# MUON REGENERATION

# IN

# MUON CATALYZED DT-FUSION



Helga E. Rafelski

A thesis submitted in partial fulfillment for the degree of
Doctor of Philosophy at the University of Cape Town

31 July 1988

## ABSTRACT

The origin of the experimentally observed density dependence of the effective muon alpha sticking fraction $\omega_s^{eff}$ in muon catalyzed deuterium- tritium fusion has been comprehensively reanalyzed with the particular emphasis put on the density dependence of the stopping power in dense hydrogen. The main technical details and improvements in this work are: The $(\alpha\mu)^+$ 2s and 2p states are treated independently and are assigned individual reaction rates. The essential muonic excitation rates have been recalculated taking into account finite nuclear mass effects. The stopping power for a charged projectile in liquid heavy hydrogen is modified to account for dynamic screening effects and a density dependent effective ionization potential. It is shown that the medium dependent stopping power for the $(\alpha\mu)^+$ ion is the crucial entity controlling the density dependance of the effective sticking fraction. It is also pointed out that the muonic helium $K_\alpha$ X-ray yield and the sticking fraction at high density can not be simultaneously brought into agreement with the experimental results without invoking novel mechanisms suppressing Stark mixing in the (He$\mu$) L-shell.

## ACKNOWLEDGEMENTS

It is a great pleasure to acknowledge friends and colleagues who through their encouragement and stimulating discussions have helped me with this research project. Thank you all in particular for providing a vibrant and stimulating atmosphere and a sense of urgency which contributed to my determination to complete this project.

**Raoul Viollier** supervised this thesis with patience and encouragement. He gave his full support whenever necessary. Without his interest and help this thesis may have never been completed.

**Dirk Trautmann** contributed the muon ionization cross sections used in this work and provided the computer code for the calculations of the inelastic excitation cross sections. My sincere thanks are also due to him for numerous clarifying discussions and encouragement.

**Berndt Müller** provided encouragement in the final phase. His interest and stimulating discussions generated the momentum during the past months leading to the completion of this thesis.

**Allard Schnabel** has been an exceptional student colleague, he listened patiently to many ideas and problems and helped in many different ways.

**Susanne and Marc Rafelski,** my lovely children, deserve a lot of credit for their understanding beyond the usual comprehension.

**Jan Rafelski,** my best friend and husband, I like to thank him most of all for his support and understanding. He rigorously kept private and business matters apart. His pointed criticism amongst many other things made him my best teacher.

TABLE OF CONTENT

# 1. INTRODUCTION

In muon catalyzed fusion (MuCF) a collection of favorable physical coincidences allows that fusion energy production becomes possible in the presence of a muon, an elementary particle not used by nature for any other obvious purpose and which poses a puzzle by its sheer existence since its discovery 50 years ago. Muons are particles akin to electrons with a mass $m_\mu = 206.77 m_e$ which decay after an average lifetime of $\tau_\mu = 2.2 \mu sec$. For MuCF to be a viable process of energy production many hundreds of fusions must occur during the short lifetime for each muon present in order to recover the cost involved in the artificial production in elementary processes of this particle. While six deuterium- tritium fusions release an energy equivalent of the muon rest mass many more fusions are needed to offset the inefficiency of the muon formation process. Aside from the negatively charged muon $\mu^-$ the positively charged anti muon $\mu^+$ is created in many elementary processes, but is of no use in MuCF.

In *appendix A* a survey of MuCF processes not directly needed in this work are presented.

The introduction of a $\mu^-$ into a mixture of hydrogen isotopes brings about a repetitive cycle of processes leading to nuclear fusion and the release of energy [1-16]. While several different fusion reactions are possible because of various fundamental processes involved, only the dt catalytic cycle, see figure 1, can be repeated hundred(s) of times during the lifetime of one muon. The main steps are summarized below, with emphasis on elementary coincidences placed in brackets.

1. The muon $\mu^-$ is slowed in the mixture of hydrogen isotopes, within less than $10^{-10}$ sec.

2. The $\mu^-$ is captured by one of the hydrogen isotopes d or t in $n \approx \sqrt{208}$ outer orbit, replacing an electron in the process.

3. a) The muon cascades down to the 1s state of t or
   b) if captured in d, the muon is transferred to the heavier tritium isotope ($\Delta E_{1s} = 48\ eV$, isotopic mass shift) either during the cascade in deuterium or only slowly after reaching the 1s orbit.
   (Even from the $d_{1s}$ the transfer rate is 100 times faster than the competing $(dd\mu)$ formation rate.)

4. A $(dt\mu)$ muomolecule is formed, due to the existence of the fortunate resonant muomolecule formation
   (this can be even more than 1000 times faster than the muon lifetime).

5. The muonic molecule deexcites to J=0 muomolecular state.

6. The nuclear fusion reaction $d+t \rightarrow \alpha+n$ takes place and 17.6 $MeV$ energy is released
(the existence of a near threshold compound nucleus resonance ${}^5He(\frac{3}{2}^+; 17.66\ MeV)$ causes the fusion reaction to be millions times faster than the natural muon decay).

7. a) If the muon is set free it can repeat the cycle, otherwise
b) the muon becomes bound to the reaction product, the $\alpha-$ particle, i.e. sticking occurs,
(sticking to the dt- fusion reaction product is $\sim 0.45\%$ compared to about 12% sticking to the nuclear reaction product $({}^3He)^+$ in dd- fusion and nearly 100% in other reactions).

**This work deals with the processes occurring when the $(\alpha\mu)^+$ muonic ion created with the energy $E = 3.46\ MeV$ is slowed down in a dense D-T mixture. In particular, the muon can be stripped (regenerated), thus allowing the muon to return to the catalytic cycle.**

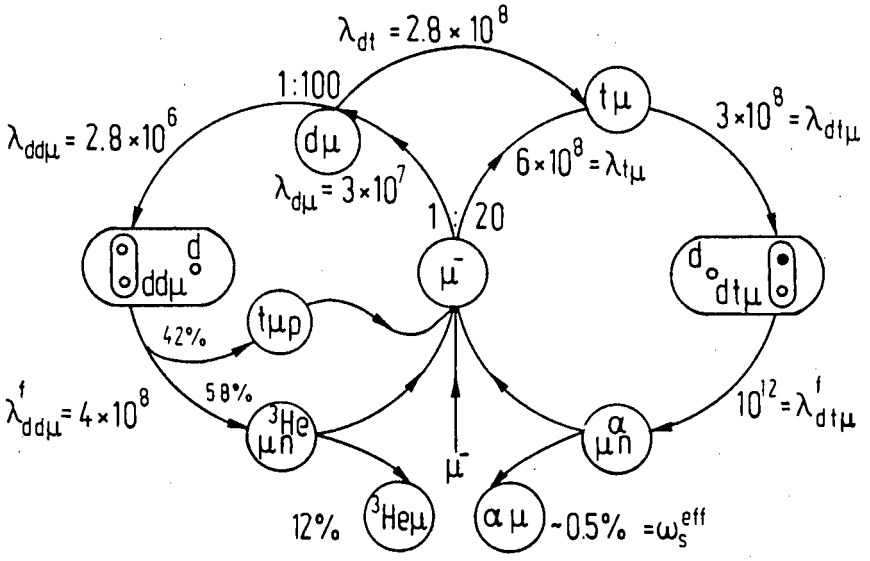


Representation of cycle processes for a muon stopping in a liquid mixture of deuterium and tritium of equal proportions. Note: the $(dt\mu)$ formation rate is dependent on the density and temperature of the mixture.

The different processes described are graphically depicted above and some important rates per sec for the processes are indicated. Because of the necessary presence of deuterium, there is a competition between the desirable $(dt\mu)$ fusion and the $(dd\mu)$ fusion. Fortunately, the ratio of rates of muon transfer process

from the $(d\mu)_{1s}$ to $(t\mu)_{1s}$ state, which can form the $(dd\mu)$ molecule resonantly,is:

$$\frac{(d\mu)_{1s} + t \rightarrow d + (t\mu)_{1s}}{(d\mu)_{1s} + d \rightarrow (dd\mu)} > 100. \tag{1}$$

Furthermore, it was expected that the $(t\mu)_{1s}$ state is populated 20 times more frequently than the $(d\mu)_{1s}$ state, even when the isotopic properties in the target are taken into account. However, these theoretical expectations are not born out in experiments.

The muomolecular formation rates $\lambda_{dt\mu}$ and $\lambda_{dd\mu}$ typically increase with temperature, due to the process of resonance tuning. In more detailed studies one has to distinguish the rates $\lambda_{dt\mu-d}$, $\lambda_{dt\mu-t}$, $\lambda_{dd\mu-d}$ and $\lambda_{dd\mu-t}$ associated with the different molecular partners and hence slight differences in the resonance conditions.

In comparison to the muon lifetime of $\tau_\mu = 2.2\mu sec$ about $(\tau_\mu \lambda)$ repetitions of the cycle can be expected. More precisely, denoting by $\lambda_c$ the cycling rate of the muon and with $\tau_{eff}$ the effective lifetime of the muon as catalyst, the total number of fusions (yield) per muon is:

$$Y = \tau_{eff} \lambda_c. \tag{2}$$

The effective lifetime of the catalyst is limited not only by the muon decay rate $\lambda_\mu = \tau_\mu^{-1} = 0.44 \times 10^6 s^{-1}$, but also by the loss rate of the catalyst

$$\lambda_l = w_s \lambda_c, \tag{3}$$

where $w_s$ is the probability of muon loss per cycle. Since the effective rate of muon loss is additive (as can be easily seen studying the population equations),

$$\lambda_\mu^{eff} = \tau_{eff}^{-1} = \lambda_\mu + \lambda_l \tag{4}$$

and the fusion yield is obtained in terms of $\lambda_c$ and $w_s$:

$$Y^{-1} = \lambda_\mu / \lambda_c + w_s. \tag{5}$$

The rapid muomolecule formation rate leads presently to the value $O(200^{-1})$ for the first factor, which is about the magnitude of the second term in *eq.*(5). Hence in order to be able to raise the yield of fusions per muon not only the cycling rate $\lambda_c$ has to be increased but also the muon loss must be kept minimal, in particular the muon poisoning processes must be well understood.

The probability of muon loss per cycle $w_s$ has as its dominant term the effective sticking probability $\omega_s^{eff}$ to the $\alpha$- particle which is the initial sticking $\omega_s^0$ reduced by the regeneration processes

$$w_s = \omega_s^{eff} + \omega_s^{cyc} + \omega_s^{scav}. \tag{6}$$

The second term $\omega_s^{cyc}$ describes the muon loss in the dd- and tt- side cycles of the fusion reaction, while $\omega_s^{scav}$ is the effect of muon scavenging by $(^3He)^+$, arising from the tritium decay. Both last terms will not be further discussed here, except to note, that they are considerably smaller than the first term due to muon sticking, especially when a 50-50% D-T mixture is used.

The sticking loss $\omega_s^{eff}$ is the sum over sticking to all possible states $(nl)$ of the $(\alpha\mu)^+$ ion, less the regeneration probability $R_{nl}$ from these states, which includes all possible stripping processes of the muon during the slow down of the $(\alpha\mu)^+$ ion.

$$\omega_s^{eff} = \sum_{n,l} \omega_{nl}^0 (1 - R_{nl}). \tag{7}$$

Figure 1 shows that only 1s and 2p states are difficult to regenerate.

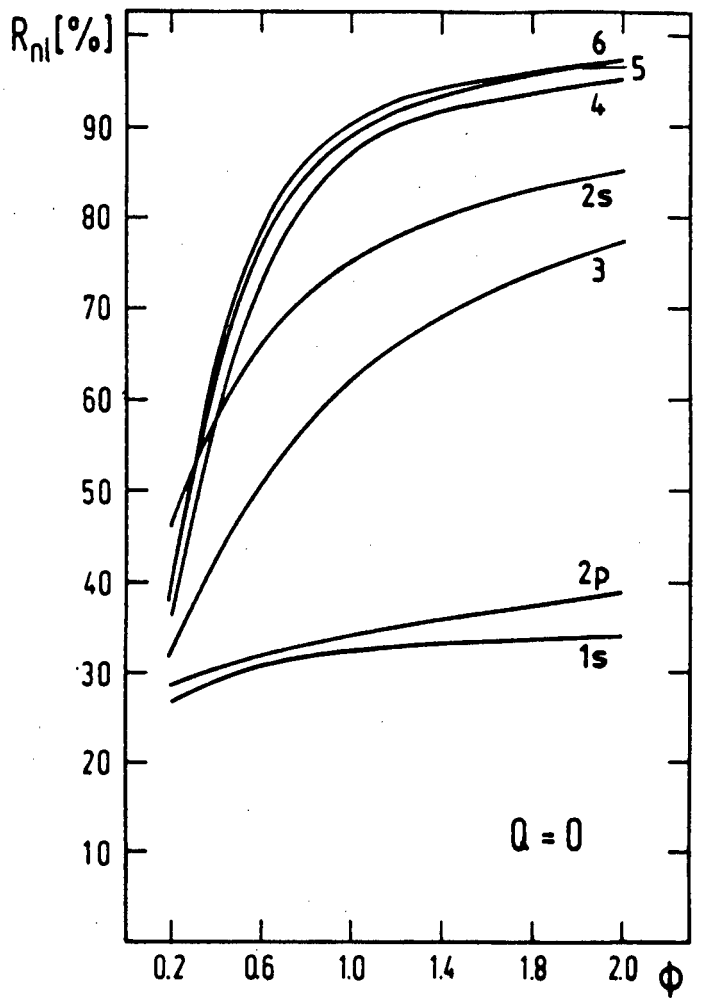


Figure 1: Regeneration probabilities $R_{nl}$ following on $(dt\mu)$ fusion. Q=0: no 2p-2s quenching.

In *section 2* the initial sticking probability $\omega_{nl}^0$ is reviewed and the quan-

titative relation to the effective sticking probability $\omega_s^{eff}$ is shown. Also the differential equation of the regeneration dynamics is given and most of the notation convention is established.

The reaction rates contributing to the regeneration mechanism are described in *section 3*. The methods for the theoretical calculation of the muonic stripping and the inelastic muonic excitation cross sections are outlined and results are shown. Results for the regeneration probability, the effective muon sticking fraction and muonic X-rays arising during the $(\alpha\mu)^+$ slow down process after dt- and dd- fusion are obtained. A comparison with existing experimental as well as to other theoretical work is presented.

Since the strong density dependence of the effective muon sticking fraction of the LAMPF experiments [13] can not be accounted for by the competition between excitation and the X-ray deexcitation the attention is focused on the $(\alpha\mu)^+$ stopping power in *section 4*. Indeed the density dependence can arise from the competition between muon stripping cross sections and the energy loss reactions of the $(\alpha\mu)^+$ ion if the latter quantity depends non linearly on the target density. The stopping power is parametrized to allow for a density dependence through the mean ionization potential and screening effects.

Under this assumption a strong density dependent reduction of the effective muon sticking fraction is obtained from a density dependent stopping power in *section 5*. However, the muonic X-ray yields for the K-transitions are shown to increase, making the already existing X-ray yield discrepancy between theory and experiment even larger. A resonant deexcitation of the 2p state [17] is introduced in *section 6* and the influences on the muon regeneration dynamics is described. Good agreement to all experimental observables can be achieved. In *section 7* a general discussion of the results of this work is presented.

In order not to disturb the flow of the physical arguments and results, technical details, some mathematical calculations and extensive formulas needed in this project are provided in the appendices.

*Appendix A* provides some background facts about muon catalyzed fusion and reviews some historical developments in this field for the non specialist reader.

In *appendix B* the muon transfer cross sections in the eikonal approximation [18] used in the present regeneration calculations is given.

The formulas for the inelastic Coulomb excitation cross sections in the modified Born approximation [19] are derived in *appendix C*.

The theory of the stopping power is described in more detail in *appendix D*.

## 2. THE REGENERATION MECHANISM

### 2.1 Initial Sticking Probability

When MuCF dt- fusion occurs the muon can end up free, i.e. it is shaken off. The muon is then available to repeat the chain of reactions. In some cases, however, the muon can end up in a bound state of the fusion product.

$$d + t + \mu \rightarrow \begin{cases} {}^4He + n + \mu \\ \alpha\mu + n \end{cases}. \tag{1}$$

The muon can stick to a charged reaction product and in dt- fusion it may stick to the recoiling $\alpha$-particle and form a $(\alpha\mu)^+$ ion with an initial kinetic energy $E^{in}_{\alpha\mu} \simeq 3.46\, MeV$ (roughly 4/5 of the $17.60\, MeV$ fusion yield), corresponding to the initial velocity $v_{(\alpha\mu)} = 5.82c/137$, c is the velocity of light and the notation $1/137$ is used for the fine structure constant $e^2/\hbar c$ to avoid confusion with the $\alpha$-particle. If not otherwise stated the velocity $v$ will be expressed in atomic units [a.u.] through out this document, i.e. omitting $[1/137c, etc.]$.

MuCF can also be viewed as a decay process of the metastable $(dt\mu)$ molecule. There are two possible reactions
the three body decay:

$$d + t + \mu \rightarrow \alpha + \mu + n, \tag{2}$$

and the two body decay:

$$d + t + \mu \rightarrow (\alpha\mu)^+_k + n. \tag{3}$$

In the latter case the muon sticks to the fusion product. The $\alpha-$ particle forms a muonic helium ion $(\alpha\mu)^+_k$ with the muon captured in the atomic bound state $k$ (the ground state or any other orbit).

Should the muon be freed in the catalyzed fusion reaction *eq.*(2), it will in general form another muomolecule leading to further fusion processes in the catalytic cycle. The practicability of the muon catalyzed fusion depends critically on the mechanism leading to muon loss from this cycle of which the muon sticking probability $\omega^0_s$ is the dominant and fundamental component. In terms of the reactions in *eqs.*(2,3) this *intrinsic* initial sticking probability $\omega^0_s$ is given by the branching ratio:

$$\omega^0_s = \frac{\Gamma(dt\mu \rightarrow n + \alpha\mu)}{\Gamma(dt\mu \rightarrow n + \alpha + \mu) + \Gamma(dt\mu \rightarrow n + \alpha\mu)}, \tag{4}$$

where $\Gamma$ denotes as usual the partial width of the reaction.

The total initial sticking probability $\omega_s^0$ is the sum of the probabilities with which the muon sticks to the different $(\alpha\mu)^+$ states.

$$\omega_s^0 = \sum_{nl} \omega_{nl}^0 \tag{5}$$

These probabilities have been obtained by several groups [20,21,22] in non adiabatic 3-body variational calculations. These results are ca. 30% smaller then results from earlier calculations [16,23]. The initial sticking depends on the quantum molecular state from which the $(dt\mu)$ molecule decays, but is otherwise independent of target conditions such as density dependence. Present calculations ignore possible effects of nuclear interactions on sticking [24,25,26,27].

Table 1 lists the initial sticking probabilities ($\omega_d^0$ for the dd- fusion reaction and $\omega_s^0$ for the dt- fusion reaction) and the initial muon distribution $P_s(nl)$ and $P_d(nl)$ normalized to 1 as used in the calculations for this document.

Table 1

Sticking probabilities: $\omega_s(\%)$ for the reaction $(dt\mu) \rightarrow (\mu^4He) + n$, $\omega_d(\%)$ for the reaction $(dd\mu) \rightarrow (\mu^3He) + n$, as well as the normalized distributions $P_s(nl)$ and $P_d(nl)$.

| nl | $\omega_{nl}^s$ | $P_s(nl)$ | $\omega_{nl}^d$ | $P_d(nl)$ |
|---|---|---|---|---|
| 1s | 0.6803 | 0.7731 | 9.36 | 0.7091 |
| 2s | 0.0973 | 0.1106 | 1.21 | 0.0917 |
| 2p | 0.0237 | 0.0269 | 1.00 | 0.0758 |
| 3 | 0.0382 | 0.0434 | 0.75 | 0.0568 |
| 4 | 0.0164 | 0.0186 | 0.35 | 0.0265 |
| 5 | 0.0079 | 0.0090 | 0.18 | 0.0139 |
| 6 | 0.0046 | 0.0052 | 0.13 | 0.0101 |
| $n \geq 7$ | 0.0116 | 0.0132 | 0.22 | 0.0167 |
| total | 0.8800 | 1.0000 | 13.20 | 1.0000 |

## 2.2 Observed Sticking Probability and Muon Regeneration Processes

Recall from the introduction that each muon is capable of catalyzing $(Y)$ fusions, a number determined by the average cycle rate $\lambda_c$ of the muon and the effective muon disappearance rate $\lambda_\mu^{eff}$:

$$Y = \lambda_c/\lambda_\mu^{eff}, \tag{6}$$

$$\lambda_\mu^{eff} = \lambda_\mu + w_s\lambda_c,$$

$\lambda_\mu = \tau_\mu^{-1}$ is the rate of muon decay in the catalytic cycle and $w_s$ is the mean probability per muon cycle to immobilize the muon whatever the cause. The probability $w_s$ comprises further mechanisms of muon loss, aside from $\alpha$ -sticking. These losses for example could be losses to inert muomolecules comprising protium, losses to the tritium decay product, losses to inevitable side chains of fusion reactions, etc.. In order to emphasize the importance of sticking *eqs.*(4) and (5) of *section 1* are used to obtain

$$Y < (w_s)^{-1} < (\omega_s^{eff})^{-1}, \tag{7}$$

the first inequality arises when $\lambda_c \gg \lambda_\mu$ which is true in favorable circumstances [2] . The last inequality is a consequence of the fact that a priori, the quantum mechanical muon loss probability $\omega_s^{eff}$, is a lower limit on $w_s$.

The quantity $\omega_s^{eff}$ used above c.f. *eq.*(6) in *section 1* is not quite the intrinsic branching ratio $\omega_s^0$, because even if a muon is captured by the $\alpha-$ particle following the fusion process, the muon may be stripped [1,3,4] in subsequent collisions with the hydrogen molecules in the target during slow down that is until the kinetic energy reaches the threshold energy $E_0$ (a few $keV$) of the appropriate reaction. This may occur either in a single step Coulomb ionization process or by multistep processes such as intrinsic Coulomb excitation followed by a transfer to a hydronic bound state, etc..

The time it takes for the $(\alpha\mu)^+$ to be slowed down from its initial velocity $v_{(\alpha\mu)} = 5.82$ to $v_{(\alpha\mu)} = 0$, depends on the actual stopping power $S(v)$ of the target. This quantity is defined by the relation

$$\frac{dE}{dx} = -\rho S(v) \tag{8}$$

or

$$\frac{dE}{dt} = -\rho v S(v). \tag{9}$$

Hence the slow down time $t_{stop}$ is:

$$t_{stop} = \int_{E_{in}}^{0} \rho v S(v) dE. \tag{10}$$

This quantity will be proportional to the density $\rho$

$$\rho = \phi\rho_0 \tag{11}$$

of the target and is usually presented for the liquid hydrogen density $\rho_0$:

$$\rho_0 = 4.25 \times 10^{22} cm^{-3}.$$

This slow down time is $t_{stop} \sim 4 \times 10^{-11} s$, if the stopping power of the $(\alpha\mu)^+$ is obtained from the scaled proton stopping power c.f. reference [16]. Thus even for $\phi = 10^{-2}$ the time needed for the muon stripping during the slow down of the $(\alpha\mu)^+$ ion is of no particular significance.

In order to understand the general expressions describing the muon regeneration, it is helpful to consider first a simplified problem, assuming that the muon can only be stripped from the $(\alpha\mu)^+$ ion by one step processes. The cross section for this will be denoted $\sigma_{str}(E)$ and comprises both ionization and transfer components. The rate for the stripping process to occur is:

$$\lambda_{str}(E) = \sigma_{str}\rho v, \tag{12}$$

where $v$ is the velocity of the $(\alpha\mu)^+$ ion. The 1s-state population $P_0$ of the $(\alpha\mu)^+$ ion is thus satisfying the equation

$$\frac{dP_0}{dt} = -\lambda_{str}(E(t))P_0 \tag{13}$$

with the solution

$$P_0(t = t_{stop}) = \exp(-\int_{t=0}^{t_{stop}} \lambda_{str} dt)$$

$$P_0(t = t_{stop}) = \exp(-\int_{E_{in}}^{0} \lambda_{str} \frac{dt}{dE} dE). \tag{14}$$

Recalling *eq.*(9) the final population is

$$P_0(t_{stop}) = \exp(-\int_0^{E_{in}} \frac{\sigma_{str}}{S} dE) \tag{15}$$

or simply

$$P_0 = 1 - R_0 = \exp(-I)$$

where

$$I = \int_0^{E_{in}} \frac{\sigma_{str}}{S} dE. \tag{16}$$

The regeneration probability $R_{nl}$ invokes the ratio of the *muon* stripping cross section $\sigma_{str}$ to the *electron* ionization cross section S (S is $\sigma$ weighted with the energy loss). The simplest estimate of the exponent thus is

$$I \sim (m_e/m_\mu)^2 \times E_{in}/\delta E \sim 0.4,$$

where $\delta E$ is the mean energy loss in the $(\alpha\mu)^+$ collision with electrons, $\delta E \sim O(20eV)$. Hence a regeneration at the level of $R_0 \sim 0.3$ can be expected.

The actual stripping processes are Coulomb ionization on target nuclei d, or t either in a single step or by multistep processes as intrinsic Coulomb excitations followed by either transfer to a hydrogenic bound state of the target (d or t) or Coulomb ionization. Once, however, the muon is found in an excited state be it by Coulomb excitation or due to initial sticking deexcitation processes (radiative decay, Auger processes and Coulomb deexcitation processes) compete with stripping. To treat the full problem the population equation has to be generalized to incorporate the individual population of all $(\alpha\mu)^+$ bound states.

The regeneration probability R of the muon and the average K-series X-ray yield after fusion can be calculated including all above processes by solving the following coupled differential equations numerically:

$$\begin{aligned}\frac{dP_i}{dt} &= -\lambda_{ion}^{i\to\infty} P_i - \sum_m \lambda_{tra}^{i\to m} P_i \\ &- \sum_{k>i} \lambda_{exc}^{i\to k} P_i + \sum_{k<i} \lambda_{exc}^{k\to i} P_k + \sum_{k>i} \lambda_{Au}^{k\to i} P_k \\ &- \sum_{k<i} \lambda_{rad}^{i\to k} P_i + \sum_{k>i} \lambda_{rad}^{k\to i} P_k\end{aligned} \tag{17}$$

$$\frac{dP_s}{dt} = \sum_i \lambda_{str}^{(i)} P_i \tag{18}$$

with

$$\lambda_{str}^{(i)} = \lambda_{ion}^{i\to\infty} + \sum_m \lambda_{tra}^{i\to m}$$

The following notation for reaction rates is used:

| | |
|---|---|
| Stripping rates: | $\lambda^i_{str}$ |
| Transfer rates: | $\lambda^{i\to m}_{tra}$ |
| Ionization rates: | $\lambda^i_{ion}$ |
| Coulomb excitation rates: | $\lambda^{i\to k}_{exc}$ |
| Coulomb deexcitation rates: | $\lambda^{k\to i}_{de}$ |
| Stark mixing rates: | $\lambda^{2s\to 2p}_{Stark}$ |
| Radiative decay rates: | $\lambda^{k\to i}_{rad}$ |
| Auger rates: | $\lambda^{k\to i}_{Au}$ |

$i$ and $k$ are $(\alpha\mu)^+$ states $(1s, 2s, 2p, 3, 4, 5, 6)$, $m$ is a tritium or deuterium state $(1s, 2s, 2p, 3, ..., 10)$. These rates will be discussed in more detail in the following section.

$P_i(t)$ is the population of the $(\alpha\mu)^+$ ion states as a function of time t, $P_s$ is the number of stripped muons. The regeneration probability or reactivation efficiency R is:

$$R = \int_0^{t_{stop}} \sum_i \lambda^i_{str} P_i(t) dt. \tag{19}$$

The K-series X-ray yield $\gamma_{K_{i\to 1}}$ per stuck muon is similarly given by

$$\gamma_{K_{i\to 1}} = \int_0^{t_s top} \lambda^{i\to 1}_{rad} P_i(t) dt \tag{20}$$

and is related to the observed X-ray yield (called XY in this document) by normalizing with the initial sticking probability.

$$XY_{i\to 1} = \gamma_{K_{i\to 1}} \omega^0_s. \tag{21}$$

The initial conditions for the differential equations at $t = 0$ are:

$E(t = 0) = 3.46\ MeV$, for sticking after dt- fusion,
$E(t = 0) = 1.08\ MeV$, for sticking after dd- fusion.
$P_s(t = 0) = 0$
$P_i(t = 0)$ is the normalized initial sticking probability distribution as given in table 1.

The rate equation *eq.*(17) was solved including the following aspects for the relevant muon excitation and stripping cross sections:

1. The 2s and 2p states are treated separately throughout the calculation.

2. Transitions from the 1s, 2s, and 2p states into the continuum, as well as transitions among all states up to the N-shell (n=4) are calculated in Born approximation, but *with recoil* and *Coulomb deflection* effects [19] included.

3. Transfer cross sections out of states up to the N-shell are calculated in the framework of the eikonal approximation [18].

All other rates are the same as given by Cohen [28,29] and references therein. For the 2s-2p Stark mixing cross section the factor $Q$ is introduced, where $Q = 1$ corresponding to the choice of Cohen [28]. Takahashi's $C_{st} = 260$ [31] and Markushin's value [32] correspond to $Q = 0.43$.

# 3. RESULTS FOR MUON REGENERATION

## 3.1 Stripping

The stripping cross section consists of two contributions a) ionization of the $(\alpha\mu)^+$ and b) transfer of the muon to either a bound state in deuterium or tritium depending on the material present in the fusion vessel. All cross sections will be presented in units of $a_\mu^2$, where $a_\mu = 255.93\ fm$ is the muonic Bohr radius.

It is noteworthy to observe that a cross section of 100 $[a_\mu^2]$ at liquid hydrogen density and at velocity 1 [a.u.] corresponds to a rate of

$$\lambda = 100 a_\mu^2 \rho_0 v = 6.088 \times 10^{11} s^{-1}.$$

The muon transfer and ionization cross sections can not be measured at present. Experimental information has only been obtained for electron capture. The literature on theoretical calculations therefore concerns itself conclusively with electronic cross sections [33] . Quantum mechanical calculations for transfer cross sections suffer form the difficulties of handling hydrogenic wave functions with high quantum numbers. An exception is the Oppenheimer Brinkman Kramers (OBK) approximation, see reference [33] and references therein, which provides a simple closed form expression for the total electron capture cross sections and of capture rates into individual subshells. The OBK approximation shows the correct behavior but otherwise it overestimates the experimental cross sections and hence is unacceptable for our treatment.

The classical trajectory eikonal approximation as presented in *appendix B* takes into account the interaction of the captured electron with the target and the projectile nucleus. This leads to a reduction of the cross section by a factor 0.14-0.4 which is needed to bring theory into accord with experiments for electronic cross sections. The eikonal theory of charge exchange allows an explicit expression for the charge exchange cross section of a single electron between the hydrogenic shells $nl$ and $n'l'$ [18]. The results obtained for electronic cross sections are in good agreement with the experimental data.

The compact expression for the electronic charge exchange cross sections can be easily adapted for the calculation of muon charge exchange between $(\alpha\mu)^+$ and the hydrogen isotopes d or t. The theoretical calculations will properly account for the existing degeneracy between some muonic projectile and target states. The final expression used in the numerical calculation of the transfer cross section as derived by Eichler [18] and modified to apply to the muonic transfer is reviewed in Appendix B.

The muon transfer cross sections obtained with the eikonal approximation for $(\alpha\mu)^+$ 1s, 2s, 2p states to $(t\mu)_{1s}$ is shown in figure 2 as a function of the slow down velocity $v$. The sum of the muon transfer cross sections over all target $(t\mu)$ states up to N=10 from the 1s, 2s and 2p state in $(\alpha\mu)^+$ is given in figure 3.

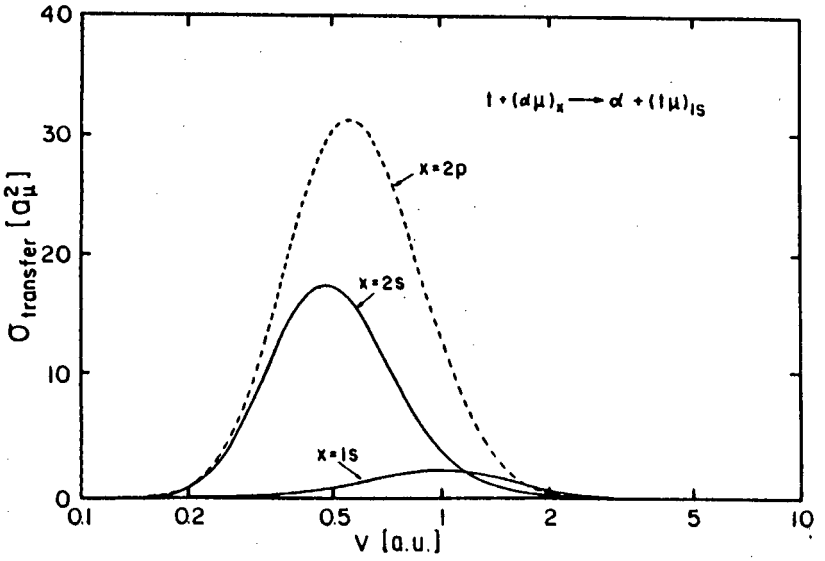


Figure 2: Cross section for the transfer of the muon from $(\alpha\mu)^+$ 1s, 2s, 2p states to $(t\mu)_{1s}$ as a function of velocity $v$.

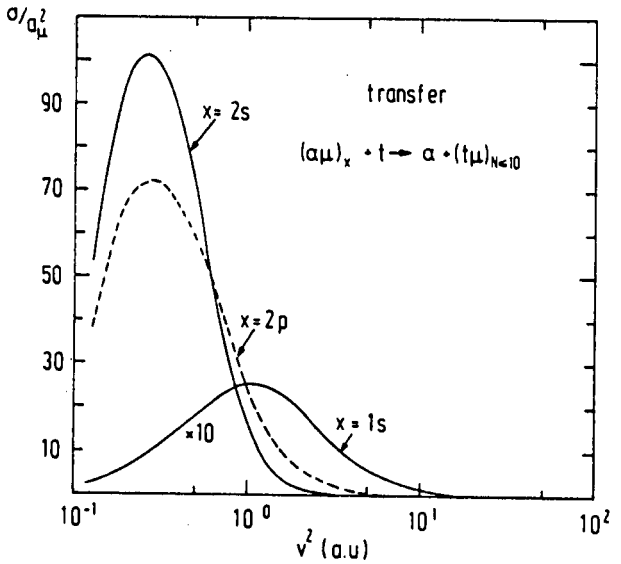


Figure 3: Cross section for transfer of the muon from $(\alpha\mu)^+$ 1s, 2s, 2p states to $(t\mu)$ including all states up to N=10 as a function of $v^2$.
Note: $\sigma_{1s}$ is multiplied by 10.

The muon ionization cross sections were calculated in the semiclassical approximation by D. Trautmann [34]. The electronic ionization cross sections obtained by the same method do agree well with experimental data [35]. Classical trajectories have been used to include Coulomb deflection, which is important for the muonic ionization cross sections and can not be neglected. Results are shown in figure 4 and figure 5.

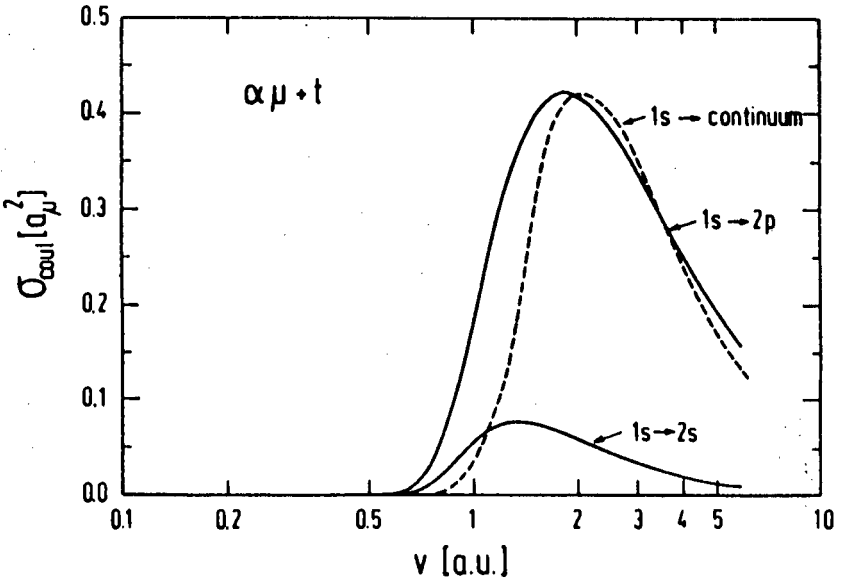


Figure 4: Cross section for the Coulomb excitation of $t + (\alpha\mu)^+$ to the continuum (dashed line) and the 2s, 2p states (full line) .

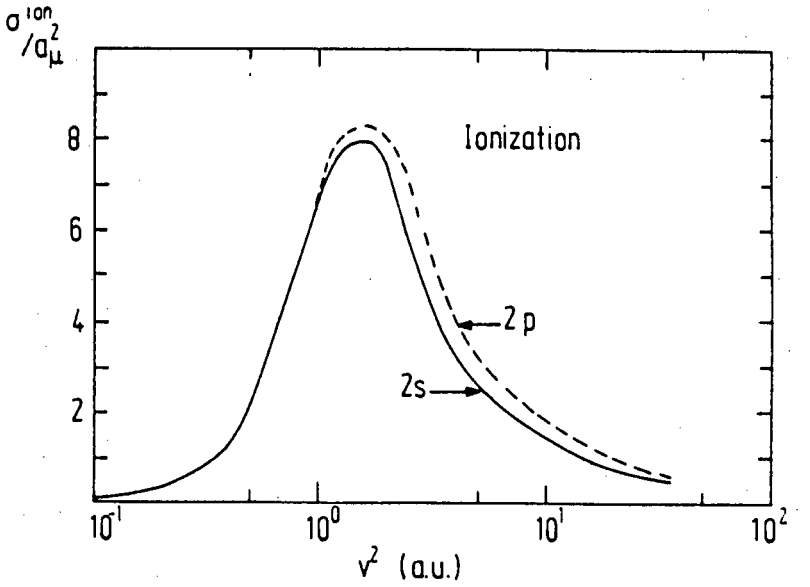


Figure 5: Ionization cross section [34] of $(\alpha\mu)^+_{2s}$ and $(\alpha\mu)^+_{2p}$ as a function of $v^2$.

The muon stripping rates, as described above and used in the present calculations are higher then those in references [36,28], see figure 6 and result dominantly from higher muon transfer rates calculated in the eikonal approximation. This is expected, since scaling of electronic cross sections neglects some near resonances in the muon transfer due to the degeneracy of some muon projectile and target states.

In order to verify the theoretical methods used, the transfer cross section was calculated with the eikonal formula for the experimentally measured [35] process

$$H^+ + He^+ \rightarrow H^+ \sum(n,l) + He^{++}.$$

The theoretical eikonal approximation is about twice as large for velocities $v < 3$. At present it is, however, not clear which value (the scaled experimental electron cross sections or the theoretically calculated cross sections) describes the 1s-muon stripping more adequately and the theoretical values are used throughout this work. This uncertainty in the 1s transfer rate does not produce any sizable effect for X-rays after fusion. Regeneration rates, however, will be somewhat different.

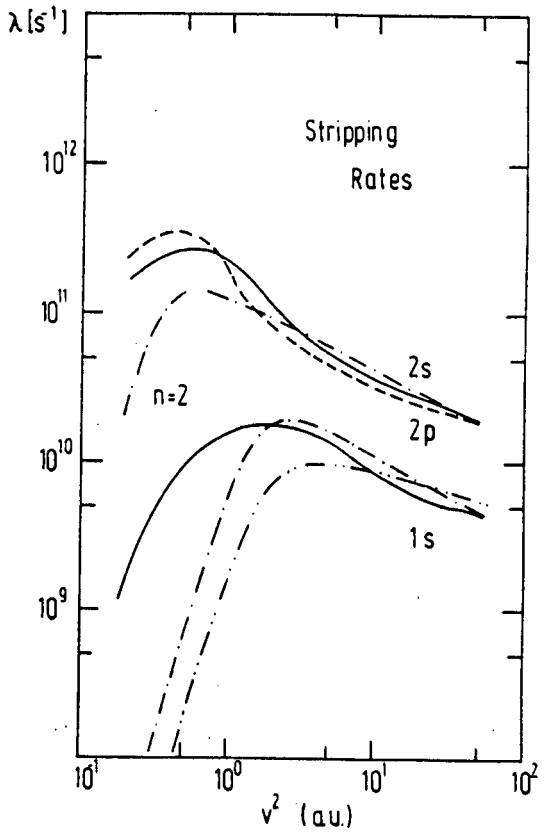


Figure 6: 1s, 2s and 2p stripping rates as a function of $v^2$. Rates by Cohen (dash dot line) [28] and (dot dash dot line) [29].

### 3.2 Coulomb Deflection and Recoil Effects for Inelastic Muon Excitation Cross Sections

The inelastic muon excitation cross sections used are calculated in a *modified* Born approximation [19] taking into account the *Coulomb deflection* of the projectile by the target system and *recoil* effects as described in *appendix C.* These effects are not taken into account in the usual procedure of using scaled electronic cross section, since they depend on the nuclear masses of target and projectile as well. They are potentially important corrections, because the ratio of muon mass to nuclear mass is not small.

Figure 7 shows the effects of the Coulomb deflection for the inelastic muon excitations of the $(\alpha\mu)^+$ during the slow down.

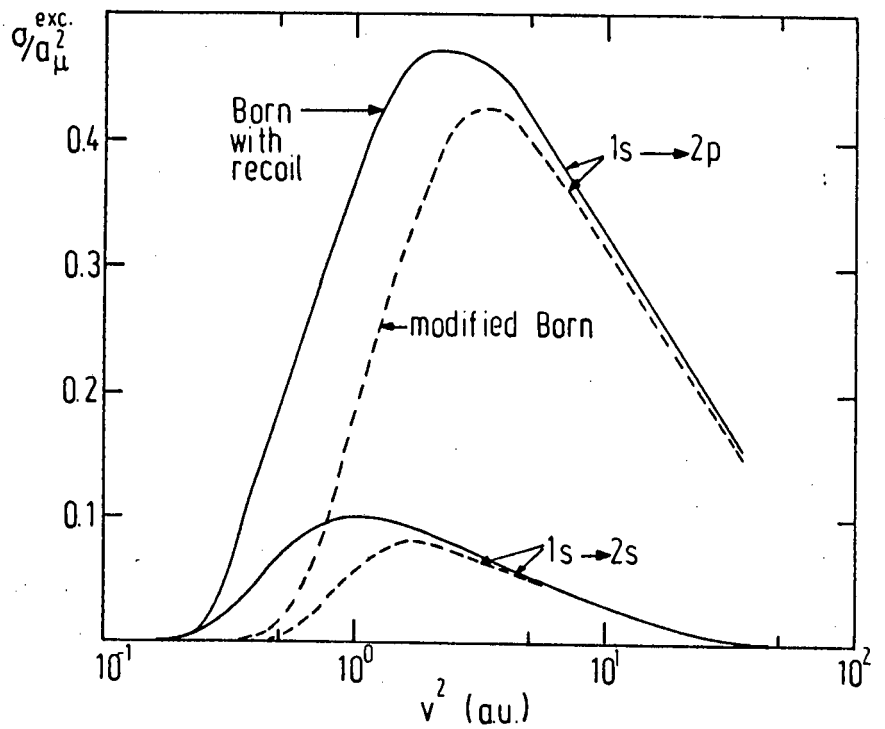


Figure 7: Excitation cross section Born approximation with recoil corrections (solid line) and modified Born (broken line) as a function of $v^2$.

Recoil effects increase the inelastic excitation cross sections. This increase is largest for the $(\alpha\mu)^+_{1s\to 2s}$ and $(\alpha\mu)^+_{1s\to 2p}$ transitions, see figure 7. The Coulomb deflection corrections reduce this increase, see figure 8.

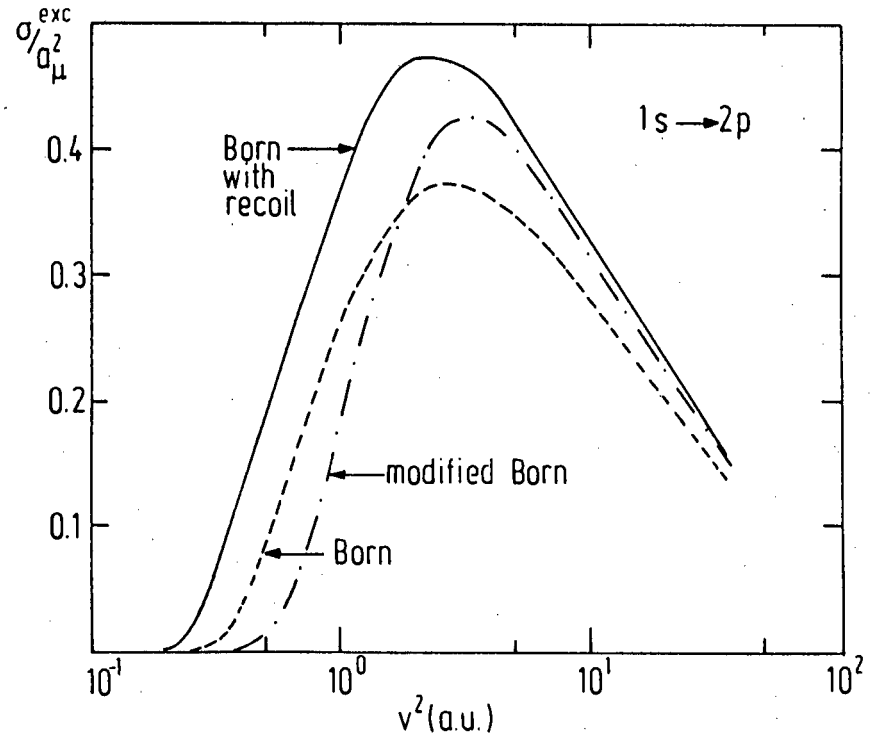


**Figure 8:** Excitation cross section for the $(\alpha\mu)^+ 1s \rightarrow 2p$ in Born approximation (broken line), with recoil corrections (solid line) and including recoil corrections and Coulomb deflection (dash dot line) .

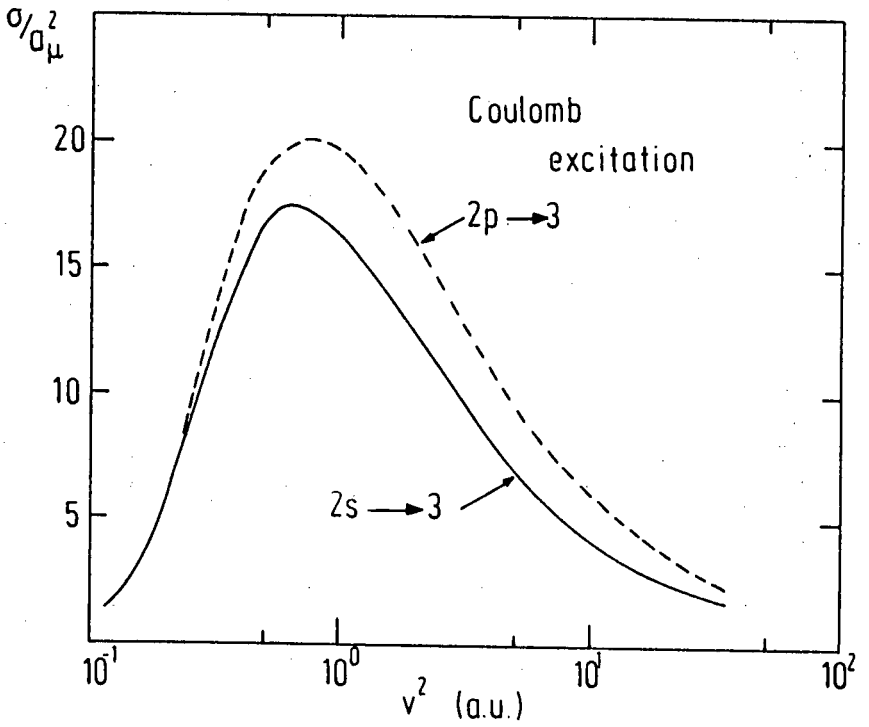


**Figure 9:** Excitation cross section with Coulomb deflection and recoil corrections as a function of $v^2$.

The inelastic Coulomb excitation cross sections $\sigma_{exc}^{2s\to 3}$ and $\sigma_{exc}^{2p\to 3}$ differ by more than 25%, see figure 9, calling for a consistently separate treatment of the $(\alpha\mu)_{2s}^{+}$ and $(\alpha\mu)_{2p}^{+}$ states.

Figure 10 distinguishes the excitation rates of the $(\alpha\mu)_{2s}^{+}$ and $(\alpha\mu)_{2p}^{+}$ stressing the importance of treating the degenerate 2s and 2p states separately.

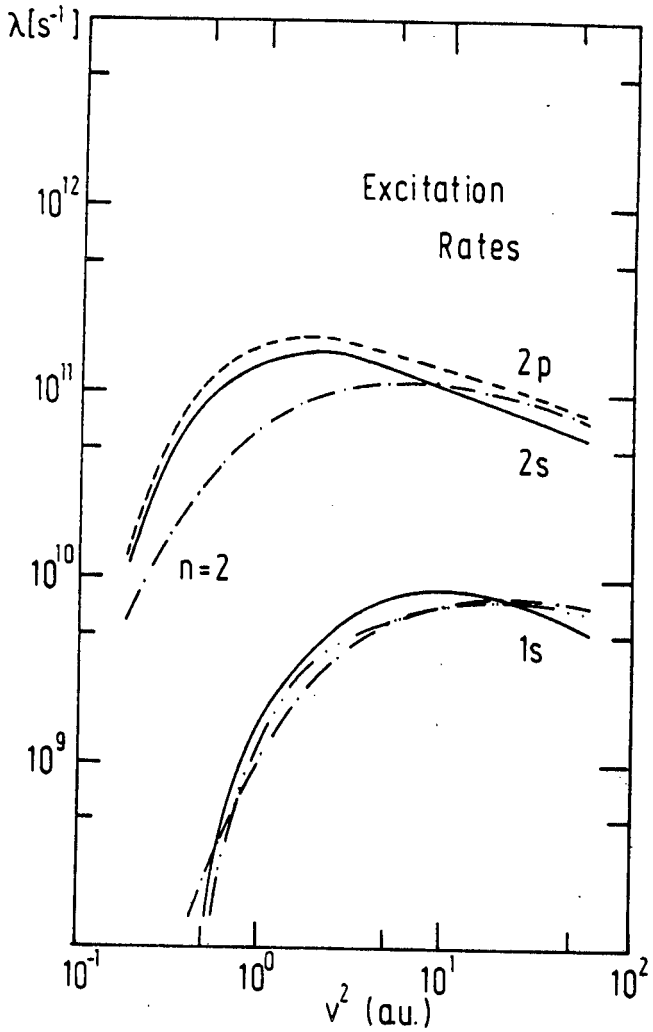


Figure 10: 1s, 2s and 2p excitation rates as a function of $v^2$. The dash dot line shows the rates by Cohen [28] and dash dot dot reference [29].

### 3.3 Deexcitation

The deexcitation processes influencing the muon regeneration are radiative decay, Auger processes on one hand and Coulomb deexcitation processes on the other hand. The first two rates are independent of the velocity of the $(\alpha\mu)^+$ ion, but the Auger process is of course proportional to the electron density and hence to the target density $\rho$. The dipole radiative decay rates used are listed in Table 2 and the Auger transition rates in Table 3. The angular momentum structure for $n \geq 3$ is not resolved and the radiative transitions are computed assuming statistical population of the angular momentum states.

Table 2

Radiative dipole transition rates for transitions $i \rightarrow k$ in $(\alpha\mu)^+$ ion. $[\lambda(\sigma = 100[a_\mu^2], v = 1 \text{ (a.u.) at } \rho_0 = 6.088 \times 10^{11} s^{-1}]$.

| i | k= 1s | 2s | 2p | 3 | 4 | 5 |
|---|---|---|---|---|---|---|
| 2 | 20.17 | | | | | |
| 3 | 1.794 | 0.240 | 1.178 | | | |
| 4 | 0.412 | 0.058 | 0.212 | 0.289 | | |
| 5 | 0.133 | 0.019 | 0.062 | 0.078 | 0.053 | |
| 6 | 0.056 | 0.008 | 0.025 | 0.026 | 0.027 | 0.018 |

Table 3

Auger transition rates [16] for transitions $i \rightarrow k$ [in units of $10^{11} s^{-1}$] for $\rho = \rho_0$.

| i | k= 1s | 2s | 3 | 4 | 5 |
|---|---|---|---|---|---|
| 2 | $4.41\times10^{-3}$ | | | | |
| 3 | $2.88\times10^{-4}$ | 0.15 | | | |
| 4 | $5.5\times10^{-5}$ | 0.001 | 1.21 | | |
| 5 | $1.6\times10^{-5}$ | $2.0\times10^{-3}$ | 0.08 | 5.4 | |
| 6 | $6.2\times10^{-6}$ | $6.4\times10^{-4}$ | 0.016 | 0.34 | 17.2 |

For the (velocity dependent) deexcitation cross sections the argumentation of Bracci and Fiorentini [16] has been adopted.

The cross sections for Coulomb deexcitation to the 1s state, $\sigma_{de}^{n\rightarrow 1s}$, averaged over the states of the initial multiplet n, can be derived from the discrete excitation cross sections, $\sigma_{exc}^{1s\rightarrow n}$. Since the dominant matrix element pertains to $1s \longleftrightarrow ns$ transitions and the phase space is practically the same for excitation and deexcitation

$$\sigma_{de}^{n\rightarrow 1s} = \sigma_{exc}^{1s\rightarrow n}/n^2.$$

The cross sections for $ns \rightarrow n's$ transitions are suppressed by a factor $n'^{-3}$ with respect to $ns \rightarrow 1s$.
Thus the deexcitation cross sections used in the present calculations are

$$\sigma_{de}^{k \rightarrow i} = \frac{\sigma_{exc}^{i \rightarrow k}}{n_k^2 n_i^3}, \tag{1}$$

where $\sigma_{exc}$ are the Coulomb excitation cross sections as calculated in the modified Born approximation, the $n_k, n_i$ are the principle quantum numbers of the states k and i.

### 3.4 Stark Mixing

During the passage of the $(\alpha\mu)^+$ ion through the D- T mixture the ion experiences often strong electrical fields, when it comes into proximity of the d or t nuclei. This leads to the mixing of levels in the same principle shell, called Stark mixing. This mixing between the 2p and 2s states has the effect of depopulating the metastable 2s state much faster during the slow down time, while the 2p state levels off in a dynamical population equilibrium at a slightly higher level see figure 11.

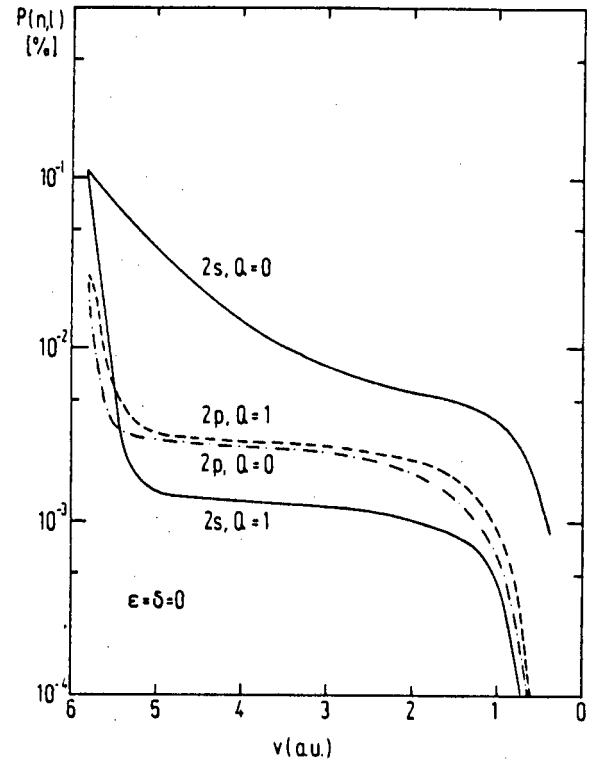


Figure 11: Influence of the Stark mixing on the $P_{2s}$ and $P_{2p}$ population of the $(\alpha\mu)^+$ during slow down.

The Stark mixing used in this work has been evaluated by Cohen [28] using the method of Leon and Bethe [30] in the limit $n^2/v < 10$:

$$\sigma_{2s\to 2p} \simeq \frac{192\pi}{v^2 M_\mu^2 Z^2} = 3\sigma_{2p\to 2s},$$

where Z=2 and $M_\mu$ is the reduced mass of $(\alpha\mu)^+$ or $(^3He\mu)^+$. The equality arises because statistically only "1/3" of the muon participates in the mixing in the J=1 state. Q is used to specify the fraction of this cross section for this Stark mixing rate used:

$$\sigma_{Stark} = Q \times \sigma_{2s\to 2p}.$$

### 3.5 Regeneration and Muonic X-rays

The reactivation probability of the muon is determined by a rather delicate balance between collisional excitation and ionization and transfer processes on one hand and the combination of electromagnetic deexcitation and slowing down of the $(\alpha\mu)^+$ particle on the other hand. In principle, the experimentally observed decrease of $\omega_s^{eff}$ with growing target density [13] could have its origin in any of these quantities.

The effective sticking fraction has been first calculated for the $(\alpha\mu)^+$ with an initial sticking $\omega_s^0 = 0.88$, see table 1. The stopping power used to obtain this result is the same as in reference [16]. The effective sticking fraction from dt- fusion and dd- fusion without Stark mixing (Q=0) and with Stark mixing (Q=1), i.e. as chosen in reference [28] are listed in table 4 and table 5 for comparison with previous theoretical results and experimental data.

Table 4
The $(\alpha\mu)^+$ sticking fraction $\omega_s^{eff} = (1 - R)\omega_s^0$ with $\omega_s^0 = 0.88\%$.

| THEORY: | $\phi$=1.2 | $\phi$=0.1 |
|---|---|---|
| PRESENT WORK: | | |
| Q=1 | 0.56 | 0.62 |
| Q=0 | 0.52 | 0.55 |
| | | |
| OTHER THEORY: | | |
| Bracci et al. [16] | 0.67 | 0.70 |
| Cohen [38] | 0.54 | 0.59 |
| Cohen [28] Q=1 | 0.53 | 0.59 |
| Cohen [28] Q=0 | 0.49 | 0.57 |
| Gershtein et al. [23] | 0.68 | |
| Markushin [32] | 0.57 | |
| Menshikov et al. [39] | 0.60 | 0.67 |
| Takahashi [31] Q=0 | 0.57 | |
| Takahashi [31] Q=0.43 | 0.61 | 0.63 |
| | | |
| EXPERIMENT: | | |
| Jones et al. [14] | 0.4±0.1 | |
| Jones et al. [13] | 0.35±0.07 | 1.1±0.5 |
| Breunlich et al. [41] | 0.45±0.05 | 0.50±0.10 |
| Nagamine [42] | 0.42±0.07 | |
| Bossy et al. [43] | 0.42±0.14 | |

density dependence becomes more clearly visible:

$$\frac{dP_i}{dE} \sim \frac{1}{S}\sum_k(\sigma^{exc}_{k\to i} + \frac{1}{v\rho}\lambda^{rad}_{ik})P_k - \frac{1}{S}\sum_k(\sigma^{exc}_{i\to k} + \frac{1}{v\rho}\lambda^{rad}_{ki})P_i - \frac{1}{S}\sigma^{str}_i P_i. \quad (2)$$

Therefore, the radiative transitions become less dominant at high density, and a larger fraction of muons can be stripped from higher states in the helium atom. This mechanism produces the weak decrease of $\omega_s^{eff}$ with increasing density. As noted in table 2, for the competition to be really effective a cross section in the range of 300 a.u. is needed, that is about a factor 10 greater than expected. Thus the strong density dependence can not be found by fine tuning the absolute values of various reactions.

Contributions to the regeneration coefficient R are mainly from ionization of the 1s state of the $(\alpha\mu)^+$ and account for 68% of the total stripping in calculations for a target density $\phi = 1.2$ and with Stark mixing Q=1, but only 56% comes from the 1s ionization if no Stark mixing (Q=0) is assumed. The main contribution to the regeneration of the $(^3He\mu)^+$ comes from the 1s transfer. For Q=1 the 1s transfer accounts for 31% of the total stripping and 24% if Q=0.

Further details about contributions from ionization and transfer to the regeneration coefficient can be found for stripping from $(\alpha\mu)^+$ in table 6 and table 7 and from $(^3He\mu)^+$ in table 8 and table 9.

Table 6

Contributions to the $(\alpha\mu)^+$ in % of the total regeneration R=0.4066 for Q=0 and $\phi = 1.2$.

| state | stripping | ionization | transfer |
|---|---|---|---|
| n=1-6 | | 83.24 | 16.76 |
| 1s | 55.56 | 39.86 | 15.70 |
| 2s | 7.95 | 7.51 | 0.44 |
| 2p | 0.93 | 0.58 | 0.35 |
| 3 | 4.81 | 4.60 | 0.21 |
| 4 | 2.58 | 2.56 | 0.02 |
| 5 | 19.43 | 19.40 | 0.03 |
| 6 | 8.74 | 8.73 | 0.01 |

Table 7

Contributions to the $(\alpha\mu)^+$ in % of the total regeneration R=0.3583 for Q=1 and $\phi = 1.2$.

| state | stripping | ionization | transfer |
|---|---|---|---|
| n=1-6 | | 80.38 | 19.62 |
| 1s | 68.37 | 49.09 | 19.28 |
| 2s | 1.48 | 1.44 | 0.04 |
| 2p | 1.49 | 1.36 | 0.13 |
| 3 | 3.54 | 3.41 | 0.13 |
| 4 | 2.13 | 2.12 | 0.01 |
| 5 | 15.88 | 15.86 | 0.02 |
| 6 | 7.11 | 7.10 | 0.01 |

Table 8

Contributions to the $(^3He\mu)^+$ in % of the total regeneration R=0.2884 for Q=0 and $\phi = 1.2$.

| state | stripping | ionization | transfer |
|---|---|---|---|
| n=1-6 | | 70.53 | 29.47 |
| 1s | 39.36 | 15.04 | 24.32 |
| 2s | 10.33 | 6.84 | 3.49 |
| 2p | 1.08 | 0.91 | 0.17 |
| 3 | 7.18 | 5.94 | 1.24 |
| 4 | 2.40 | 2.30 | 0.10 |
| 5 | 23.88 | 23.74 | 0.14 |
| 6 | 15.77 | 15.76 | 0.01 |

Table 9

Contributions to the $(^3He\mu)^+$ in % of the total regeneration R=0.2416 for Q=1 and $\phi = 1.2$.

| state | stripping | ionization | transfer |
|---|---|---|---|
| n=1-6 | | 67.80 | 32.20 |
| 1s | 50.75 | 19.27 | 31.48 |
| 2s | 1.46 | 1.38 | 0.08 |
| 2p | 2.03 | 1.78 | 0.25 |
| 3 | 5.25 | 4.98 | 0.27 |
| 4 | 0.43 | 0.42 | 0.01 |
| 5 | 23.14 | 23.08 | 0.06 |
| 6 | 16.94 | 16.89 | 0.05 |

Contributions to the muon regeneration after dt- fusion from deexcitation rates are smaller than 0.3%. Auger effects account only for about 0.5%. Even so recoil and Coulomb deflection effects give quite some differences in the Coulomb excitation cross sections (see figures 8 and 9), these differences bring about only a 1.7% (0.9%) difference in the regeneration rate and a 1.8% (0.4%) difference in the $K_\alpha$ X-ray yield after fusion during the $(\alpha\mu)^+$ respectively $(^3He\mu)^+$ slow down. Much larger differences are brought about through the choice of the Stark mixing Q see table 10 and 11. The choice of Q=0 or Q=1 changes the reactivation probability by about 13% and the $K_\alpha$ X-ray yields change by 30%.

The results obtained with the theoretically calculated cross sections as described above show only a *weak* density dependance for the muon regeneration from $(\alpha\mu)^+$ and $(^3He\mu)^+$ similar to calculation obtained with different cross sections [38,31,32]. The $K_\alpha$ X-rays after dt- and dd- fusion, however, do agree better with experiments if only a small or even no Stark mixing is assumed. This distinguishes the present results from all calculations that do use the CTMC (classical trajectory Monte Carlo) method for the calculation of the inelastic excitation cross sections, see for example reference [38].

Figure 12 shows the ratio $\sigma_{1s\to 2p}/\sigma_{1s\to 2s}$ in comparison with this ratio from reference [38]. The larger modified Born approximation excitation cross section results in a considerably higher population of the 2p state, as a consequence the $K_\alpha$ X-ray yield is larger and in good agreement with experiment for small or even zero Stark mixing.

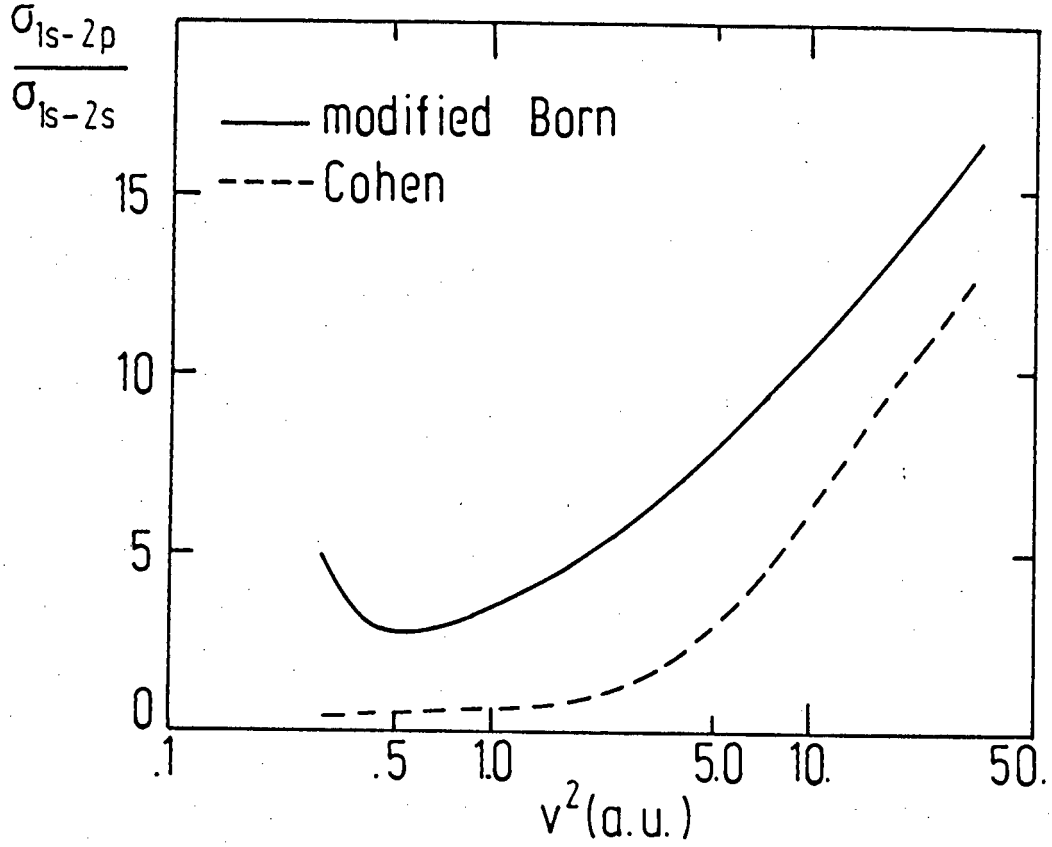


Figure 12: Ratio of $1s \to 2p$ to $1s \to 2s$ inelastic excitation cross section as a function of $v^2$, present calculation (solid line), reference [38] (broken line).

Table 10

Number of X-rays per 100 fusions $XY_{K_\alpha} = \gamma_{K_\alpha}\omega_s^0$ with $\omega_s^0 = 0.88\%$ .

| THEORY: | $XY_{K_\alpha}$ | $XY_{K_\alpha}$ | $XY_{K_\beta}$ | $\gamma_{K_\beta}/\gamma_{K_\alpha}$ | $\gamma_{K_\gamma}/\gamma_{K_\alpha}$ |
|---|---|---|---|---|---|
| PRESENT WORK: | $\phi = 1.2$ | $\phi = 0.1$ | $\phi = 1.2$ | $\phi = 1.2$ | $\phi = 1.2$ |
| Q=1 | 0.30 | 0.38 | 0.021 | 0.07 | 0.012 |
| Q=0 | 0.21 | 0.32 | 0.026 | 0.12 | 0.017 |
| OTHER THEORY: | | | | | |
| Cohen [38] | 0.24 | 0.30 | | 0.12 | 0.019 |
| Cohen [28] Q=1 | 0.23 | 0.28 | | | |
| Cohen [28] Q=0 | 0.15 | 0.20 | | | |
| Markushin [32] | 0.25 | 0.29 | | 0.12 | |
| Takahashi [31] Q=0 | 0.13 | | 0.042 | 0.32 | 0.043 |
| Takahashi [31] Q=0.43 | 0.24 | | 0.043 | 0.18 | 0.024 |
| Takahashi [36] | 0.36 | | 0.046 | 0.13 | 0.019 |
| EXPERIMENT: | | | | | |
| Bossy et al. [43] | 0.21±0.05 | | | | |
| Bossy et al. [37] | 0.19±0.05 | | | | |
| Nagamine [42] | 0.049±0.04 | | | | |

Table 11

Number of X-rays per 100 fusions $XY_{K_\alpha} = \gamma_{K_\alpha}\omega_d^0$ with $\omega_d^0 = 13.3\%$ .

| THEORY: | $XY_{K_\alpha}$ | $XY_{K_\alpha}$ | $\gamma_{K_\beta}/\gamma_{K_\alpha}$ | $\gamma_{K_\gamma}/\gamma_{K_\alpha}$ |
|---|---|---|---|---|
| PRESENT WORK: | $\phi = 1.2$ | $\phi = 0.05$ | $\phi = 1.2$ | $\phi = 1.2$ |
| Q=1 | 3.6 | 4.5 | 0.09 | 0.019 |
| Q=0 | 2.5 | 3.4 | 0.13 | 0.027 |
| OTHER THEORY: | | | | |
| Cohen [38] | 2.2 | 2.9 | 0.11 | 0.015 |
| Cohen [44] | 2.2 | | 0.11 | 0.015 |
| Markushin [32] | 2.5 | 3.0 | 0.19 | 0.039 |
| Takahashi [31] Q=0 | 1.4 | | 0.31 | 0.042 |
| Takahashi [31] Q=260 | 2.5 | 5.6 | 0.18 | 0.024 |
| EXPERIMENT: | | | | |
| Bossy et al. [46] | 1.6±0.4 | | 0.13±0.02 | 0.011±0.012 |
| Bossy et al. [43] | 1.6±0.2 | | 0.13±0.02 | 0.023±0.013 |

The stopping power is most reasonably known at very low densities. The theoretical values for the K-series X-ray yields for very low densities are therefore independent of a possible density dependence of the stopping power as discussed in the following sections. The theoretical $K_\alpha$ X-ray yield is however sensitively dependent on the Stark mixing rates used in the calculations. Figure 13 shows the results of the present calculations for the $K_\alpha$ X-rays per initial sticking $\gamma_{K_\alpha}$ as a function of the slow down energy of the $(\alpha\mu)^+$ ion for Stark mixing strength Q=1 and Q=0.

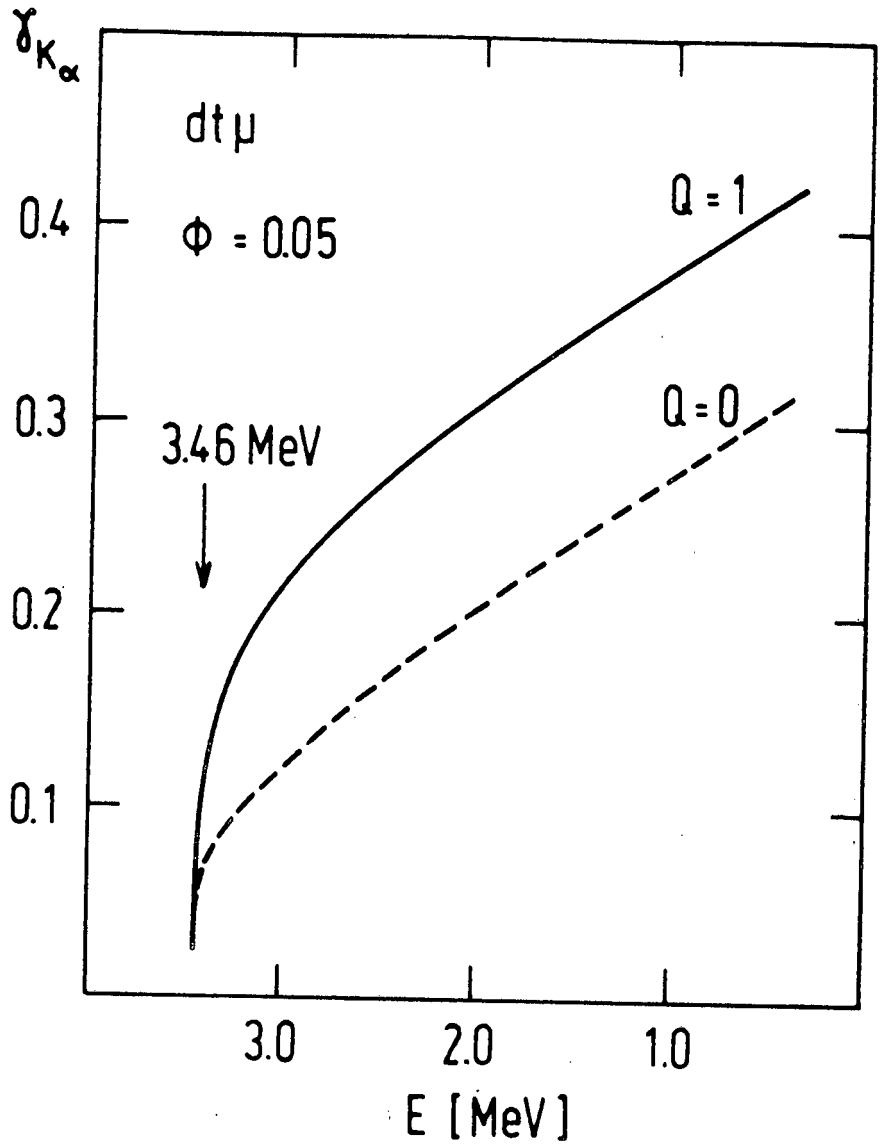


Figure 13: X-rays per initial sticking $\gamma_{K_\alpha}$ as a function of the slow down energy of the $(\alpha\mu)^+$ after fusion. .

# 4. THE STOPPING POWER

In *section 3* the reactivation probability of the muon was determined by a rather delicate balance between collisional excitation and ionization and transfer processes on one hand and the combination of electromagnetic deexcitation and slowing down of the $(\alpha\mu)^+$ particle on the other hand. In principle, the observed decrease of $\omega_s^{eff}$ with growing target density can have its origin in any of these contributions. However, only a *weak* density dependence as already established could be confirmed. Its origin is revealed by the observation that the $(\alpha\mu)^+$ energy loss rate $dE/dt$ has been assumed to grow linearly with density $\rho$ like the excitation rates $\lambda_{exc}^{i\to k}$, the stripping rates $\lambda_{str}^{i}$, whereas the radiative deexcitation rates $\lambda_{rad}^{i\to k}$ do not. This linear density dependence effectively cancels from the rate equations when these are rewritten in terms of the kinetic energy $E$ of the $(\alpha\mu)^+$, with the exception of an effective density variability introduced in this way into the radiative rates.

If the point of view is taken that regeneration is responsible for the *strong* density dependence reported by Jones et al. [13] a different mechanism must be invoked. The observed density dependence must then originate from an additional, i.e. nonlinear, density dependence. The rate of energy loss of the $(\alpha\mu)^+$ is the most promising mechanism for an explanation of the observed phenomena: $S(\rho)$. Such non-linearities are known to exist in condensed matter targets at ion velocities below and around the equivalent K-shell velocity. As this is the region in which the stripping cross sections peak, it is not inconceivable that a strong density dependence could result from this effect. For more detailed discussion see appendix D.

As will be seen, in order to account for the experimentally observed density effect in sticking the linear increase of $dE/dx$ as a function of density has to be reduced. This means that $S(v)$ in *eq.*(8) in *section 2* becomes density dependent and in particular it is decreasing with $\rho$.

Such a nonlinearity of the stopping power with target density can have two clearly distinct origins. Firstly, the electronic structure of the target usually changes with density when the interatomic spacings are comparable to the atomic radii, and even discontinuously so when a phase transition occurs, e.g. from gas to liquid or solid. Therefore, stopping powers based on the values measured in, or calculated for, the gaseous phase [47] need not apply to liquid or solid targets. Secondly, the response of the electronic structure of the medium, of which the energy loss of the penetrating ion is one particular manifestation, may not be a linear function of the target density. Such effects arise, e.g., due to partial screening of the projectile charge by the target electrons, and are usually taken

into account through a velocity dependent effective projectile charge.

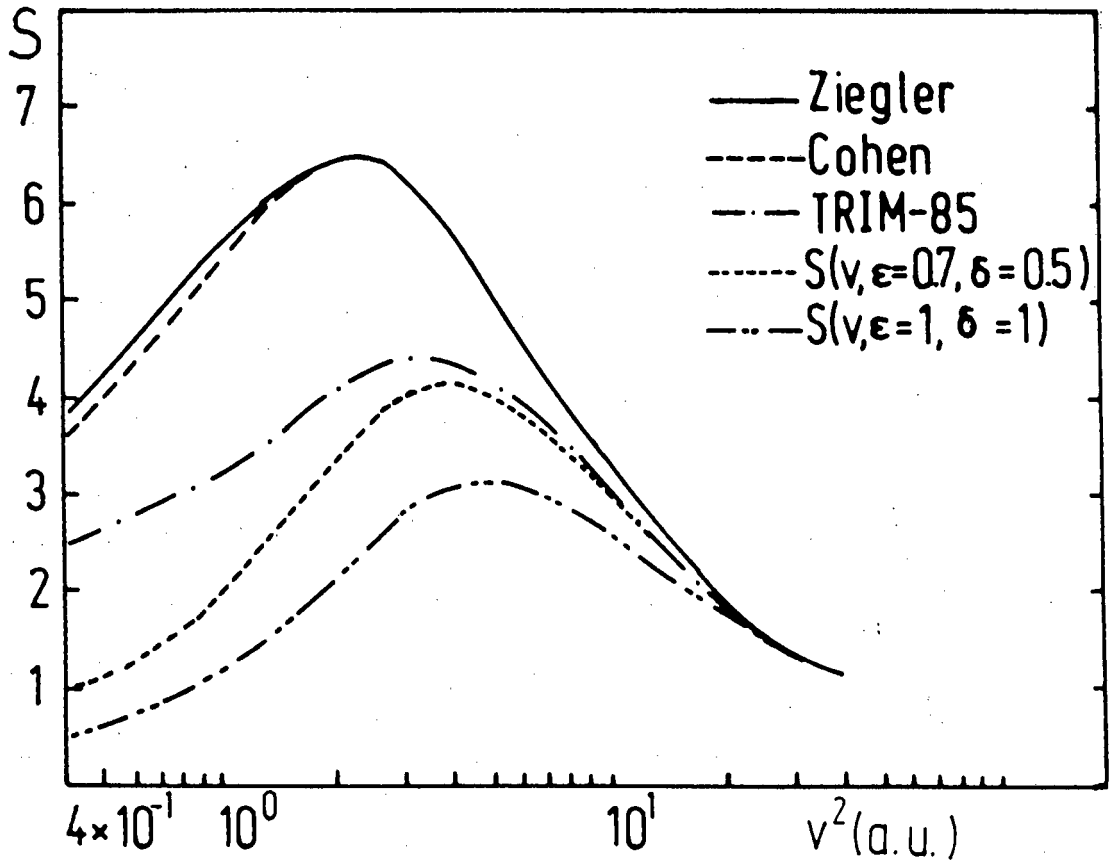


Figure 14: Various choices for the stopping power function $S(v)$ in units of $[eV\ cm^2/1E15]$. The curve denoted 'Cohen' is from reference [38], 'Ziegler' [47] is for hydrogen gas and is identical to $S(\epsilon = \delta = 0)$, the curve 'TRIM-85' [48] is for solid hydrogen. The curves labelled by values of $\epsilon$ and $\delta$ are obtained from stopping power parametrization.

Lacking a more reliable description of the nonlinear density dependence of the stopping power function $S(v;\epsilon,\delta)$ applicable to a $(\alpha\mu)^+$ ion in hydrogen, the calculations were carried out with a simple parametrized model form of $S(v;\epsilon,\delta)$ The two parameters in this ansatz, $\delta$ and $\epsilon$, describe the effects of a density dependence of the mean ionization potential $I$ and of the effective charge $Z_{eff}$, respectively.

If $\phi$ is the target density in units of liquid hydrogen density ($4.25 \times 10^{22}\text{cm}^{-3}$) the explicit forms chosen are:

$$I_{eff} = I(1 + \phi\delta), \tag{1}$$

$$Z_{eff} = Z_p(1 + \epsilon\phi e^{-v^2})^{-1}, \tag{2}$$

where $v$ is in atomic units. For $\epsilon = \delta = 0$ the function $S(v)$ for gaseous hydrogen from Ziegler [47] is taken.

For other values of $\epsilon$, $\delta$ the density dependence arises according to the analyctical form of the Bethe formula:

$$S(v, Z_{eff}(\epsilon), I_{eff}(\delta)) = \frac{4\pi Z_{eff}^2 e^4}{mv^2} Z_t(ln\frac{2mv^2}{I_{eff}} + ln\frac{1}{1-\beta^2} - \beta^2 - C) \tag{3}$$

The velocity dependence of the parametrized function

$$S(v; \epsilon, \delta) = S(v, Z_{eff}(\epsilon), I_{eff}(\delta))$$

is shown in figure 14 for two non zero values of the parameters. The smaller set of values, ($\epsilon = 0.7$ and $\delta = 0.5$), appears to mark the borderline of acceptable modification of the gas stopping power. The second, larger set, ($\epsilon = \delta = 1$) was chosen to explore the range of effects beyond these limits on a purely speculative basis, without any claim that it may be realized under experimental conditions.

An experimental observable as a measure of the stopping power is the range $R_{\alpha\mu}$ of the $(\alpha\mu)^+$ ion:

$$R_{\alpha\mu} = \int dx = \int dE / \frac{dE}{dx}.$$

Since

$$\frac{dE}{dx} = -\rho S,$$

the range is

$$R_{\alpha\mu} = -\frac{1}{\rho} \int \frac{dE}{S}. \tag{4}$$

Due to the fact that the various stopping power functions deviate from one another only for small ion velocities they result only in small differences in the range of the $(\alpha\mu)^+$ ion emitted originally with $v = 6$. As shown in figure 15, the difference is less than 40% at $\phi = 1$ even for the larger parameter set $\epsilon = \delta = 1$.

Finally, note that a different stopping power will result in a different slow down time $t_{stop}$, see section 2 *eq.*(11). The energy loss during slow down is compared for $S(v; \epsilon = \delta = 0)$ with $S(v; \epsilon = \delta = 1)$ in figure 16. The relevant slow down times differ by a factor of $\sim 1.2$.

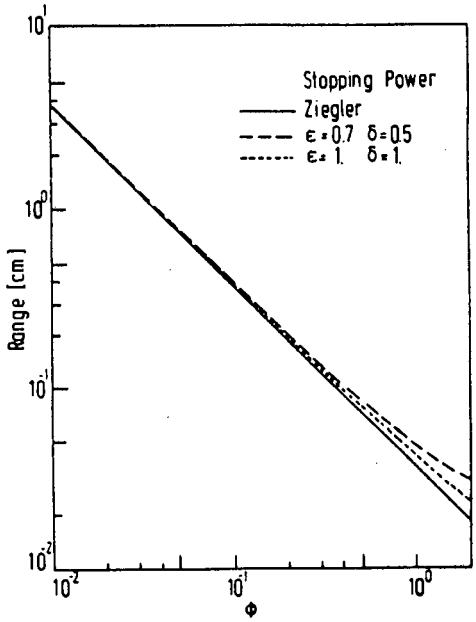


Figure 15: Range of $(\alpha\mu)^+$ ions in liquid hydrogen at $\phi = 1.2$. (For the notation see figure 14.)

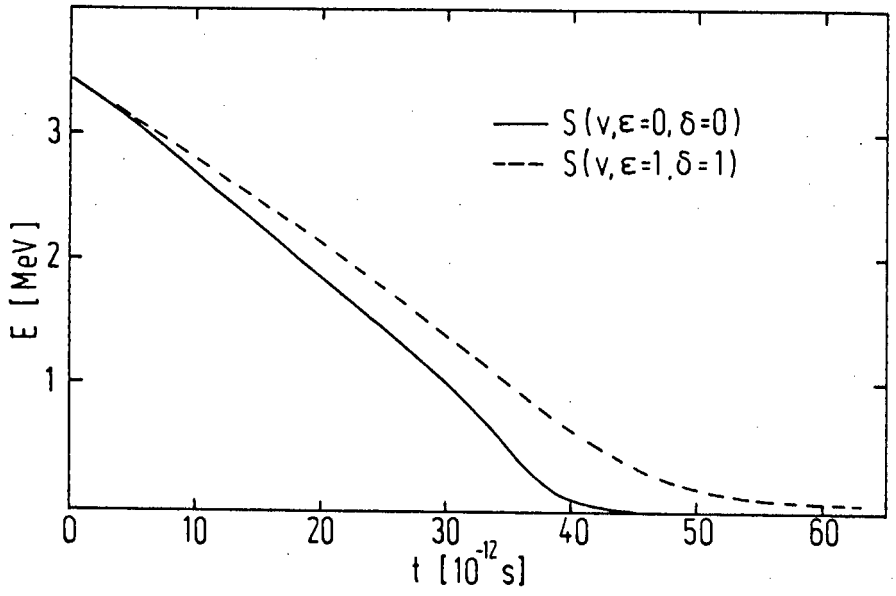


Figure 16: Energy loss of the $(\alpha\mu)^+$ ion during slow down for the parameter set $(\epsilon = \delta = 0)$ and $(\epsilon = \delta = 1)$.

For the three parameter sets and the target density $\phi = 1.0$ the stopping power in units of [MeV/cm] is given in table 12.

Table 12

Stopping power [MeV/cm] for $0.2 \leq v \leq 6$, $\phi$=1.0 for the parameter sets $(\epsilon = \delta = 0)$, $(\epsilon = 0.7, \delta = 0.5)$ and $(\epsilon = \delta = 1)$.

| $v$ [a.u.] | $S(v; \epsilon = \delta = 0)$ [MeV/cm] | $S(v; \epsilon = 0.7, \delta = 0.5)$ [MeV/cm] | $S(v; \epsilon = \delta = 1)$ [MeV/cm] |
|---|---|---|---|
| .20 | .6139E+02 | .1219E+02 | .5847E+01 |
| .40 | .1140E+03 | .2491E+02 | .1221E+02 |
| .60 | .1619E+03 | .4097E+02 | .2083E+02 |
| .80 | .2038E+03 | .6178E+02 | .3302E+02 |
| 1.00 | .2374E+03 | .8723E+02 | .4949E+02 |
| 1.20 | .2605E+03 | .1150E+03 | .6954E+02 |
| 1.40 | .2720E+03 | .1409E+03 | .9063E+02 |
| 1.60 | .2725E+03 | .1608E+03 | .1094E+03 |
| 1.80 | .2640E+03 | .1727E+03 | .1232E+03 |
| 2.00 | .2492E+03 | .1766E+03 | .1314E+03 |
| 2.20 | .2308E+03 | .1742E+03 | .1345E+03 |
| 2.40 | .2112E+03 | .1676E+03 | .1338E+03 |
| 2.60 | .1919E+03 | .1585E+03 | .1305E+03 |
| 2.80 | .1739E+03 | .1482E+03 | .1253E+03 |
| 3.00 | .1575E+03 | .1375E+03 | .1191E+03 |
| 3.20 | .1429E+03 | .1271E+03 | .1123E+03 |
| 3.40 | .1301E+03 | .1173E+03 | .1054E+03 |
| 3.60 | .1189E+03 | .1082E+03 | .9853E+02 |
| 3.80 | .1091E+03 | .9986E+02 | .9193E+02 |
| 4.00 | .1006E+03 | .9235E+02 | .8571E+02 |
| 4.20 | .9302E+02 | .8559E+02 | .7992E+02 |
| 4.40 | .8637E+02 | .7954E+02 | .7458E+02 |
| 4.60 | .8047E+02 | .7412E+02 | .6970E+02 |
| 4.80 | .7522E+02 | .6925E+02 | .6524E+02 |
| 5.00 | .7052E+02 | .6488E+02 | .6119E+02 |
| 5.20 | .6628E+02 | .6095E+02 | .5750E+02 |
| 5.40 | .6245E+02 | .5739E+02 | .5415E+02 |
| 5.60 | .5897E+02 | .5417E+02 | .5109E+02 |
| 5.80 | .5580E+02 | .5123E+02 | .4831E+02 |
| 6.00 | .5290E+02 | .4855E+02 | .4576E+02 |

## 5. THE INFLUENCE OF A DENSITY DEPENDENT STOPPING POWER ON REGENERATION DYNAMICS

The density dependent stopping power $S(v;\phi)$ introduced in *section 4 eq.*(3) is shown in figure 17 as a function of $v^2$ for the parameter set ($\epsilon = 0.7$, $\delta = 0.5$) evaluated at densities $\phi = 0.1$, $\phi = 1$ and $\phi = 2$.

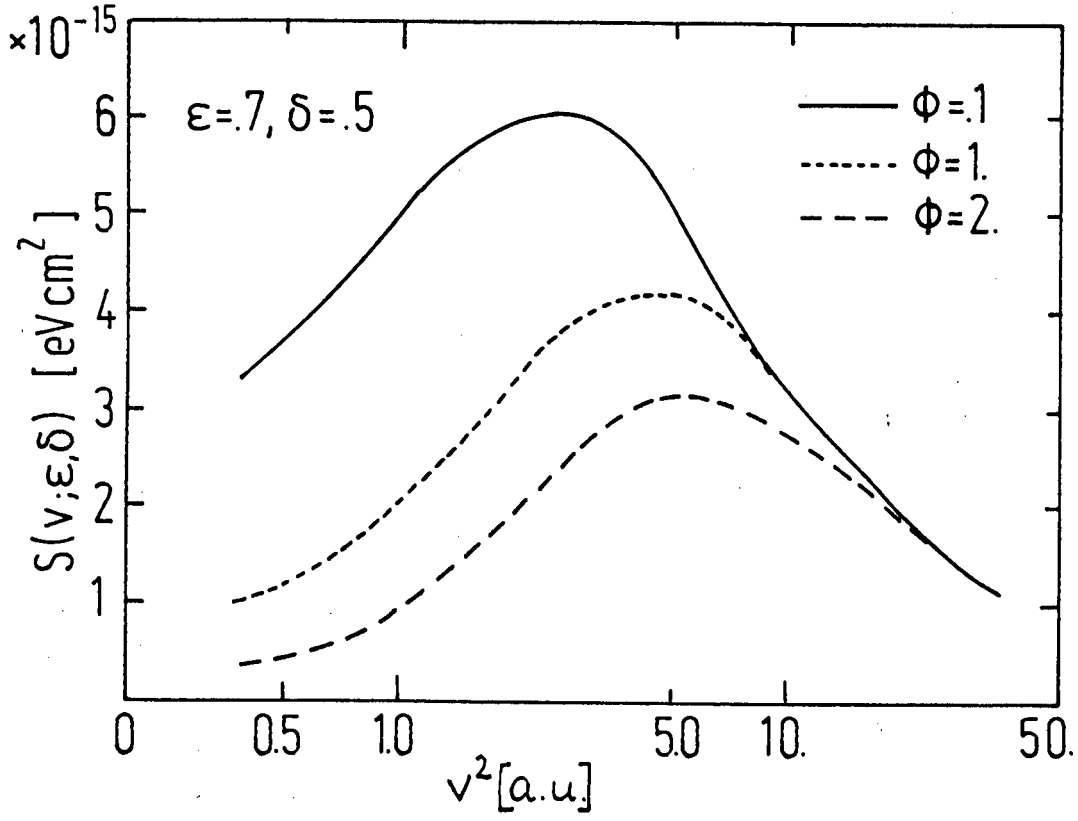


Figure 17: Density dependence of the stopping power $S(v;\epsilon = 0.7, \delta = 0.5)$ in units $[eV\ cm^2/1E15]$ for the density parameter $\phi = \rho/\rho_0 = 0.1, 1.0, 2.0$

Such a density dependence of the stopping power has the potential to introduce a strong density dependence into both the effective muon sticking fraction through the regeneration probability and the X-ray yields after fusion. A quantitative study of these effects follows.

### 5.1 Density Dependence of the Effective Muon Sticking Fraction

The effective sticking fraction is calculated for the $(\alpha\mu)^+$ with an initial sticking $\omega_s^0 = 0.88\%$ and a parametrized stopping power $S(v;\epsilon,\delta)$ as described in *section* 4 and shown in figure 17. Results for the effective muon sticking fraction are shown for Q=1 in figure 18 and for Q=0 in figure 19 for three sets of values for the parameters $\epsilon$ and $\delta$ describing the density dependence of the stopping power. *Solid* marks the use of the stopping power for solid hydrogen [47].

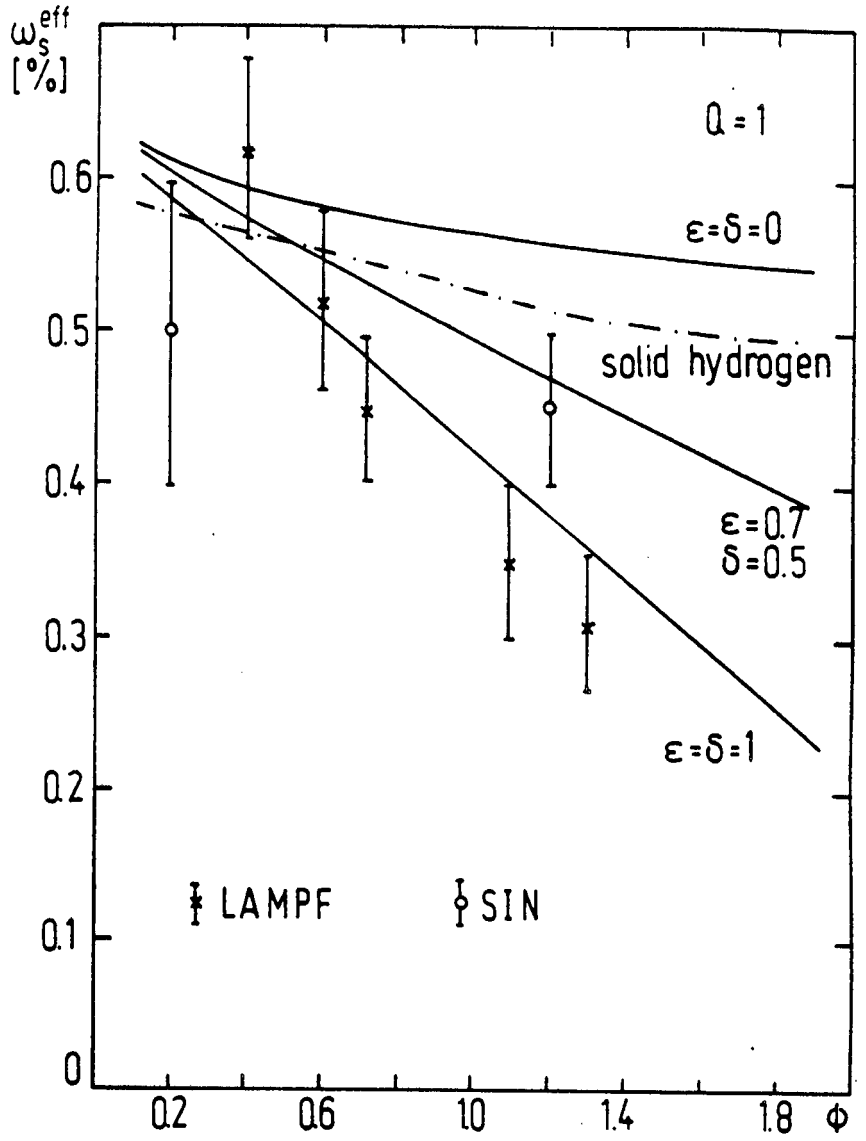


Figure 18: Effective sticking fraction $\omega_s^{eff}$ as function of density in units of liquid hydrogen density for Q=1. The dash-dot line showes results obtained with the stopping power for liquid hydrogen. The experimental data point are from references [13] and [41].

For the parameter values $\epsilon = \delta = 0$ corresponding to the stopping power in hydrogen gas also used by Bracci *et al.* [16] the present results, see figure 18 and figure 19, show the same *weak* density dependence as reported e.g. by Cohen [44]. A much stronger density dependence is found, however, for the two other choices of the stopping power parameters considered. The smaller parameter set ($\epsilon = 0.7, \delta = 0.5$) does not fully account for the density dependence reported by the LAMPF collaboration [13] but shows a better agreement with experimental data if only a small stark mixing or even no stark mixing is assumed, see figure 19.

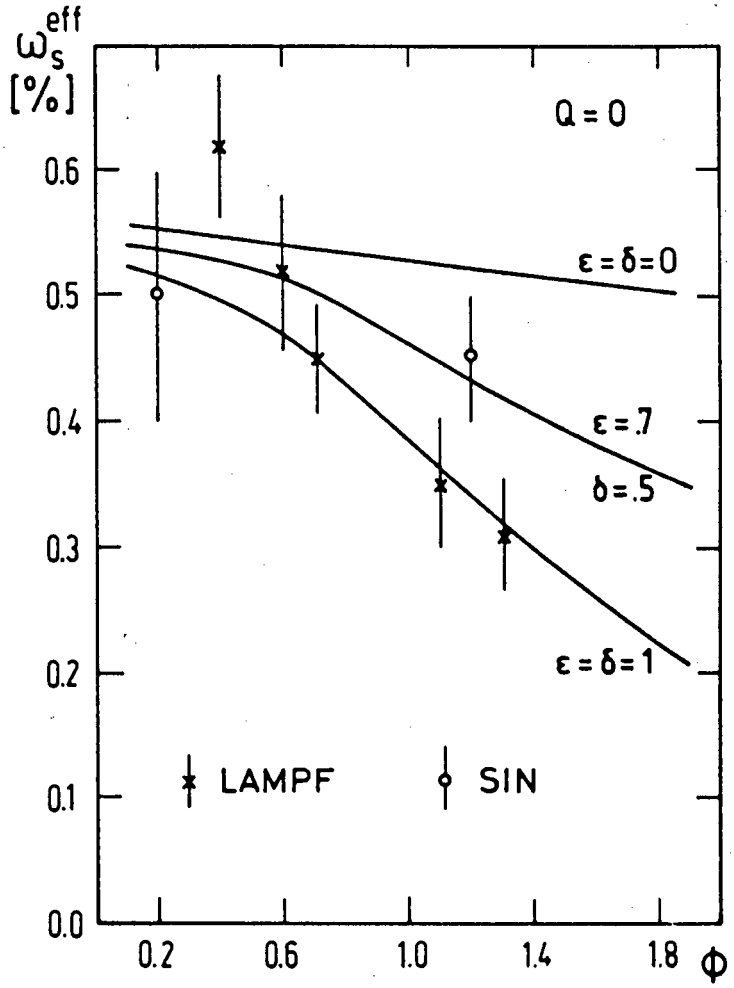


Figure 19: Effective sticking fraction $\omega_s^{eff}$ as function of density in units of liquid hydrogen density for Q=0. The experimental data point are from references [13] and [41].

The larger parameter set ($\epsilon = \delta = 1$) does yield the desired steep density dependence, but the corresponding stopping power can not be considered to be very realistic. However, should this agreement be taken seriously, an effective sticking probability of less than $2 \times 10^{-3}$ at $\phi = 2.5$ would be found. A density of $\phi \sim 2.5$ is planed with the next generation of target vessels [49].

Given a particular set of values for the parameters $\epsilon$ and $\delta$ the calculations predict a similar density dependence of the effective sticking fraction for the $(dd\mu)$ reaction. In this case the reduction compared to the standard value of $\omega_s^{eff}$ is 15% for the parameter set ($\epsilon = 0.7, \delta = 0.5$) and 30% for the set ($\epsilon = \delta = 1$) at $\phi = 1.2$.

The effective sticking fraction $\omega_d^{eff}$ calculated for the $(^3He\mu)^+$ with an initial sticking of $\omega_d^0 = 13.3\%$ and a parametrization of the stopping power $S(v; \epsilon, \delta)$ as used above is shown in figure 20 for Q=0 and Q=1.

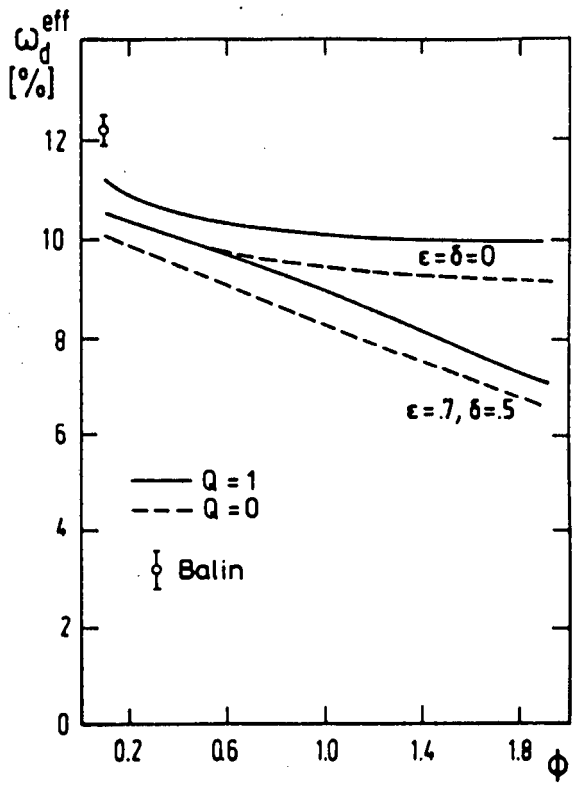


Figure 20: Effective sticking fraction $\omega_d^{eff}$ as function of density $\phi$ for Q=0 and Q=1. The experimental data are from reference [45].

The density dependent stopping power $S(v;\epsilon,\delta)$ results in different population probabilities $P_i(v)$ of the $(\alpha\mu)^+$ states during slow down and a different stripping fraction R. For the parameter sets $(\epsilon = \delta = 0)$ and $(\epsilon = 0.7,\ \delta = 0.5)$ and Q=0 the population probabilities $P_i(v)$ for $i$ =1s, 2s, 2p, 3, 4 and R($v$) are shown as a function of the slow down velocity $v$ of the $(\alpha\mu)^+$ ion in figure 21.

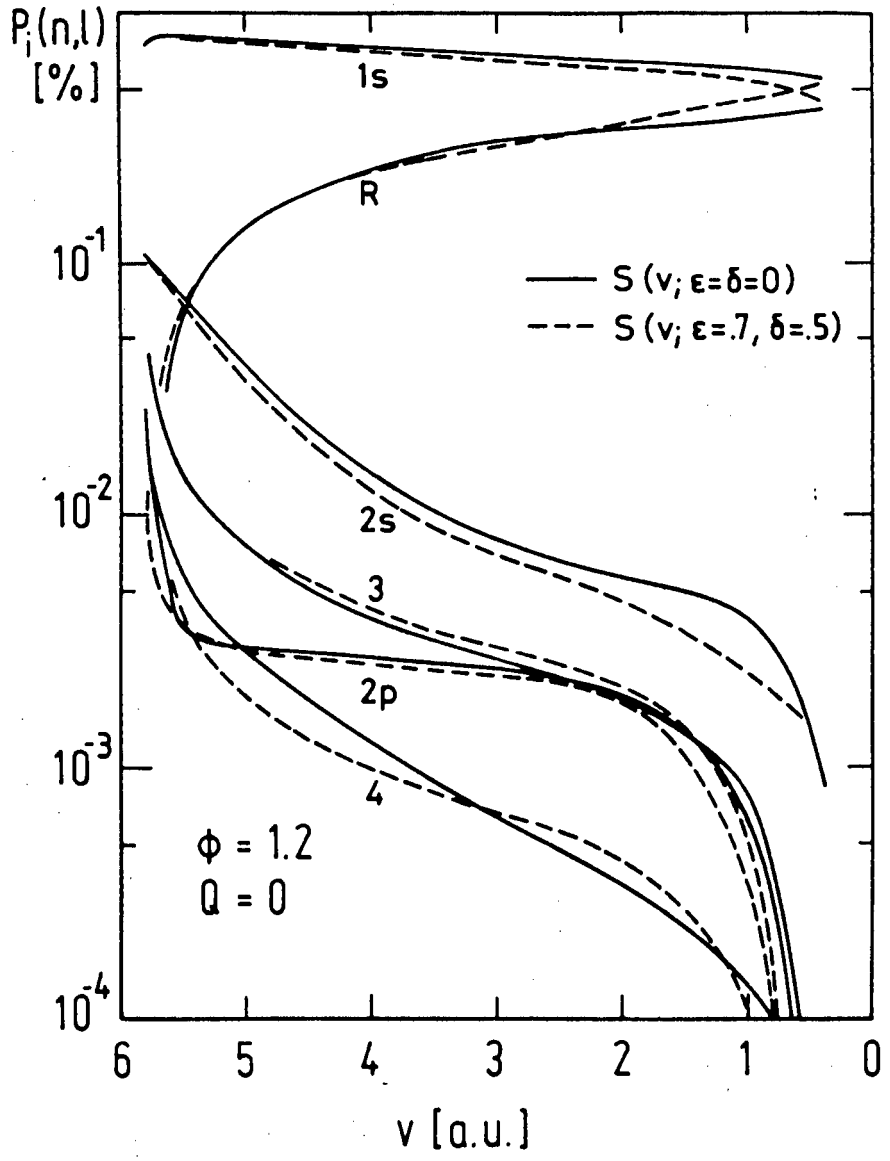


Figure 21: The population $P_i(v)$ of the $(\alpha\mu)^+$ during slow down for i=1s, 2s, 2p, 3, 4 and stripping fraction R($v$) with Q=0 for S($\epsilon = \delta = 0$) solid lines and S($\epsilon = 0.7, \delta = 0.5$) broken lines.

The present calculations of the effective muon sticking fraction after the $(dt\mu)$ and $(dd\mu)$ fusion are compared with previous theoretical calculations and experiments in table 13 and table 14.

Table 13

The $^3$He$\mu$ sticking fraction $\omega_d^{eff} = (1 - R)\omega_d^0$ with $\omega_d^0 = 13.3\%$ for different d-d target densities $\phi = \rho/\rho_0$.

| THEORY: | $\phi$=1.2 | $\phi$=0.05 |
|---|---|---|
| PRESENT WORK: | | |
| Q=1, $S(\epsilon = \delta = 0)$ | 10.0 | 11.2 |
| Q=1, $S(\epsilon = .7, \delta = .5)$ | 8.5 | 11.1 |
| Q=1, $S(\epsilon = \delta = 1)$ | 7.0 | 11.1 |
| Q=1, $S_{solid}$ | 9.4 | 10.6 |
| Q=0, $S(\epsilon = \delta = 0)$ | 9.4 | 10.6 |
| Q=0, $S(\epsilon = .7, \delta = .5)$ | 7.9 | 10.5 |
| Q=0, $S(\epsilon = \delta = 1)$ | 6.4 | 10.4 |
| OTHER THEORY: | | |
| Cohen [50] | 10.8 | 11.9 |
| Cohen [44] | 10.7 | 11.9±0.5 |
| Markushin [32] | | 12.3±0.2 |
| Takahashi [31] Q=0.43 | 11.3 | 11.7 |
| EXPERIMENT: | | |
| Balin [45] | | 12.2±0.3 |

Table 14

The $(\alpha\mu)^+$ sticking fraction $\omega_s^{eff} = (1 - R)\omega_s^0$ with $\omega_s^0 = 0.88\%$ for different d-t target densities $\phi = \rho/\rho_0$.

| THEORY: | $\phi$=1.2 | $\phi$=0.1 |
|---|---|---|
| PRESENT WORK: | | |
| Q=1, $S(\epsilon = \delta = 0)$ | 0.56 | 0.62 |
| Q=1, $S(\epsilon = .7, \delta = .5)$ | 0.47 | 0.62 |
| Q=1, $S(\epsilon = \delta = 1)$ | 0.37 | 0.60 |
| Q=1, $S_{solid}$ | 0.52 | 0.59 |
| Q=0, $S(\epsilon = \delta = 0)$ | 0.52 | 0.55 |
| Q=0, $S(\epsilon = .7, \delta = .5)$ | 0.42 | 0.54 |
| Q=0, $S(\epsilon = \delta = 1)$ | 0.34 | 0.53 |
| | | |
| OTHER THEORY: | | |
| Bracci et al. [16] | 0.67 | 0.70 |
| Cohen [50] | 0.57 | |
| Cohen [38] | 0.54 | 0.59 |
| Cohen [28] Q=1 | 0.53 | 0.59 |
| Cohen [28] Q=0 | 0.49 | 0.57 |
| Gershtein et al. [23] | 0.68 | |
| Markushin [32] | 0.57 | |
| Menshikov et al. [39] | 0.60 | 0.67 |
| Takahashi [31] Q=0 | 0.57 | |
| Takahashi [31] Q=0.43 | 0.61 | 0.63 |
| | | |
| EXPERIMENT: | | |
| Jones et al. [14] | 0.4±0.1 | |
| Jones et al. [13] | 0.35±0.07 | 1.1±0.5 |
| Breunlich et al. [41] | 0.45±0.05 | 0.50±0.10 |
| Nagamine [42] | 0.42±0.07 | |
| Bossy et al. [43] | 0.42±0.14 | |

## 5.2 Muonic X-rays after Fusion

Any modification of the stopping power also has an influence on the yield of muonic X-rays emitted after fusion. These X-rays originate from muons that are either initially captured into excited states or excited during the slow down of the $(\alpha\mu)^+$ in the target. Once the muon enters into an excited state, e.g. the L-shell, the radiative deexcitation competes with all other processes leading to depopulation of the state. A simple consideration for $P_i$ for *eq.* (3) of this section shows that the K X-ray yield due to excitations into the L-shell is proportional to

$$XY(K_\alpha) \sim \frac{\sigma_{exc}^{1\to 2}}{S(v;\phi)} \left(1 + \frac{\lambda_{exc}^2}{\lambda_{rad}^{2p}}\right)^{-1}, \qquad (1)$$

where the ratio of the K-L excitation cross section $\sigma^{1\to 2}$ and the stopping power $S(v;\phi)$ enters.

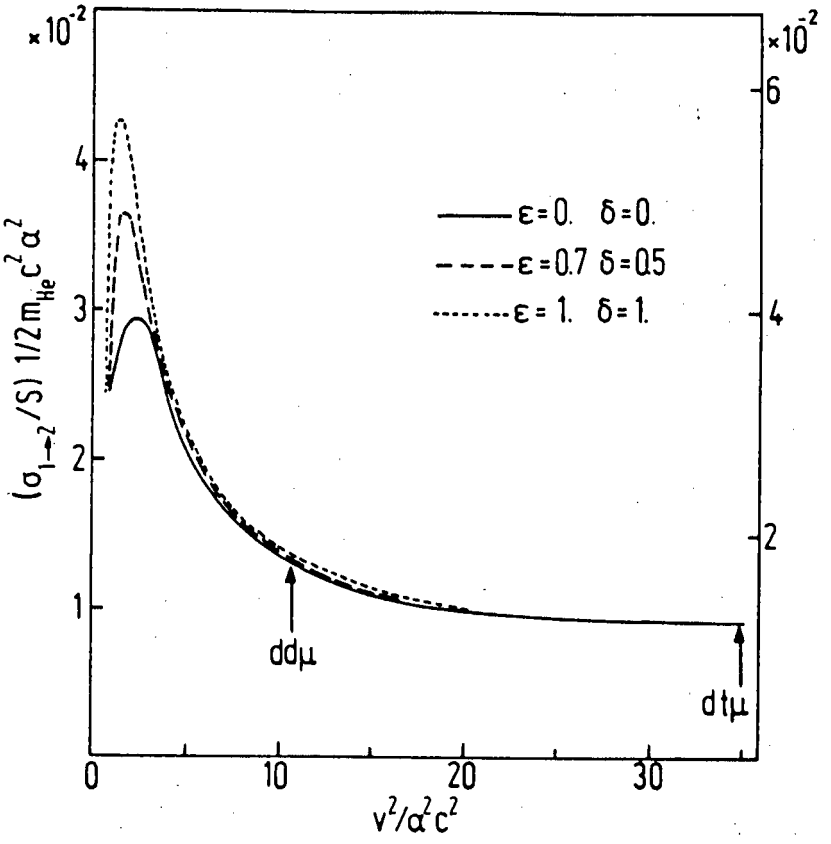


Figure 22: Ratio of the K- to L-shell excitation cross section $\sigma_{exc}^{1\to 2}$ and stopping cross section $S(v;\phi)$ as function of the ion velocity.

The velocity dependence of this ratio $\sigma_{exc}^{1\to 2}/S(v;\phi)$ is shown in figure 22 for the three standard parameter sets for $\epsilon$ and $\delta$ at $\phi = 1.2$. The curves are normalized such that the surface area is a direct measure for the X-ray yield at higher densities. The initial velocities of the helium nuclei produced in (dd$\mu$) and (dt$\mu$) fusion are also shown. Note, that the left scale is for $(^3\mathrm{He}\mu)^+$ and the right scale for $(\alpha\mu)^+$. Obviously, a reduced stopping power will result in an increase in the excitation of the L-shell and hence in an increase of the $K_\alpha$ X-ray yield.

Figure 23 shows the $XY_{K_\alpha}$ X-ray yield for these parameter sets and Q=0 as a function of the target density $\phi$ after ($dt\mu$) fusion and figure 24 after ($dd\mu$) fusion.

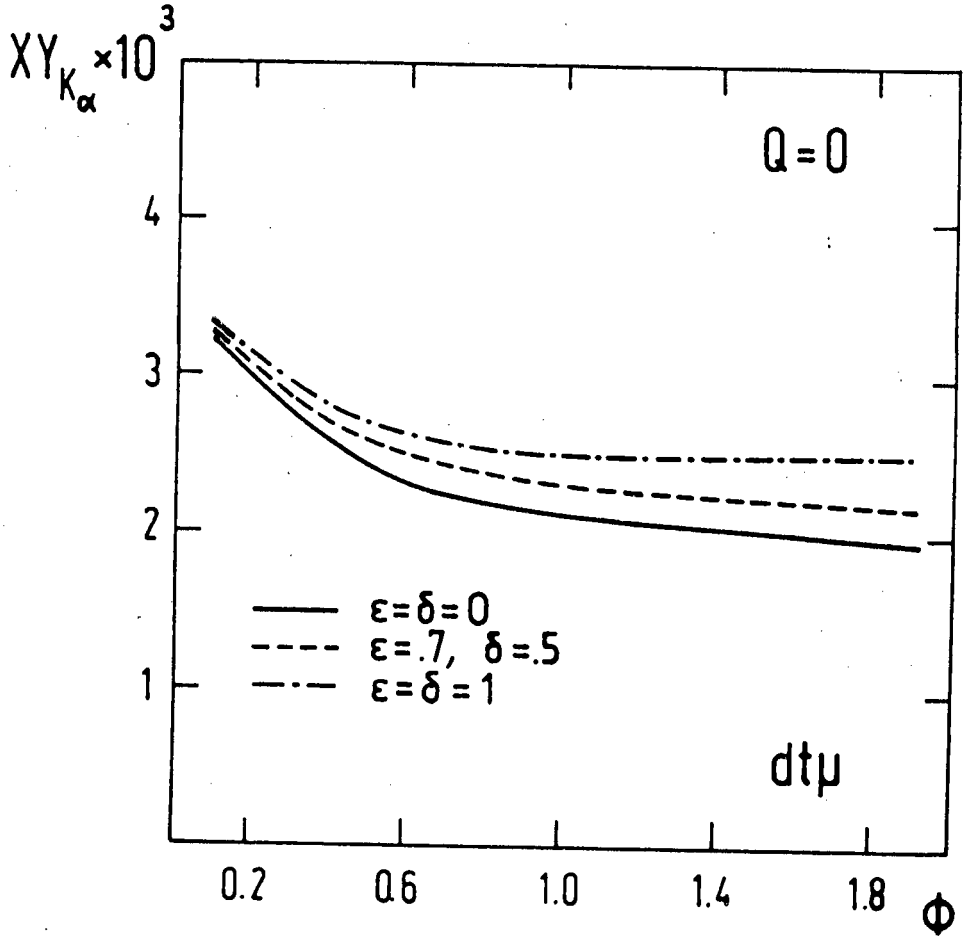


Figure 23: Yield of muonic helium $K_\alpha$ radiation emitted after ($dt\mu$) fusion as a function of the target density $\phi$ for different stopping power parametrizations $S(v;\epsilon,\delta)$.

This increase will be more pronounced for the (dd$\mu$) reaction, since in this case the $(^3He\mu)^+$ starts with a lower velocity ($v \approx 2$), whereas the $(\alpha\mu)^+$ particle created in the ($dt\mu$) reaction spends most of its time in the energy range $v > 2$ where no change occurs.

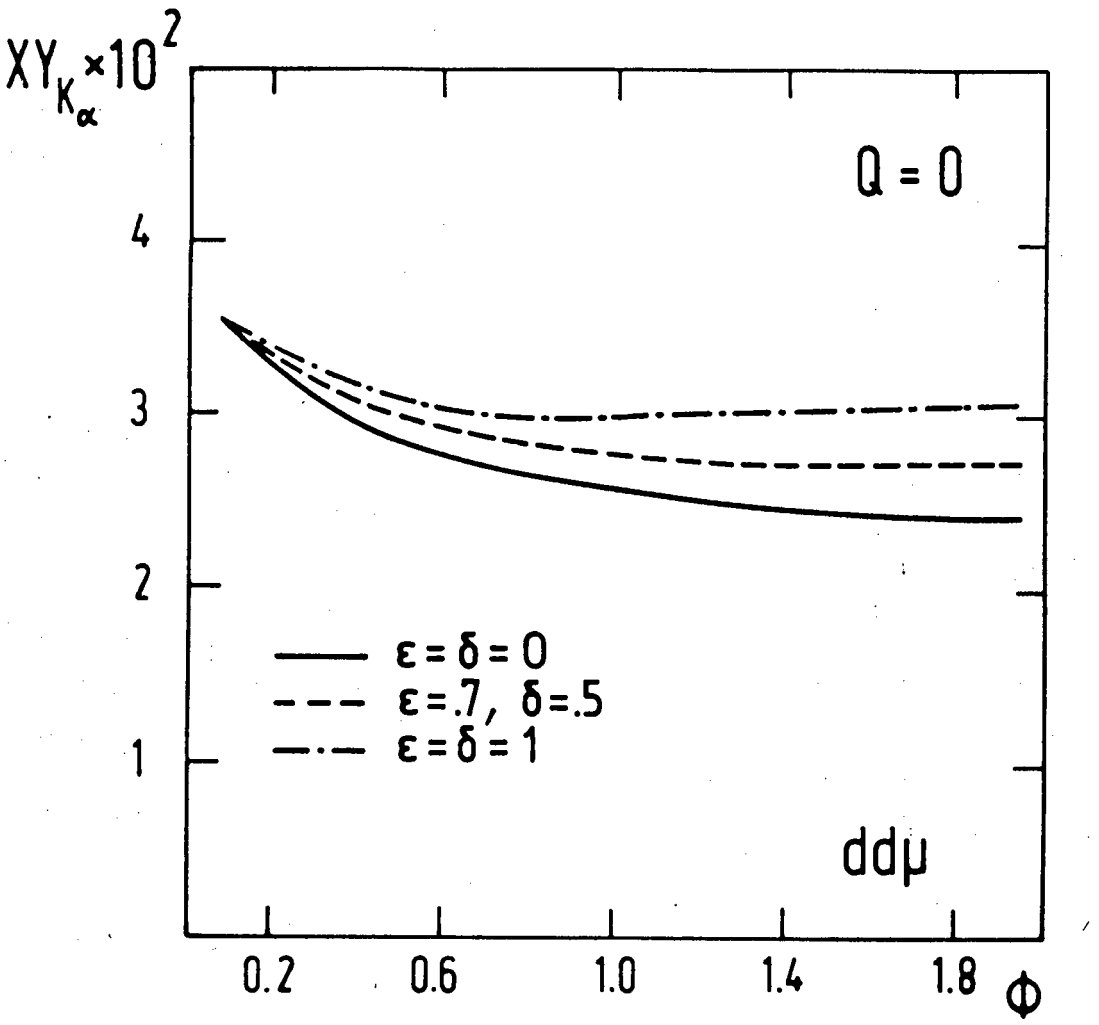


Figure 24: Yield of muonic helium $K_\alpha$ radiation emitted after ($dd\mu$) fusion as a function of the target density for different stopping power parametrizations $\hat{S}(v; \epsilon, \delta)$.

The results of the calculations for the total muonic helium $K_\alpha$ X-ray yield emitted after (dd$\mu$) and (dt$\mu$) reactions (i.e. per fusion) are represented in figure 25 and figure 26. The values obtained for the standard hydrogen stopping power ($\epsilon = \delta = 0$) can be compared with those of other authors.

As can be seen in the tables below, the values for full Stark mixing ($Q = 1$) lie higher than those of references [44] and [32] but lower than those of reference [36]. This is probably caused by the differences in the matrix elements for excitation used in the various calculations, and may be taken as an indication of the theoretical uncertainties.

Table 15

Number of X-rays per 100 fusions $XY_{K_\alpha} = \gamma_{K_\alpha}\omega_s^0$ with $\omega_s^0 = 0.88\%$.

| THEORY: | $XY_{K_\alpha}$ | $XY_{K_\alpha}$ | $XY_{K_\beta}$ | $\gamma_{K_\beta}/\gamma_{K_\alpha}$ | $\gamma_{K_\gamma}/\gamma_{K_\alpha}$ |
|---|---|---|---|---|---|
| PRESENT WORK: | $\phi = 1.2$ | $\phi = 0.1$ | $\phi = 1.2$ | $\phi = 1.2$ | $\phi = 1.2$ |
| Q=1, $S(\epsilon = \delta = 0)$ | 0.30 | 0.38 | 0.021 | 0.07 | 0.012 |
| Q=1, $S(\epsilon = .7, \delta = .5)$ | 0.32 | 0.38 | 0.022 | 0.07 | 0.011 |
| Q=1, $S_{solid}$ | 0.31 | 0.39 | 0.022 | 0.07 | 0.011 |
| Q=0, $S(\epsilon = \delta = 0)$ | 0.21 | 0.32 | 0.026 | 0.12 | 0.017 |
| Q=0, $S(\epsilon = .7, \delta = .5)$ | 0.23 | 0.32 | 0.026 | 0.11 | 0.016 |
| Q=0, $S_{solid}$ | 0.22 | 0.30 | 0.026 | 0.12 | 0.016 |
| OTHER THEORY: | | | | | |
| Cohen [50] | 0.26 | 0.30 | | | |
| Cohen [38] | 0.24 | 0.30 | | 0.12 | 0.019 |
| Cohen [28] Q=1 | 0.23 | 0.28 | | | |
| Cohen [28] Q=0 | 0.15 | 0.20 | | | |
| Markushin [32] | 0.25 | 0.29 | | 0.12 | |
| Takahashi [31] Q=0 | 0.13 | | 0.042 | 0.32 | 0.043 |
| Takahashi [31] Q=0.43 | 0.24 | | 0.043 | 0.18 | 0.024 |
| Takahashi [36] | 0.36 | | 0.046 | 0.13 | 0.019 |
| EXPERIMENT: | | | | | |
| Bossy et al. [43] | 0.21±0.05 | | | | |
| Bossy et al. [37] | 0.19±0.05 | | | | |
| Nagamine [42] | 0.049±0.04 | | | | |

Table 16

Number of X-rays per 100 fusions $XY_{K_\alpha} = \gamma_{K_\alpha}\omega_d^0$ with $\omega_d^0 = 13.3\%$.

| THEORY: | $XY_{K_\alpha}$ | $XY_{K_\alpha}$ | $\gamma_{K_\beta}/\gamma_{K_\alpha}$ | $\gamma_{K_\gamma}/\gamma_{K_\alpha}$ |
|---|---|---|---|---|
| PRESENT WORK: | $\phi = 1.2$ | $\phi = 0.05$ | $\phi = 1.2$ | $\phi = 1.2$ |
| Q=1, $S(\epsilon = \delta = 0)$ | 3.6 | 4.5 | 0.092 | 0.019 |
| Q=1, $S(\epsilon = .7, \delta = .5)$ | 3.8 | 4.5 | 0.087 | 0.018 |
| Q=1, $S(\epsilon = \delta = 1)$ | 4.1 | 4.5 | 0.083 | 0.017 |
| Q=1, $S_{solid}$ | 3.7 | 4.7 | 0.089 | 0.018 |
| Q=0, $S(\epsilon = \delta = 0)$ | 2.5 | 3.4 | 0.136 | 0.027 |
| Q=0, $S(\epsilon = .7, \delta = .5)$ | 2.8 | 3.5 | 0.130 | 0.025 |
| Q=0, $S(\epsilon = \delta = 1)$ | 3.0 | 3.5 | 0.123 | 0.023 |
| Q=0, $S_{solid}$ | 2.6 | 3.6 | 0.134 | 0.025 |
| OTHER THEORY: | | | | |
| Cohen [50] | 1.8 | 2.2 | | |
| Cohen [38] | 2.2 | 2.9 | 0.11 | 0.015 |
| Markushin [32] | 2.5 | 3.0 | 0.19 | 0.039 |
| Takahashi [31] Q=0 | 1.4 | | 0.31 | 0.042 |
| Takahashi [31] Q=0.43 | 2.5 | 5.6 | 0.18 | 0.024 |
| EXPERIMENT: | | | | |
| Bossy et al. [46] | 1.6±0.4 | | 0.13±0.02 | 0.011±0.012 |
| Bossy et al. [43] | 1.6±0.2 | | 0.13±0.02 | 0.023±0.013 |

It is worth noting, however, that all theoretical results are higher than the experimental values of the SIN collaboration [43] for both systems. Results obtained for the other two parameter sets ($\epsilon = 0.7, \delta = 0.5$) and ($\epsilon = \delta = 1$) show that this systematical discrepancy is increased as the stopping power decreases, if a strong Stark mixing of Q=1 is used in the calculations. A density dependent reduction in the stopping power increases the difference between theory and experiment. Modifying the stopping power to explain the X-ray yield means S has to be increased with $\rho$ and therefore the density dependence of sticking is reduced.

Thus unless another phenomena is identified which influences the X-ray yield the discrepancy of the X-ray and $\omega_s^{eff}$ measurements are to be seen as mutually aggravating in the sense that attempts to explain one of them increases the discrepancy in the other. A larger value for the Stark mixing cross section, e.g. $Q = 2$ as advocated in reference [50], would even further increase the discrepancy. The ratios of $K_\beta$ and $K_\gamma$ to $K_\alpha$ X-rays, however, are only slightly affected by the modifications in the stopping power function.

The parametrization of the stopping power leads to different ranges (see *section 4*). For a target density of $\phi = 1.2$ and the $(\alpha\mu)^+$ ion velocity $v = 5.82$ [a.u.] these ranges are: $R_{(\alpha\mu)}(\epsilon = \delta = 0) = 0.03$ cm, $R_{(\alpha\mu)}(\epsilon = 0.7, \delta = 0.5) = 0.035$ cm, $R_{(\alpha\mu)}(\epsilon = \delta = 1) = 0.04$ cm and for the $(^3He\mu)^+$ ion velocity $v = 3.25$ [a.u.] these ranges are: $R_{(^3He\mu)}(\epsilon = \delta = 0) = 0.004$ cm, $R_{(^3He\mu)}(\epsilon = 0.7, \delta = 0.5) = 0.007$ cm and $R_{(^3He\mu)}(\epsilon = \delta = 1) = 0.010$ cm.

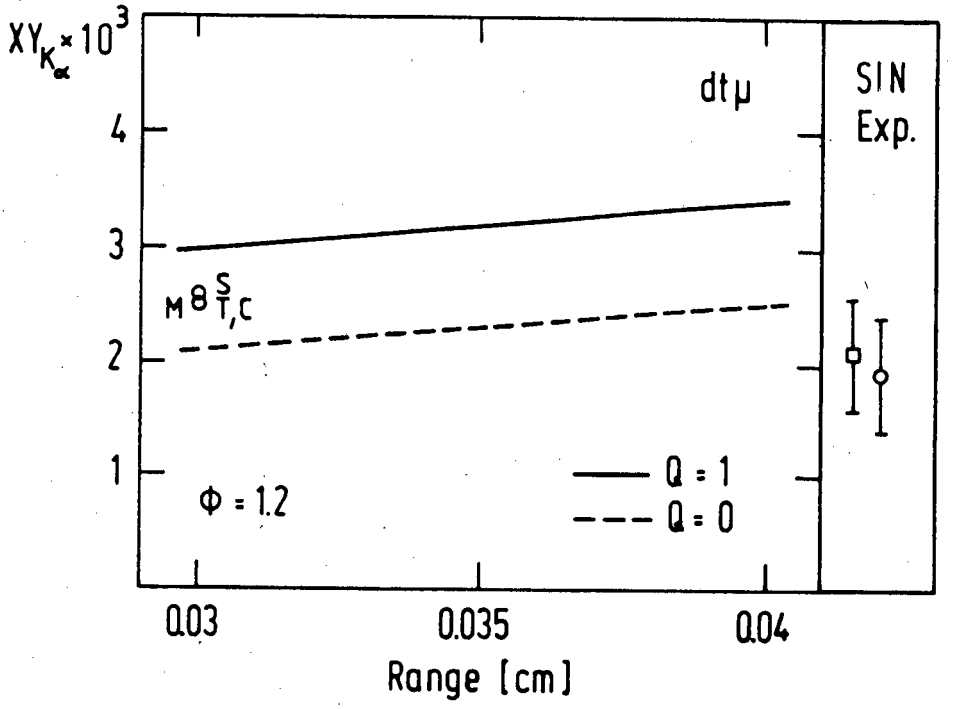


Figure 25: Yield of muonic helium $K_\alpha$ radiation emitted after dt- fusion as a function of the range. The open circles denote results obtained by other authors T [36], C [44], M [32] and S [50]. The experimental data are those of Bossy *et al.* [43] and [37].

All theoretical results, see figure 25 and figure 26 (with the exception of reference [50] for $(dd\mu)$ $XY_{K_\alpha}$), show a discrepancy between theory and experiment. The density dependent reduction in stopping power tends to make the discrepancy for muonic helium $K_\alpha$ radiation emitted after fusion between theory and experiment even larger. Note, however, that the present calculations do agree with the experimental data for $XY_{K_\alpha}$ emission after $(dt\mu)$ fusion for the parameter range $\epsilon \leq 0.7$ and $\delta \leq 0.5$, if no Stark mixing is assumed.

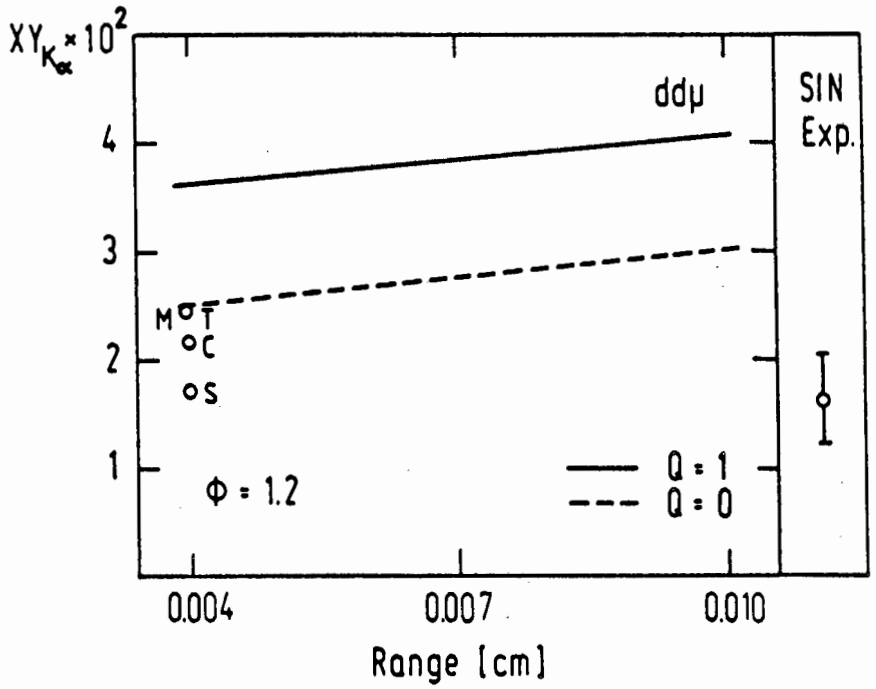


Figure 26: Yield of muonic helium $K_\alpha$ radiation emitted after dd- fusion as a function of the range. The open circles denote results obtained by other authors T [36], C [44], M [32] and S [50]. The experimental data are those of Bossy *et al.* [43] and [46].

If a smaller stopping power makes the yield X-ray radiation from muonic helium emitted after fusion too large, a larger stopping power would get the X-rays of the present calculation into agreement with experiment. An arguable increase of the stopping power is however not enough to accomplish this. A twice as large stopping power as normally used does change the X-ray yield in the present calculation by a suitable amount. The consequences, however, result in an effective sticking fraction of 0.61% for $\phi = 1.2$, much too high to be compatible with experimental results.

## 6. THE INFLUENCE OF A POSSIBLE RESONANT DEEXCITATION OF THE 2P STATE

It is very difficult to properly account for the L-shell population dynamics of the $[(\alpha\mu^+)_{2s}, (\alpha\mu)^+_{2p}]$ or $[(^3\mathrm{He}\mu)^+_{2s}, (^3\mathrm{He}\mu)^+_{2p}]$ states during the slow down process. The cross sections depend crucially on the approximations made. For the transfer reactions there is an additional difficulty because of the near degeneracy with some target states.

The $(\alpha\mu)^+_{2p}$ states are 1.39 $eV$ $(2p_{\frac{1}{2}})$ and 1.53 $eV$ $(2p_{\frac{3}{2}})$ above the $(\alpha\mu)^+_{2s}$ state. The $(\alpha\mu)^+_{2s\to 2p}$ transition may therefore resonate with the vibrational excitations of electronic $T_2(\nu = 0 \to \nu = 5)$ (1.43 $eV$) and $D_2(\nu = 0 \to \nu = 4)$ (1.40 $eV$) molecules. Thus there is a possibility that the $(\alpha\mu)^+_{2p}$ state is resonantly deexcited to the $(\alpha\mu)^+_{2s}$ state in collisions with hydrogenic molecules during the slow down process [17], reversing the effect of the Stark quenching. Similar considerations apply to the $(^3\mathrm{He}\mu)$ slow down process. The energy difference of the $2p-2s$ state is 83 $meV$ smaller here due to a larger nuclear radius.

Lacking more an exact theoretical study of this mechanism a constant resonant deexcitation (RDX) rate of $15 \times 10^{12} s^{-1}$ is assumed in a schematic study to explore the influence of such an effect on the dynamics of the $2s$ and $2p$ population during the slow down. The same constant resonant deexcitation rate is used in the present calculations for the $(^3\mathrm{He}\mu)$ case. This resonant deexcitation rate (RDX) does lower the effective sticking probability, bringing the theoretical calculations for $(\alpha\mu)^+$ sticking closer to the experimentally observed data, see figure 27. The still physically realistic density dependent stopping power $S(v; \epsilon = 0.7, \delta = 0.5)$ and the assumed RDX do give a very good agreement with the SIN data and the LAMPF data for $\phi < 1$. The LAMPF data for $\phi \geq 1$ are still lower and would require a higher RDX rate or a stronger non linearly density dependent stopping power, see solid line $\epsilon = \delta = 1$ in figure 27. The later proposition must be excluded, however, since the large parameter set $(\epsilon = \delta = 1)$ seems to be physically unrealistic.

Figure 27 shows the effective sticking fraction $\omega_s^{eff}$ obtained with three previously employed sets of values for the parameters $\epsilon$ and $\delta$ describing the density dependence of the stopping power and a resonant 2p deexcitation contribution. Results obtained with the stopping power for solid hydrogen [47] and a resonant 2p deexcitation is given as dash dot line. For comparison results from the density independent stopping power $S(v)$ are included in figure 27 as a broken line.

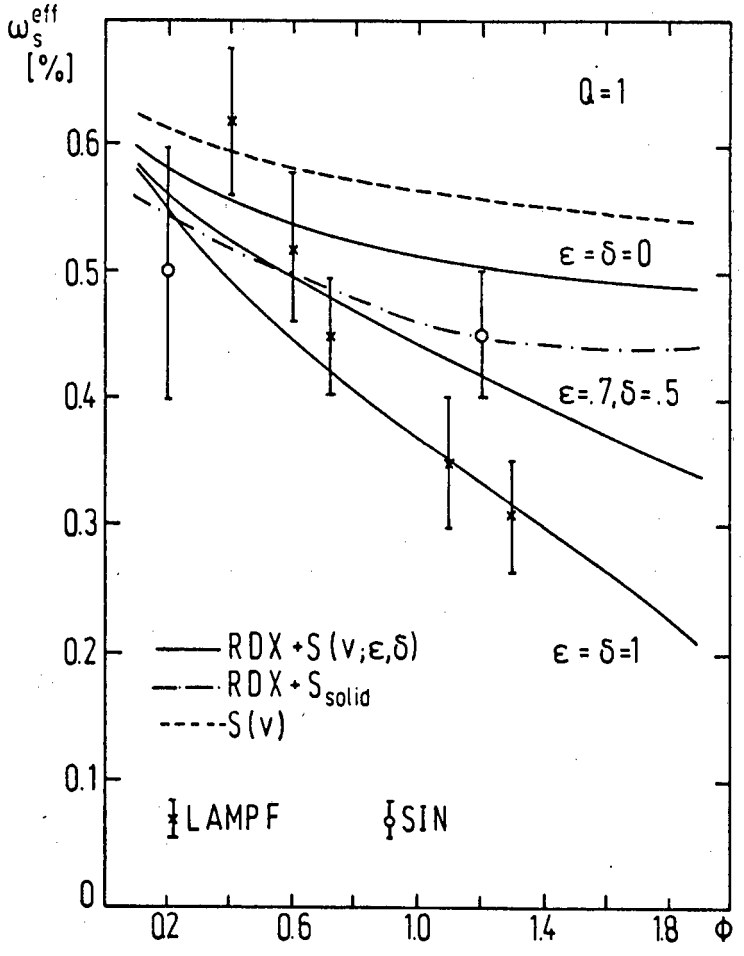


Figure 27: Effective sticking fraction $\omega_s^{eff}$ calculated with RDX and S($v;\phi$) as function of density [in units of liquid hydrogen density]. The experimental data points are from references [13] and [41].

Further results are shown in comparison with other theoretical calculations [36,44,32,50] and experimental data [43,37,46] for X-rays after $(dt\mu)$ fusion in figure 29 and for X-rays after $(dd\mu)$ fusion in figures 30, 31 and 32.

RDX substantially influences $\gamma_{K_\alpha}$, the X-rays per initial sticking. For the density $\phi = 0.05$ figure 28 compares the $\gamma_{K_\alpha}$ obtained with RDX as a function of the slow down energy of the $(\alpha\mu)^+$ ion to the results obtained in *section 3*. Please note that the RDX rate was chosen in this section to over compensate the Stark mixing effects of Q=1.

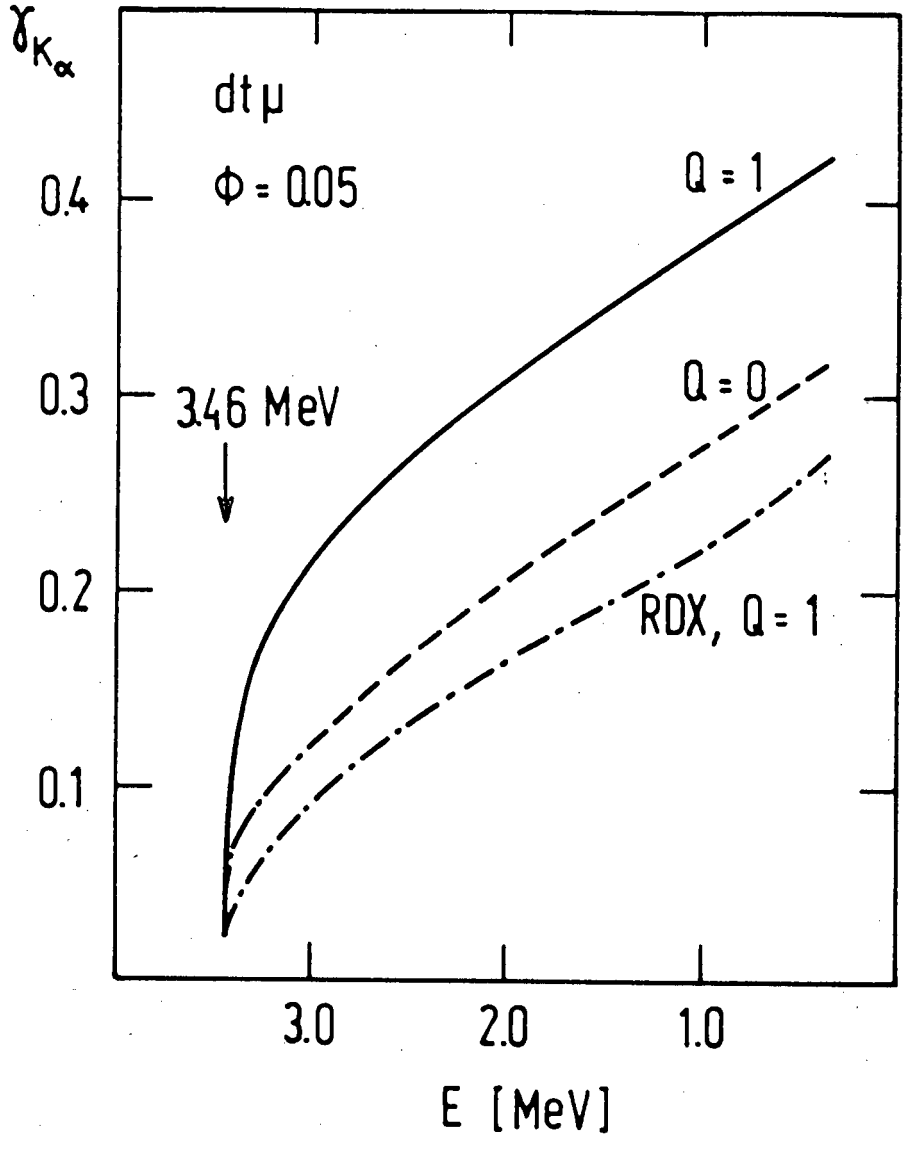


Figure 28: X-rays per initial sticking $\gamma_{K_\alpha}$ as a function of the slow down energy of the $(\alpha\mu)^+$ after fusion for $\phi = 0.05$ .

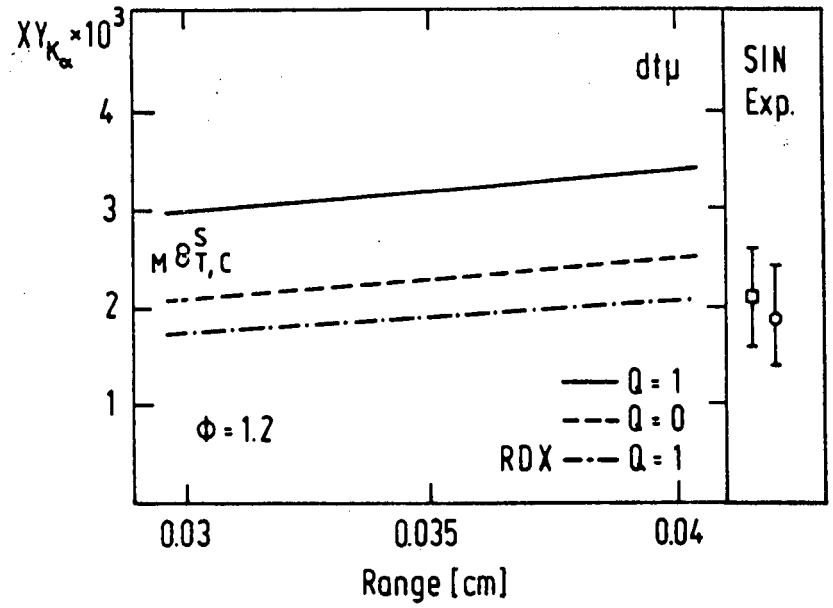


Figure 29: Yield of muonic helium $K_\alpha$ radiation emitted after dt- fusion. The open circles denote results obtained by other authors T [36], C [44], M [32] and S [50]. The experimental data are those of Bossy *et al.* [43] and [37].

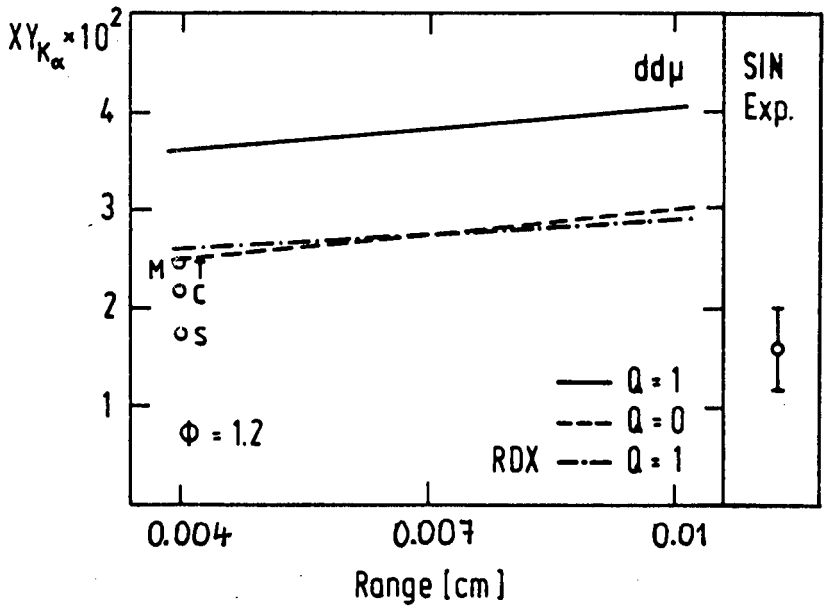


Figure 30: Yield of muonic helium $K_\alpha$ radiation emitted after dd- fusion. The open circles denote results obtained by other authors T [36], C [44], M [32] and S [50]. The experimental data are those of Bossy *et al.* [43] and [46].

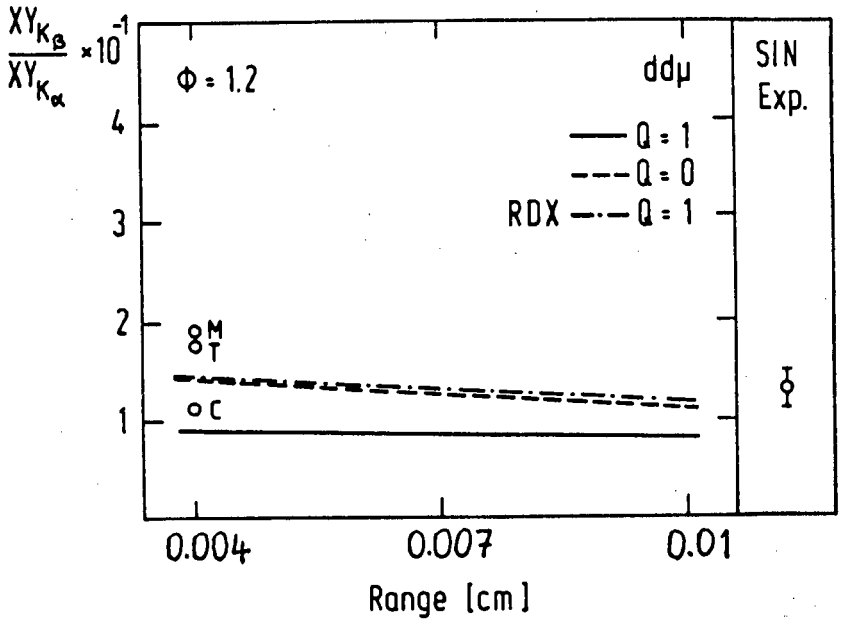


Figure 31: Ratio of the yields of muonic helium radiation $K_\beta/K_\alpha$ emitted after dd- fusion. For notation see figure 30.

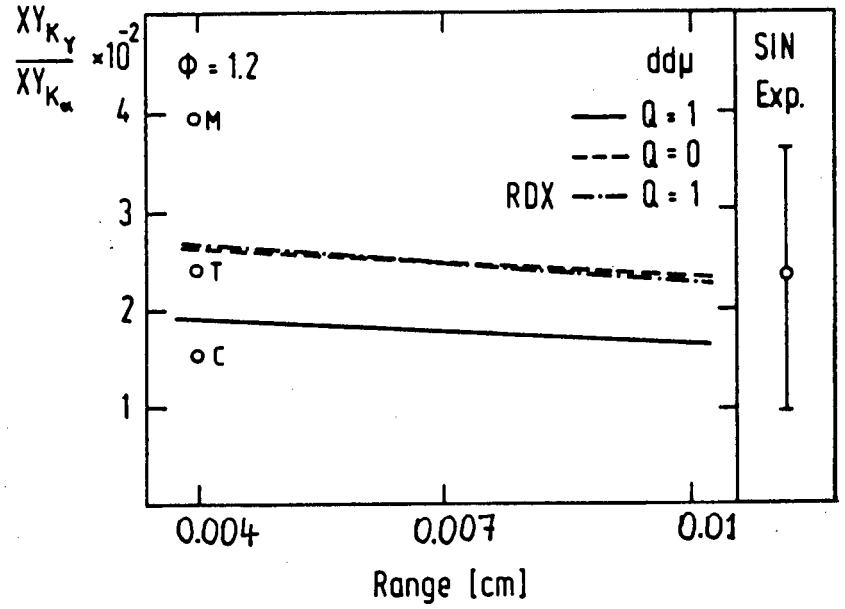


Figure 32: Ratio of the yields of muonic helium radiation $K_\gamma/K_\alpha$ emitted after dd- fusion. For notation see figure 30.

Calculations including a RDX effect and allowing for a density dependent stopping power can consistently explain all existing measurements of muon regeneration and X-rays after $(dt\mu)$ and $(dd\mu)$ fusion and are in an overall better agreement with all experiments including the LAMPF data for higher densities.

Table 17

The $(\alpha\mu)^+$ sticking fraction $\omega_s^{eff} = (1 - R)\omega_s^0$ with $\omega_s^0 = 0.88\%$ for different d-t target densities $\phi = \rho/\rho_0$.

| THEORY: | $\phi$=1.2 | $\phi$=0.1 |
|---|---|---|
| PRESENT WORK: | | |
| RDX, $S(\epsilon = \delta = 0)$ | 0.50 | 0.60 |
| RDX, $S(\epsilon = .7, \delta = .5)$ | 0.42 | 0.59 |
| RDX, $S_{solid}$ | 0.45 | 0.56 |
| Q=1, $S(\epsilon = \delta = 0)$ | 0.56 | 0.62 |
| Q=1, $S(\epsilon = .7, \delta = .5)$ | 0.47 | 0.62 |
| Q=1, $S_{solid}$ | 0.52 | 0.59 |
| Q=0, $S(\epsilon = \delta = 0)$ | 0.52 | 0.55 |
| Q=0, $S(\epsilon = .7, \delta = .5)$ | 0.42 | 0.54 |
| OTHER THEORY: | | |
| Bracci et al. [16] | 0.67 | 0.70 |
| Cohen [50] | 0.57 | |
| Cohen [38] | 0.54 | 0.59 |
| Cohen [44] | 0.56 | 0.62 |
| Cohen [28] Q=1 | 0.53 | 0.59 |
| Cohen [28] Q=0 | 0.49 | 0.57 |
| Gershtein et al. [23] | 0.68 | |
| Markushin [32] | 0.57 | |
| Menshikov et al. [39] | 0.60 | 0.67 |
| Takahashi [31] Q=0 | 0.57 | |
| Takahashi [31] Q=0.43 | 0.61 | 0.63 |
| EXPERIMENT: | | |
| Jones et al. [14] | 0.4±0.1 | |
| Jones et al. [13] | 0.35±0.07 | 1.1±0.5 |
| Breunlich et al. [41] | 0.45±0.05 | 0.50±0.10 |
| Nagamine [42] | 0.42±0.07 | |
| Bossy et al. [43] | 0.42±0.14 | |

Table 17 presents results for the $(\alpha\mu)^+$ effective sticking fraction $\omega_s^{eff}$ for the present calculations in comparison to results from other theoretical calculations and experiments. In table 18 the effective sticking fraction $\omega_d^{eff}$ of $(^3He\mu)$ is shown.

Table 18

The $^3He\mu$ sticking fraction $\omega_d^{eff} = (1 - R)\omega_d^0$ with $\omega_d^0 = 13.3\%$ for different d-d target densities $\phi = \rho/\rho_0$.

| THEORY: | $\phi$=1.2 | $\phi$=0.05 |
|---|---|---|
| PRESENT WORK: | | |
| RDX, $S(\epsilon = \delta = 0)$ | 9.4 | 10.9 |
| RDX, $S(\epsilon = .7, \delta = .5)$ | 8.0 | 10.9 |
| RDX, $S_{solid}$ | 8.8 | 10.3 |
| Q=1, $S(\epsilon = \delta = 0)$ | 10.0 | 11.2 |
| Q=1, $S(\epsilon = .7, \delta = .5)$ | 8.5 | 11.1 |
| Q=1, $S_{solid}$ | 9.4 | 10.6 |
| Q=0, $S(\epsilon = \delta = 0)$ | 9.4 | 10.6 |
| Q=0, $S(\epsilon = .7, \delta = .5)$ | 7.9 | 10.5 |
| OTHER THEORY: | | |
| Cohen [50] | 10.8 | 11.9 |
| Cohen [44] | 10.7 | 11.9±0.5 |
| Markushin [32] | | 12.3±0.2 |
| Takahashi [31] Q=0.43 | 11.3 | 11.7 |
| EXPERIMENT: | | |
| Balin [45] | | 12.2±0.3 |

A collection of X-ray results of the present work, other theoretical calculations and experiments is presented in table 19 for the case of dt- fusion and for dd- fusion in table 20.

Table 19

Number of X-rays per 100 fusions $XY_{K_\alpha} = \gamma_{K_\alpha}\omega_s^0$ with $\omega_s^0 = 0.88\%$ for different d-t target densities $\phi = \rho/\rho_0$.

| THEORY: | $XY_{K_\alpha}$ $\phi = 1.2$ | $XY_{K_\alpha}$ $\phi = 0.1$ | $XY_{K_\beta}$ $\phi = 1.2$ | $\gamma_{K_\beta}/\gamma_{K_\alpha}$ $\phi = 1.2$ | $\gamma_{K_\gamma}/\gamma_{K_\alpha}$ $\phi = 1.2$ |
|---|---|---|---|---|---|
| PRESENT WORK: | | | | | |
| RDX, $S(\epsilon = \delta = 0)$ | 0.18 | 0.23 | 0.027 | 0.15 | 0.020 |
| RDX, $S(\epsilon = .7, \delta = .5)$ | 0.19 | 0.24 | 0.028 | 0.14 | 0.019 |
| RDX, $S_{solid}$ | 0.19 | 0.25 | 0.027 | 0.15 | 0.019 |
| Q=1, $S(\epsilon = \delta = 0)$ | 0.30 | 0.38 | 0.021 | 0.07 | 0.012 |
| Q=1, $S(\epsilon = .7, \delta = .5)$ | 0.32 | 0.38 | 0.022 | 0.07 | 0.011 |
| Q=1, $S_{solid}$ | 0.31 | 0.39 | 0.022 | 0.07 | 0.011 |
| Q=0, $S(\epsilon = \delta = 0)$ | 0.21 | 0.32 | 0.026 | 0.12 | 0.017 |
| Q=0, $S(\epsilon = .7, \delta = .5)$ | 0.23 | 0.32 | 0.026 | 0.11 | 0.016 |
| Q=0, $S_{solid}$ | 0.22 | 0.30 | 0.026 | 0.12 | 0.016 |
| OTHER THEORY: | | | | | |
| Cohen [50] | 0.26 | 0.30 | | | |
| Cohen [38] | 0.24 | 0.30 | | 0.12 | 0.019 |
| Cohen [28] Q=1 | 0.23 | 0.28 | | | |
| Cohen [28] Q=0 | 0.15 | 0.20 | | | |
| Markushin [32] | 0.25 | 0.29 | | 0.12 | |
| Takahashi [31] Q=0 | 0.13 | | 0.042 | 0.32 | 0.043 |
| Takahashi [31] Q=0.43 | 0.24 | | 0.043 | 0.18 | 0.024 |
| Takahashi [36] | 0.36 | | 0.046 | 0.13 | 0.019 |
| EXPERIMENT: | | | | | |
| Bossy et al. [43] | 0.21±0.05 | | | | |
| Bossy et al. [37] | 0.19±0.05 | | | | |
| Nagamine [42] | 0.049±0.04 | | | | |

Table 20

Number of X-rays per 100 fusions $XY_{K_\alpha} = \gamma_{K_\alpha}\omega_d^0$ with $\omega_d^0 = 13.3\%$ for different d-d target densities $\phi = \rho/\rho_0$.

| THEORY: | $XY_{K_\alpha}$ $\phi = 1.2$ | $XY_{K_\alpha}$ $\phi = 0.05$ | $\gamma_{K_\beta}/\gamma_{K_\alpha}$ $\phi = 1.2$ | $\gamma_{K_\gamma}/\gamma_{K_\alpha}$ $\phi = 1.2$ |
|---|---|---|---|---|
| PRESENT WORK: | | | | |
| RDX, $S(\epsilon = \delta = 0)$ | 2.6 | 3.3 | 0.136 | 0.026 |
| RDX, $S(\epsilon = .7, \delta = .5)$ | 2.8 | 3.3 | 0.132 | 0.025 |
| RDX, $S_{solid}$ | 2.7 | 3.5 | 0.134 | 0.025 |
| Q=1, $S(\epsilon = \delta = 0)$ | 3.6 | 4.5 | 0.092 | 0.019 |
| Q=1, $S(\epsilon = .7, \delta = .5)$ | 3.8 | 4.5 | 0.087 | 0.018 |
| Q=1, $S_{solid}$ | 3.7 | 4.7 | 0.089 | 0.018 |
| Q=0, $S(\epsilon = \delta = 0)$ | 2.5 | 3.4 | 0.136 | 0.027 |
| Q=0, $S(\epsilon = .7, \delta = .5)$ | 2.8 | 3.5 | 0.130 | 0.025 |
| Q=0, $S_{solid}$ | 2.6 | 3.6 | 0.134 | 0.025 |
| OTHER THEORY: | | | | |
| Cohen [50] | 1.8 | 2.2 | | |
| Cohen [38] | 2.2 | 2.9 | 0.11 | 0.015 |
| Markushin [32] | 2.5 | 3.0 | 0.19 | 0.039 |
| Takahashi [31] Q=0 | 1.4 | | 0.31 | 0.042 |
| Takahashi [31] Q=0.43 | 2.5 | 5.6 | 0.18 | 0.024 |
| EXPERIMENT: | | | | |
| Bossy et al. [46] | 1.6±0.4 | | 0.13±0.02 | 0.011±0.012 |
| Bossy et al. [43] | 1.6±0.2 | | 0.13±0.02 | 0.023±0.013 |

# CONCLUSIONS

Our comprehensive analysis of the muon regeneration process after sticking in the muon catalyzed dt- fusion has shown that the two dominant sources of a potential target density dependence are:

1. population dynamics of the L-shell of the $(\alpha\mu)^+$ projectile and
2. non linear density dependence of the $(\alpha\mu)^+$ stopping power in heavy hydrogen.

Both mechanisms, which have not been systematically investigated previously, are not well understood theoretically. In the present work these quantities have been parametrized and it has been shown how they influence the regeneration processes in MuCF.

The validity of the standard stopping power formulas in liquid hydrogen at low velocities has not been established. Substantial variation of the stopping power between liquid and gas phase are known to exist. It has been shown that an assumed medium dependence of the stopping power can lead to a substantial density dependence of the effective muon sticking fraction similar to that observed in the LAMPF experiments.

On the other hand our knowledge of the magnitude of Stark mixing in muonic helium is based solely on theoretical calculations, for which no general consensus exists in the present literature. In particular the difficulty to obtain simultaneous agreement with the experimental results for the muonic effective sticking fraction and the muonic $K_\alpha$ X-ray yield provides strong indication that the Stark mixing has not been fully understood. X-ray data from $(dd\mu)$ fusion lend further support to this conclusion.

The present calculations which are based on a complete new set of muonic cross sections have also revealed that the other remaining uncertainties in the stripping cross section do not appear to be the likely source of the observed density dependence.

This work has shown, that it is possible to obtain a theoretical description consistent with experiment given the latitude within the theory. Complete understanding of the density dependence of muon sticking requires further experimental and theoretical studies.

# APPENDIX A

## SOME BACKGROUND AND HISTORICAL DEVELOPMENT OF THE MUON CATALYZED FUSION

Fusion is the mechanism by which our sun generates energy. The energy is gained when at extreme temperatures light elements like hydrogen overcome the repulsive Coulomb forces and the short ranged nuclear forces bind them to a heavier element (helium). The larger light nucleus typically represents an energetically lower configuration, and the energy difference is released in this process.

Nuclear fusion described above is normally thought to work only under very high temperatures found in the interior of a star or in the early universe. These conditions may be simulated in the laboratory utilizing enormous magnets, powerful lasers and extremely hot plasmas. But high temperature is not the only way to overcome the Coulomb repulsion. The Coulomb field of a hydrogen isotope can be shielded by a single bound heavy, negatively charged particle. As the muon survives the fusion process and does not participate in the actual fusion reaction. it can be viewed as a catalyst of the fusion reaction, In contrast to plasma fusion (hot fusion) muon catalyzed fusion [1,2,3,4] (cold fusion) can take place at room temperatures and in a relatively small vessel. It is in the production of the elementary particle, the muon, that technological difficulties will arise.

Muons are subatomic particles similar to the electron though 207 times heavier. They come in two forms, negative muons and their positive antiparticle. They were discovered 1936 but initially misidentified as a strongly interacting particle, the pion, in cloud chamber photographs of cosmic rays. These muons were produced by naturally occurring processes in which cosmic rays collide with the earth's upper atmosphere and the initially formed pions subsequently decay into muons. Muons can also be made artificially with the help of particle accelerators, in so called meson factories. When fast moving ions from the accelerator collide with matter, charged pions ($\pi^+$ and $\pi^-$) are produced and decay rapidly ($10^{-8} sec$) into a muon and a muon neutrino. Unlike $\pi^-$ mesons, however, a muon ($\mu$) does not react with nuclei or other particles through strong interaction. Aside from the electromagnetic interaction associated with its charge, it also decays by weak interaction into an electron accompanied by the associated $e^-$ and $\mu^-$ neutrinos. The average lifetime of a free muon is $2.2 \times 10^{-6}$ sec. Because the muon is charged it can take the place of an electron in an atomic or a molecular orbit typically 207 times closer to the nucleus or the center of nuclei.

If a negative muon enters a mixture of different kinds of heavy isotopes of hydrogen (deuterium and tritium) it starts the process cycle leading to nuclear fusion and the release of energy. That this phenomenon could occur has been predicted independently by Frank [2],Sakharov [3] and Zel'dovich [4]. However, the experimental discovery by Alvarez [1] was an accident. The excitement generated by the first observation of muon catalyzed fusion in ordinary hydrogen with a naturel deuterium contamination was substantial. However, a new process, the muon sticking, ignored previously has been noted in the following study by Jackson [6], that destroyed the hope for a clean way to generate energy. With a sticking fraction of 1% seemingly no more than 100 fusion reactions could be achieved during the lifetime of a muon. Despite this fundamental barrier many physicists continued to study muon catalyzed fusion because of its intrinsic beauty. It became clear that muons could catalyze fusion more quickly involving deuterium. Experiments at the Joint Institute for Nuclear Research in Dubna [7] found that the rate of such a process was temperature dependent, yielding more fusions at higher temperatures. Though this surprising result appeared to be due to an experimental error, it has stimulated the development of the key theoretical understanding of the *resonant mesomoleculear model* by Vesman [8] and Gershtein and Ponomarev [9]. Detailed calculations by Ponomarev and colleagues [10] first showed that the resonance condition is even more pronounced in the $(dt\mu)$ muomolecule. This led to a revival of interest in the muon catalysis and to suggestions that perhaps more than 100 fusions were possible in a mixture of deuterium and tritium [11]. Since 1982, experiments initially carried out at the Los Alamos Meson Physics Facility reached 150 fusions per muon in a dense deuterium tritium [13] mixture are possible. The interest in muon catalyzed fusion has since spread not only amongst physicists but in public as well because of its potential as a possible commercial energy source [14,15].

In the following subsections the key issues of MuCF are described in more detail:
A.1 Different Fusion Processes
A.2 The Muon Catalytic Cycle and Reaction Rates
A.3 Resonant Muomolecule Formation

## A.1 Different Fusion Processes

The first muon catalyzed fusion considered as early as 1947 [2] was proton deuteron fusion:

$$p + d + \mu \rightarrow {}^3He + \mu + 5.4MeV. \qquad (A1)$$

The $(pd\mu)$ catalyzed fusion process was later established theoretically [3,4] and observed experimentally [1] in a bubble chamber filled with hydrogen containing the natural small deuterium contamination (about 1 in 5000).

In fact fusion will occur in all different muonic hydrogenic molecules, some slower, some faster, releasing different amount of energies. The Alvarez group extended their study of muon catalysis to the case of pure liquid deuterium observing the reactions

$$d + d + \mu \rightarrow \begin{cases} {}^3He + n + \mu + 3.3MeV \\ t + p + \mu + 4MeV \end{cases} . \qquad (A2)$$

In Dubna experiments by Dzhelepov *et al.* [7] it was found that temperature changes by several hundred °K in the fusion vessel influences the cycle rate and hence the yield of fusions per muon.

But indeed it was only 20 years later, that the $(dt\mu)$ catalyzed fusion reaction was experimentally investigated by Jones *et al.* [12,13]

$$d + t + \mu \rightarrow {}^4He + n + \mu + 17.6MeV. \qquad (A3)$$

Other reactions of hydrogen isotopes known to bring about nuclear synthesis with energy liberation can be catalyzed by the muon:

$$p + d \rightarrow {}^3He + 5.4MeV, \qquad (A4)$$

$$p + t \rightarrow {}^4He + 20MeV \qquad (A5)$$

and

$$t + t \rightarrow {}^4He + n + n + 11.3MeV. \qquad (A6)$$

In principle the muon could induce fusion reactions with elements heavier than hydrogen for example:

$$d + {}^3He \rightarrow {}^4He + p + 18.3MeV. \qquad (A7)$$

$$d + {}^6Li \rightarrow {}^4He + {}^4He + 22.4MeV. \qquad (A8)$$

More possible fusion reactions are listed below:

## FUSION REACTIONS

| | | | | | | |
|---|---|---|---|---|---|---|
| p + d | $\longrightarrow$ | | $^3$He | | + | (5.4*MeV*) |
| d + d | $\longrightarrow$ | 42% | t | (1.01*MeV*) | + p | (3.02*MeV*) |
| | | 58% | $^3$He | (0.82*MeV*) | + n | (2.45*MeV*) |
| d + t | $\longrightarrow$ | | $^4$He | (3.5*MeV*) | + n | (14.1*MeV*) |
| d + $^3$He | $\longrightarrow$ | | $^4$He | (3.6*MeV*) | + p | (14.7*MeV*) |
| t + t | $\longrightarrow$ | | $^4$He | + 2n | + | (11.3*MeV*) |
| $^3$He + t | $\longrightarrow$ | 51% | $^4$He | + p + n | + | (12.1*MeV*) |
| | | 43% | $^4$He | (4.8*MeV*) | + d | (9.5*MeV*) |
| | | 6 % | $^5$He | (2.4*MeV*) | + p | (11.9*MeV*) |
| p + $^6$Li | $\longrightarrow$ | | $^4$He | (1.7*MeV*) | + $^3$He | (2.3*MeV*) |
| p + $^7$Li | $\longrightarrow$ | | $^4$He | + $^4$He | + | (17.3*MeV*) |
| d + $^6$Li | $\longrightarrow$ | | $^4$He | + $^4$He | + | (22.4*MeV*) |
| d + $^7$Li | $\longrightarrow$ | | $^4$He | + $^4$He + n | + | (15.1*MeV*) |
| p + $^{11}$B | $\longrightarrow$ | | 3 $^4$He | | + | (8.7*MeV*) |
| n + $^6$Li | $\longrightarrow$ | | $^4$He | (2.1*MeV*) | + t | (2.7*MeV*) |

## A.2 The Muon Catalytic Cycle and Reaction Rates

As an example let us first consider here a natural hydrogen target containing a small concentration of deuterium (a target mixture could consist of combinations of different concentrations of $H, D, T-$ atoms and non equilibrium concentrations of $H_2, D_2, T_2, DT, etc.$ molecules). When a negative muon enters a target of hydrogen isotopes, the muon is slowed down to an energy of some $eV$, before a muonic molecule is formed through the Auger process.

$$X + \mu^- \rightarrow (h\mu) + e; \quad \begin{cases} X = H, D, T \\ h = p, d, t \end{cases} . \tag{A9}$$

The muonic hydrogen atom $(p\mu)$ is electrically neutral and rather small, its muonic Bohr radius being

$$a_\mu = a_0 m_e/m_\mu = 255.93 fm, \tag{A10}$$

where $a_0 = 0.529 \times 10^5 fm$ is the electron Bohr radius and

$$m_e/m_\mu \approx 1/206.77.$$

This small size makes the $(h\mu)$-atom neutron like and it can diffuse freely through liquid hydrogen. If a muonic hydrogen atom comes close to a heavier isotope the muon can be transferred rapidly and irreversibly, e.g.

$$(p\mu) + d \rightarrow (d\mu) + p + 135eV, \tag{A11}$$

because the binding energy for the ground state of the $(d\mu)$ is 135 $eV$ greater than that of the $(p\mu)$ atom (reduced mass effect). The rate for reaction *eq.*(A11) is of course proportional to the deuterium density. In a natural hydrogen target (H + 1/2000 D) a $(pd\mu)$ molecule is formed subsequently

$$(d\mu) + H \rightarrow (pd\mu) + e. \tag{A12}$$

Molecules of the above type are referred to as *mesomolecules* in older literature (this goes back to the time when the muon was thought to be a meson). This object is called *muomolecule* in this document. The more appropriate expression *muonic molecular ion* is even more precise.

Hydrogenic muomolecules are composed of two heavy hydrogen isotopes and bound together by muon. In first approximation, in the classical image they resemble the $H_2^+$ ion in the same way as muonic atoms resemble ordinary atoms. From dimensional consideration follows that the size and groundstate energy for the muomolecule is scaling with the mass of the light binding particle.

Hence muomolecules are
a) extremely small objects $\sim 500\ fm$ and
b) characterized by much higher energies $\sim 300\ eV$.

The quantum structure of the muomolecules is, however, considerably different from the larger *model*, since the mass ratio of the third, binding particle to the *heavy* hydrogen vibrating in the molecule is not so much different from unity. Hence the molecular spectrum is greatly different from the scaled values of usual hydrogen molecules. This will be discussed further in *section* A.3.

A proton and a deuteron fuse through electromagnetic interaction:

$$p + d \rightarrow^3 He + \gamma + 5.4MeV. \qquad (A13)$$

In the muomolecule a virtual photon can be absorbed by the muon in a so called conversion process (see figure 33) giving rise to the fusion reaction

$$(pd\mu) \rightarrow^3 He + \mu + 5.4MeV. \qquad (A14)$$

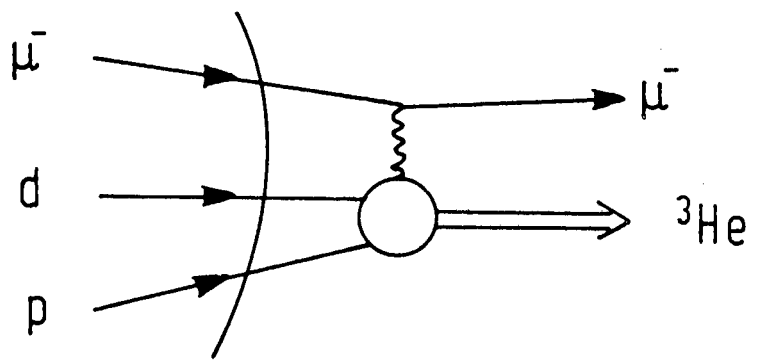


Figure 33: Reaction $(pd\mu) \rightarrow^3$He$+\mu$.

The energy of the muon is 5.4 $MeV$ equivalent to a range of 1.7 $cm$ (distances B-C and D-E) in the sketch of the bubble chamber picture, (see figure 34). This was the clue for the understanding of the puzzling reaction chain.

The mystery of the gap between C, the stopped muon and D, the ejected muon was also solved by Edward Teller, when he suggested that the muon would

be initially bound to a proton and then transferred to the deuteron. The neutral $(d\mu)$ atom could then recoil some distance producing the observed gap, followed by $(pd\mu)$ formation and fusion.

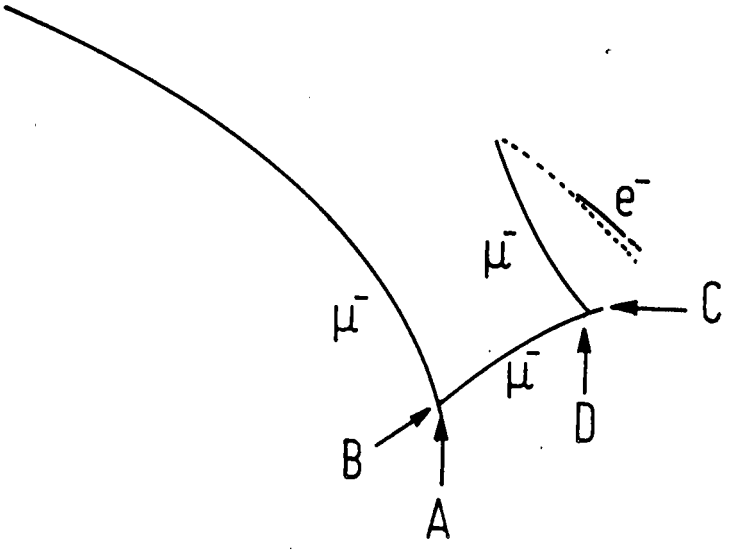


Figure 34: Sketch of a $(pd)$ fusion catalyzed by $\mu^-$. The incident muon comes to rest, drifts as a neutral muonic atom, is ejected with 5.4 $MeV$ by the $HD$ reaction, comes to rest again after 1.7 $cm$, repeats drift and ejection and decays.

The catalysis of the nuclear synthesis reaction (*cold fusion*) is only effective if one muon can repeat the catalytic cycle several times. For this to be possible the muon lifetime must be considerably larger than the reaction times for processes within the catalytic cycle. Each process is associated with a characteristic reaction rate $\lambda_x = 1/\tau_x$, where $\tau_x$ is the mean wait time before the reaction occurs. The conditions for the muon to be able to complete several cycles are

$$\lambda_{pd\mu} > \lambda_0 \qquad (A15)$$

and

$$\lambda_{pd}^f > \lambda_0, \qquad (A16)$$

where $\lambda_0 = 0.455 \times 10^6 s^{-1}$ is the decay rate of the free muon, $\lambda_{pd\mu}$ is the formation rate of the $(pd\mu)$ muomolecule and $\lambda_{pd}^f$ is the nuclear fusion reaction rate in the muomolecule. All atomic and molecular rates are usually normalized to refer to the density $\rho_0 = 4.25 \times 10^{22} cm^{-3}$ of natural hydrogen at liquidizing point at 1At. In a mixture of isotopes $c_p$, $c_d$, $c_t$ refer to the respective normalized partial densities.

The muonic atom formation time which is shorter than $10^{-11}$ sec including the slow down process will not be further considered here. The muon transfer rate from the 1s-(p$\mu$) state to the heavier isotope is

$$(\lambda_{pd})_{1s} \approx 10^8 s^{-1} c_d \qquad (A17)$$

and a similar value holds for $(\lambda_{dt})_{1s}$. The muomolecule formation, *eq.*(A4), proceeds with a formation rate of $\lambda_{pd\mu} \approx 6 \times 10^6 s^{-1}$.

The actual fusion reaction time is

$$\frac{1}{\lambda_{pd}^f} \approx 3 \times 10^{-6} s, \qquad (A18)$$

since the muon conversion in process is not a *strong* interaction. It should be noted that the nuclear reaction normally occurs from the J=0 muomolecular state. Should the muomolecule be formed in the J=1 state, the Auger transition to J=0 will occur rapidly with a rate of $10^{11} s^{-1}$ (except for $(dd\mu)$ and other molecules which do not have a dipole moment).

*Eq.*(A18) implies that the mean time required for the muon to induce fusion exceeds the mean muon lifetime $\tau_\mu = 2.2 \times 10^{-6} s$ and the muon usually decays before it can repeat the $(pd\mu)$ fusion cycle, either while waiting in the $(pd\mu)$ molecule for fusion to occur or while waiting in a $(p\mu)$ atom to find a deuteron. The latter could resolved by putting more deuterium into the reaction vessel. Thus it is the nuclear reaction time which constitutes the barrier here. Similar catalytic cycles exist for the reactions in *eq.*(A2) and *eq.*(A3).

The fusion reaction times for the dd- cycle and the dt- cycle are faster. The dd- and dt- fusion reaction rates are

$$\lambda_{dd}^f = 0.43 \times 10^9 s^{-1} \quad \lambda_{dt}^f = 1.1 \times 10^{12} s^{-1}. \qquad (A19)$$

The $(dd\mu)$ formation rate at room temperature was also remeasured recently. Jones [13] finds:

$$\lambda_{dd\mu}(T = 300^\circ K) = 3 \times 10^6 s^{-1}. \qquad (A20)$$

Table 21

Some characteristic rates in MuCF [51], normalized to liquid hydrogen density $\rho_0 = 4.25 \times 10^{22} cm^{-3}$.

| Rates | Theory | Experiment | T[° K] |
|---|---|---|---|
| $\lambda_{dt}$ | $2 \times 10^8 s^{-1}$ | $2.8 \pm 0.4 \times 10^8 s^{-1}$ | |
| $\lambda_{dd\mu}$ | $2.8 \times 10^6 s^{-1}$ | $2.76 \pm 0.08 \times 10^6 s^{-1}$ | 300 |
| $\lambda_{dt\mu}$ | $\sim 4 \times 10^8 s^{-1}$ | $6.56 \pm 0.58 \times 10^8 s^{-1}$ | $<130$ |
| $\lambda^f_{pd\mu}$ | $\sim 3 \times 10^6 s^{-1}$ | | |
| $\lambda^f_{dd\mu}$ | $4.3 \times 10^8 s^{-1}$ | | |
| $\lambda^f_{dt\mu}$ | $1.1 \times 10^{12} s^{-1}$ | | |
| $\lambda^f_{tt\mu}$ | | $15 \pm 2 \times 10^6 s^{-1}$ | |

## A.3 Resonant Muomolecule Formation

Conventional direct $(dd\mu)$ formation rate was computed to be

$$\lambda_{dd\mu} \approx 0.5 \times 10^5 s^{-1}, \qquad (A21)$$

which differed significantly from the experimental data which also indicated a temperature dependence. This led Vesman [8] to suggest the possibility of a *resonant* $dd\mu$ formation.

A muonic hydrogen is neutral and quite small; it can therefore approach other hydrogenic isotopes closely. Normally the binding energy of the muomolecule will be transferred to an Auger electron (*non resonant* process),

$$(d\mu) + D_2 \rightarrow [(dd\mu)de] + e. \qquad (A22)$$

If the binding energy of the muomolecule is very small on the muonic scale, of the order of $eV$, this binding can be absorbed in the excitation of the vibrational and rotational degrees of freedom of the electronic molecules, exploiting possibly an accidental degeneracy between the $\mu$ and e molecules (*resonant muomolecule formation*),

$$(d\mu) + D_2 \rightarrow [(dd\mu)^* d2e]^*_\nu. \qquad (A23)$$

To obtain such a degeneracy, energies of electronic molecular hydrogen of the order of $eV$ have to correspond to those of muonic atoms and molecules that are usually about 207 *times* larger. In the case of muomolecules only *weakly* bound excited states satisfy this condition.

Table 22 summarizes the energies of the Coulombic, spinless, Schrödinger 3-body system [52]. The binding energies were obtained using the following particle masses: $m_t = 5496.918 m_e$, $m_d = 3670.481 m_e$, $m_p = 1836.1515 m_e$, $m_\mu = 206.7686 m_e$ and $Ry = 13.6058041 eV$. Noticeable is the presence of weakly bound states in the $(dd\mu)$ and $(dt\mu)$ molecules with J=1 and $\nu = 1$.

Table 22
Muomolecular spectrum, energies in $eV$.

| $J\nu$ | $(pd\mu)$ | $(dd\mu)$ | $(dt\mu)$ | $(tt\mu)$ |
|---|---|---|---|---|
| 00 | 221.55 | 325.07 | 319.14 | 362.91 |
| 01 | - | 35.844 | 34.834 | 83.771 |
| 10 | 97.498 | 226.68 | 232.47 | 289.14 |
| 11 | - | 1.9748 | 0.66017 | 45.206 |

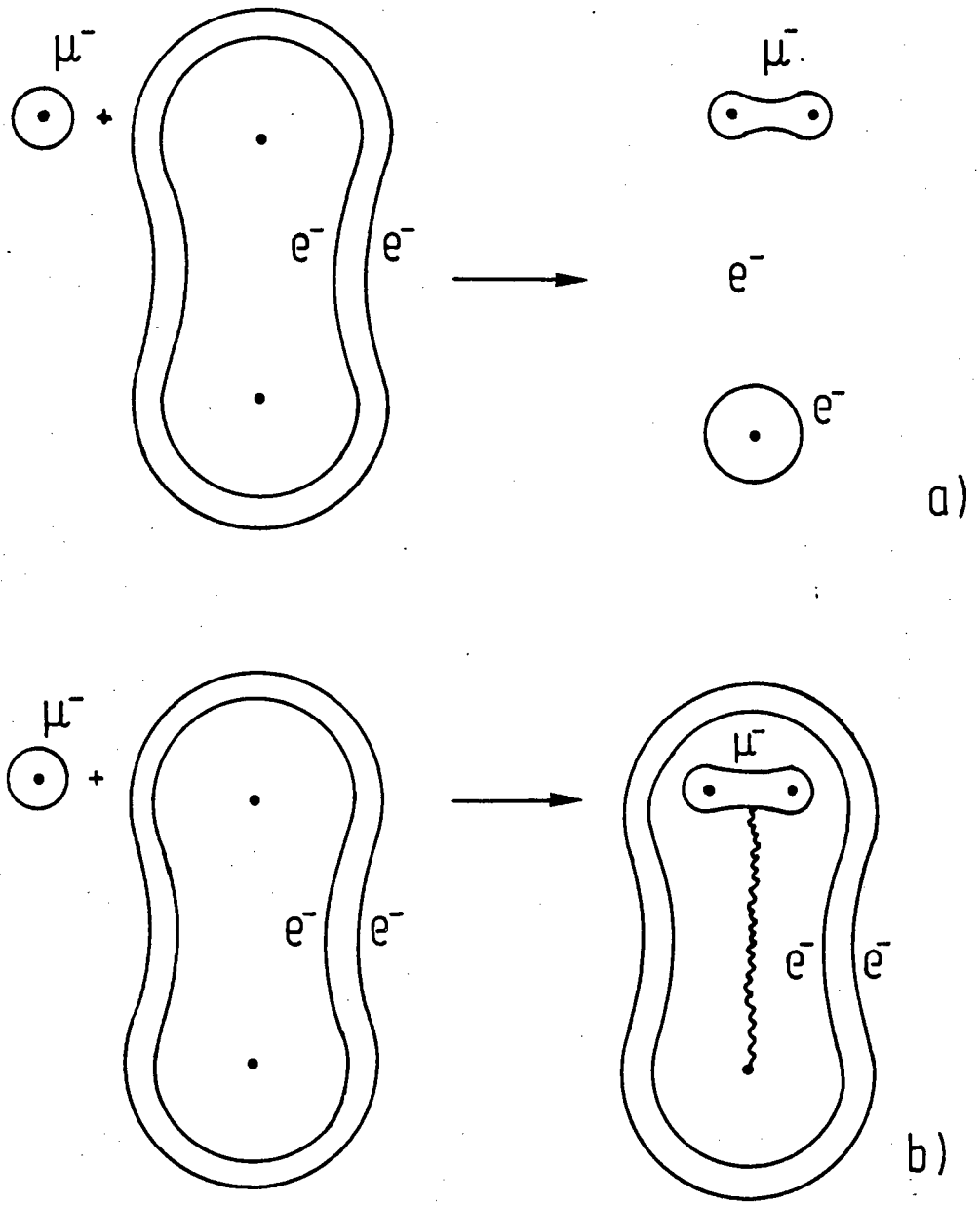


Figure 35: Muomolecule formation: a) non resonant, b) resonant.

The muomolecular states have been obtained by different methods. Initial calculations by Ponomarev and collaborators [9,10] have yielded adequate results except for the weakly bound states, however, only the sophisticated variational calculations by Szalewicz *et al.* [53], Hu [21], led to finally accepted values for weakly bound states, though the wave functions are still being improved on. The finding of the weakly bound $(dt\mu)$ state was the major accomplishment of the soviet group under Ponomarev which led to the further studies in muomolecular quantum structure.

In case of a possible degeneracy between the vibrational and rotational states of the electronic molecule and the muomolecule the thermal energy $\epsilon_T$ at the temperature $T$ is of considerable importance. The thermal distribution

$$\gamma(\epsilon, \epsilon_T) = (\frac{27}{2\pi}\frac{\epsilon}{\epsilon_T})^{\frac{1}{2}}\frac{1}{\epsilon_T}\exp(-\frac{3}{2}\frac{\epsilon}{\epsilon_T}) \qquad (A24)$$

is weakly peaked. The resonance condition on the energy of the electronic molecule $(\epsilon_r)$

$$\epsilon_r = \epsilon_T + \epsilon^{\mu}_{mol} \qquad (A25)$$

is not very pronounced in the above distribution. Therefore in the temperature range $30^0K < T < 1000^0K$ an appreciable probability exists to find a particular value $\epsilon$ in the domain $0.005 < \epsilon < 0.1\ eV$. Also it turns out that the electron molecular states have a natural collisional width which facilitates the resonance matching of the level.

Another component in the energy balance is the rotational energy of the electronic molecule, before and after the attachment of the muonic deuterium or tritium to one of the molecular centers. This energy is

$$E^J = \frac{J(J+1)}{2\Theta}, \qquad (A26)$$

with

$$\Theta = R^2 M_r. \qquad (A27)$$

$M_r$ is the reduced mass of the electronic molecule, different before and after muomolecule formation and R the separation of the two molecular centers. At $T > 300^0K$ several rotational states of the molecule can be excited, in this way preparing the rotational vibrational states for the accidental degeneracy.

## APPENDIX B

## MUON TRANSFER CROSS SECTIONS IN EIKONAL APPROXIMATION

In the laboratory frame, the projectile with a muon bound in orbit (n,l) is assumed to move with a constant velocity v along the trajectory $\mathbf{R}(t)=\mathbf{b}+\mathbf{v}t$, where b is the impact parameter. When consulting the references [18,54,55,56] the reader should remember that in the presented arguments the projectile is the $(\alpha\mu)^+$ ion colliding with a target consisting of completely ionized $d^+$ and $t^+$, while the usual way is computing collisions of $d^+$ and $t^+$ ions with a $He^{++}$ target. The cross section averaged over initial and summed over final magnetic substates can be written as [18]

$$\sigma_{nl\to n'l'} = \frac{1}{2l+1}\sum_{m,m'}\int |A_{nlm\to n'l'm'}(\mathbf{b},v)|^2 d^2b. \qquad (B1)$$

The transition amplitude is given by

$$A_{nlm\to n'l'm'}(\mathbf{b},v) = -i\int_{-\infty}^{\infty}\langle\Psi_{n'l'm'}|-\frac{Z_p}{r_p}|\Psi_{nlm}\rangle dt, \qquad (B2)$$

with

$$\Psi_{nlm} = \varphi_{nlm}(\mathbf{r}_t)e^{-i\epsilon_t t}e^{-i\mathbf{v}\mathbf{r}/2-iv^2t/8} \qquad (B3)$$

and

$$\Psi_{n'l'm'} = \varphi_{n'l'm'}(\mathbf{r}_p)e^{-i\epsilon_p t}e^{i\mathbf{v}\mathbf{r}/2-iv^2t/8}\exp\left(-Z_t'\int_t^{\infty}\frac{dt'}{r_t}\right). \qquad (B4)$$

The vectors $\mathbf{r}, \mathbf{r}_t = \mathbf{r}+\frac{1}{2}\mathbf{R}$ and $\mathbf{r}_p = \mathbf{r}-\frac{1}{2}\mathbf{R}$ refer to the position of the muon with respect to the geometrical center of the target and projectile nucleus. The $\varphi_{nlm}$ and $\varphi_{n'l'm'}$ are hydronic wave functions.

$$\epsilon_t = -\frac{1}{2}Z_t^2/n^2\frac{m_t}{m_\mu+m_t} \qquad (B5)$$

and

$$\epsilon_p = -\frac{1}{2}Z_p^2/n^2\frac{m_p}{m_\mu+m_p} \qquad (B6)$$

are the asymptotic eigenenergies of target and projectile. The velocity dependent phase factors are the translational factors and the last term in *eq.*(B4) is the eikonal phase factor. The effective target charge in the final state is denoted by $Z_t'$, but if no screening is assumed $Z_t' = Z_t$.

The time integral in the eikonal phase is evaluated for a fixed position $\mathbf{r}_p$ of the muon with respect to the projectile. With these equations the complete framework of the theory is set. For more details the reader may consult the works of Eichler [18] and references therein.

The transfer cross section [in muonic units] as used in this work for the exchange of a muon between the hydrogenic shells $nl$ and $n'l'$ is given by

$$\sigma_{nl\to n'l'} = \frac{2^{8-l}\pi Z_p^5 Z_t^{5+2l}}{n^{5+2l}n'^3v^2(q_n^2+p_-^2)^{5+2l}} \frac{\pi\eta Z_t'}{\sinh(\pi\eta Z_t')}$$

$$\times \exp[-2\eta Z_t' \tan^{-1}(-p_-/q_n)]S(nl,n'l'), \qquad (B7)$$

with:

$$\eta = 1/v, \qquad (B8)$$

$$p_\pm = \epsilon\,\eta \pm \frac{1}{2}v, \qquad (B9)$$

with

$$\epsilon = \epsilon_p - \epsilon_t, \qquad (B10)$$

and

$$q_n = \frac{Z_t}{n}\frac{m_t}{(m_\mu+m_t)}, \quad q_{n'} = \frac{Z_p}{n'}\frac{m_p}{(m_\mu+m_p)}. \qquad (B11)$$

Hence

$$S(nl,n'l') = \sum_{\lambda=l'}^{2n'-2} F_\lambda(n'l')q_{n'}^{2\lambda}$$

$$\times \sum_{\alpha,\alpha'}\sum_{\gamma=0}^{[l/2]}\sum_{\omega_1\omega_2\omega_3\omega_4} \frac{(-1^\gamma)(2l-2\gamma)!}{(l-\gamma)!(l-2\gamma)!\gamma!} i^{\omega_3-\omega_2}(l-2\gamma;\omega_1\omega_2\omega_3\omega_4)$$

$$\times \sum_{\rho=0}^{\omega_1+\sigma_1+\sigma_1'} (-1)^{\omega_1-\rho}(5+2l+\lambda+\beta+\beta'-s-s'-\rho)^{-1} \qquad (B12)$$

$$\times \binom{\omega_1+\sigma_1+\sigma_1'}{\rho} q_n^{2\omega_1-2\rho}p_-^{\omega_2+\omega_3}(q_n^2+p_-^2)^{\rho-\beta-\beta'-\lambda} D_{\alpha\gamma}D^*_{\alpha'\gamma},$$

with

$$F_\lambda(n'l') = 2^{4l'}(2l'+1)\frac{(n'+l')!}{n'(n'-l'-1)!}\left(\frac{l'!}{(2l'+1)!}\right)^2$$

$$\times \sum_{\mu=0}^{l'}\sum_{\beta,\beta'=0}^{n'-l'-1}(-1)^\mu \binom{l'}{\mu} B_\beta(n'l')B_{\beta'}(n'l'). \qquad (B13)$$

The summations in *eq.*(B13) are subject to the constraint

$$\mu+\beta+\beta'+l' = \lambda. \qquad (B14)$$

Here the coefficients

$$B_\beta(n'l') = \frac{(-n'+l'+1)_\beta(n'+l'+1)_\beta}{(l'+\frac{3}{2})_\beta\beta!} \qquad (B15)$$

are expressed by the Pochammer symbols

$$(a)_\beta = \Gamma(a+\beta)/\Gamma(a) \tag{16}$$

and

$$(a)_0 = 1.$$

$$D_{\alpha\gamma} = (-1)^{\sigma_1+\sigma_3+s}(-i)^{\sigma_2}2^{\sigma_2-s}A_{\beta\nu}(nl)(\gamma+\nu;\sigma_1\sigma_2\sigma_3)\binom{\beta+1-2\nu}{\tau}$$

$$q_n^{\beta-2\nu-\tau+2\sigma_1}p_-^{\sigma_2}(q_n+ip_-)^s\binom{s-1-i\eta Z_t'}{l+1+\beta}. \tag{B17}$$

The label $\alpha$ in the equations above stands for a set of integers.
$\alpha = \{\beta\nu\sigma_1\sigma_2\sigma_3\tau\}$ and correspondingly $\alpha' = \{\beta'\nu'\sigma_1'\sigma_2'\sigma_3'\tau'\}$.

The square brackets denote the integral part, the ranges of the summations are given by
$\beta = 0,1,\ldots,n-l-1,$
$\nu = 0,1,\ldots,[\frac{1}{2}\beta+\frac{1}{2}],$
$\gamma = 0,1,\ldots,[\frac{l}{2}],$
$\sigma_1,\sigma_2,\sigma_3 = 0,1,\ldots,\gamma+\nu,$ subject to $\sigma_1+\sigma_2+\sigma_3 = \gamma+\nu,$
$\tau = 0,1,\ldots,\beta+1-2\nu,$
$\omega_1,\omega_2,\omega_3+\omega_4 = 0,1,\ldots,l-2\gamma,$ subject to $\omega_1+\omega_2+\omega_3+\omega_4 = l-2\gamma.$

The binomial coefficient is the usual finite product.
The parentheses $(k;k_1,k_2,\ldots,k_m) = k!/(k_1!k_2!\ldots k_m!),$
$s = \tau+\omega_2+\omega_4+\sigma_2+2\sigma_3$ and $s' = \tau'+\omega_3+\omega_4+\sigma_2'+2\sigma_3'.$

Furthermore, from the initial wavefunction,

$$A_{\beta\nu}(nl) = n^{-1/2}[(n-l-1)!(n+l)!]^{1/2}\left(-[\frac{1}{2}\beta]-\frac{1}{2}\right)_\nu 2^{2l+\beta+2\nu}q_n^\beta$$

$$\times\frac{(l+1+\nu)!(2l+2+\beta)([\frac{1}{2}\beta+\frac{1}{2}])!}{(2l+2+2\nu)!(n-l-1-\beta)!([\frac{1}{2}\beta+\frac{1}{2}]-\nu)!\beta!\nu!}. \tag{B18}$$

The electron cross section *eq.*(B7) has been tested in various cases by Eichler and coworkers and it is found to describe adequately the transfer reactions in the main region of interest.

## APPENDIX C

## COULOMB EXCITATION CROSS SECTIONS IN THE MODIFIED BORN APPROXIMATION

To describe the effect of recoil of the target in inelastic collisions of a tritium atom of mass $m_t$ and charge $Z_t e$ as *projectile* with a muonic helium ion of mass $m_\alpha$ and nuclear charge $Z_\alpha e$ as *target* the coordinate system has to be defined properly. The consideration below follow closely the developments initiated by Trautmann [34].

The center of mass coordinate is:

$$\mathbf{S} = \frac{m_t \mathbf{r}_t + m_\mu \mathbf{r}_\mu + m_\alpha \mathbf{r}_\alpha}{m_t + m_\mu + m_\alpha}, \tag{C1}$$

the relative coordinate between target and projectile is:

$$\mathbf{R} = \mathbf{r}_t - \frac{m_\mu \mathbf{r}_\mu + m_\alpha \mathbf{r}_\alpha}{m_\mu + m_\alpha} \tag{C2}$$

and the relative coordinate between the target atomic center and the muon is:

$$\mathbf{r} = \mathbf{r}_\mu - \mathbf{r}_\alpha. \tag{C3}$$

The total cross section if averaged over the initial states and summed over the final states is given by:

$$\sigma_{total} = \int \frac{M^2}{(2\pi)^2 \hbar^4} \frac{K_f}{K_i} \frac{1}{(2l+1)} \sum_{m,m'} |T_{if}|^2 d\Omega, \tag{C4}$$

with

$$K_i = \frac{v_i M}{\hbar} \tag{C5}$$

and

$$M = \frac{m_t(m_\mu + m_\alpha)}{m_t + m_\mu + m_\alpha}, \tag{C6}$$

is the reduced mass of the target - projectile system and $v_i$ is the relative incoming velocity between the target system and the projectile.

The T matrix in the Born approximation is given by

$$T_{if}^{Born} = \langle \phi_f(\mathbf{r}) e^{i\mathbf{K}_f \mathbf{R}} | V | \phi_i(\mathbf{r}) e^{i\mathbf{K}_i \mathbf{R}} \rangle, \tag{C7}$$

where $\phi_f(\mathbf{r})$ is the atomic wave function of the target system and the scattering solution of the Coulomb potential is approximated by a plane wave $e^{i\mathbf{K}_f\mathbf{R}}$. The potential $V$ is:

$$V = \frac{Z_t Z_\alpha e^2}{|\mathbf{R} + \frac{m_\mu \mathbf{r}}{m_\mu + m_\alpha}|} - \frac{Z_t Z_\alpha e^2}{|\mathbf{R}|} - \frac{Z_t e^2}{|\mathbf{R} - \frac{m_\alpha \mathbf{r}}{m_\mu + m_\alpha}|}. \tag{C8}$$

If recoil effects are neglected the potential reduces to the last term

$$V_{no\ recoil} = -\frac{Z_t e^2}{|\mathbf{R} - m_r \mathbf{r}|}, \tag{C9}$$

where

$$m_r = \frac{m_\alpha}{m_\mu + m_\alpha}. \tag{C10}$$

Calculations for this document do include recoil effects and the potential used is

$$V = V_{no\ recoil} + V_{recoil} \tag{C11}$$

and

$$T_{if} = T_{if\ no\ recoil} + T_{if\ recoil} \tag{C12}$$

$$T^{Born}_{if\ no\ recoil} = -Z_t e^2 \int d^3R d^3r \frac{e^{i\mathbf{QR}}}{|\mathbf{R} - m_r \mathbf{r}|} \phi_f^*(\mathbf{r}) \phi_i(\mathbf{r}). \tag{C13}$$

The total momentum transfer is $\mathbf{Q} = \mathbf{K}_i - \mathbf{K}_f$ and the integration over $d^3r$ can be fourier transformed

$$\int d^3R \frac{e^{i\mathbf{QR}}}{|\mathbf{R} - m_r \mathbf{r}|} = 4\pi \frac{e^{im_r \mathbf{Qr}}}{Q^2}. \tag{C14}$$

Using the atomic wave function

$$\phi(\mathbf{r}) = R_{nl}(r) Y_{lm}(\hat{r}). \tag{C15}$$

The main quantum number is $n$, $l$ is the angular momentum quantum number and $m$ is its projection on the z-axis.

Expanding in spherical harmonics:

$$e^{im_r \mathbf{Qr}} = 4\pi \sum_{\lambda=0}^{\infty} \sum_{\nu=-\lambda}^{+\lambda} i^\lambda j_\lambda(m_r Q r) Y^*_{\lambda\nu}(\hat{Q}) Y_{\lambda\nu}(\hat{r}). \tag{C16}$$

The **T** matrix [57] then becomes:

$$T^{Born}_{if\ no\ recoil} = \frac{-Z_t e^2}{Q^2}(4\pi)^{\frac{3}{2}}(-1)^{m'}\sqrt{(2l'+1)(2l_i+1)}$$

$$\sum_{\lambda=0}^{\infty}\sum_{\nu=-\lambda}^{+\lambda} i^{\lambda}Y^*_{\lambda\nu}(\hat{Q})\sqrt{(2\lambda+1)}\begin{pmatrix} l & l' & \lambda \\ 000 & & \end{pmatrix}\begin{pmatrix} l & l' & \lambda \\ m & -m'\nu & \end{pmatrix}F^{\lambda}_{if\ no\ recoil} \qquad (C17)$$

with

$$F^{\lambda}_{if\ no\ recoil} = \int_o^{\infty} dr r^2 j_{\lambda}(m_r Q r) R_{n'l'}(r) R_{nl}(r) \qquad (C18)$$

and

$$R_{nl} = \hat{N} e^{-\beta r}(\beta r)^l \sum_{k=0}^{n_r} c_k (\beta r)^k, \qquad (C19)$$

where $n_r$ is the radial quantum number $n_r = n - l - 1$,

$$c_k = \frac{(-n_r)_k 2^k}{(2l+2)_k k!}, \quad \beta = \frac{Z_\alpha}{\hat{a}_\mu n} \qquad (C20)$$

with

$$\hat{a}_\mu = \frac{\hbar^2}{e^2 m_\mu m_r} = \frac{a_\mu}{m_r}. \qquad (C21)$$

The normalization is defined by:

$$\hat{N} = \frac{2^{l+1}\beta^{\frac{3}{2}}}{(2l+1)!}\left(\frac{(n+l)!}{n_r! n}\right)^{\frac{1}{2}}. \qquad (C22)$$

The total cross section is

$$\sigma^{Born}_{total} = \int 4\frac{(-Z_t e^2)^2 M^2}{\hbar^4}\frac{K_f}{K_i}(2l'+1)\sum_{\lambda}(2\lambda+1)\begin{pmatrix} l & l' & \lambda \\ 000 & & \end{pmatrix}^2$$

$$|F^{\lambda}_{if\ no\ recoil}|^2 \frac{1}{Q^4} d\Omega, \qquad (C23)$$

Using

$$d\Omega = d(\cos\Theta)d\phi, \qquad (C24)$$

with

$$\mathbf{K}_i \cdot \mathbf{K}_f = K_i K_f \cos(\Theta) \qquad (C25)$$

the integration in *eq.*13 is:

$$\ldots \int \frac{K_f}{K_i Q^4}|F^{\lambda}_{if}|^2 d\Omega = \ldots \frac{2\pi}{K_i^2}\int_{Q-}^{Q+}|F^{\lambda}_{if}|^2 \frac{dQ}{Q^3}. \qquad (C26)$$

where

$$Q_{\pm} = K_i \pm K_f. \tag{C27}$$

With the substitutions

$$x = \frac{Z_\alpha r}{a_\mu}\left(\frac{1}{n'} + \frac{1}{n}\right), \tag{C28}$$

and

$$t = \frac{\hat{a}_\mu}{Z_\alpha}\frac{n'nm_r}{n'+n}Q \tag{C29}$$

the radial integral takes the form

$$F^{\lambda}_{if\ no\ recoil} = N_{if}\sum_{k=0}^{n'_r+n_r}\sum_{s=Max(0;k-n'_r)}^{Min(k;n_r)}\frac{c'_s c_{k-s}}{n'^s n^{k-s}}\left(\frac{n'n}{n'+n}\right)^k$$

$$\times\int_0^\infty dx x^{l+l'+2k}e^{-x}j_\lambda(tx). \tag{C30}$$

The above integral can be expressed as a series [19]:

$$\int_0^\infty dx x^\gamma e^{-x}j_\lambda(tx) = 2\frac{\Gamma(\gamma+\lambda+1)}{(2t)^{\lambda+1}}(1+t^2)^{\frac{\lambda-\gamma}{2}}$$

$$\sum_\nu(-)^\nu\binom{\lambda}{\nu}\frac{\sin[(\gamma-\lambda+2\nu)\arctan(t)]}{(\gamma+\nu-\lambda)_{\lambda+1}} \tag{C31}$$

The recoil part of $F^{\lambda}_{if}$ can be calculated along the same line substituting for the recoil integral:

$$(phase)\times Z_\alpha\int_0^\infty dx x^{l+l'+2k}e^{-x}j_\lambda(p_m tx) \tag{C32}$$

with

$$p_m = \frac{1-m_r}{m_r}. \tag{C33}$$

The normalization factor in *eq.*(14) is:

$$N_{if} = \frac{4}{(2l'+1)!(2l+1)!}\left(\frac{2n'}{n'+n}\right)^l\left(\frac{2n}{n'+n}\right)^{l'}\frac{n'n}{(n'+n)^3}$$

$$\times\sqrt{\frac{(n'+l')!(n+l)!}{(n'-l'-1)!(n-l-1)!}}. \tag{C34}$$

Then the total cross section will be

$$\sigma_{total}^{Born} = 8\pi \left(\frac{a_\mu Z_t}{v_i \cdot 137/cZ_\alpha}\right)^2 \left(\frac{n'n}{n'+n}\right)^2 (2l'+1)$$

$$\sum_\lambda (2\lambda+1) \begin{pmatrix} ll'\lambda \\ 000 \end{pmatrix}^2 \int_{t_-}^{t_+} |F_{if}^\lambda|^2 \frac{dt}{t^3}. \qquad (C35)$$

The integration boundaries are:

$$t_\pm = \sqrt{\frac{Mm_r}{m_\alpha}\left(\frac{n'-n}{n'+n}\right)} \left(\sqrt{\frac{E_i}{\Delta E}} \pm \sqrt{\frac{E_i}{\Delta E} - 1}\right), \qquad (C36)$$

where $\Delta E$ is the energy difference between the eigenstate of the target system $n \rightarrow n'$. The eigenenergy of eigenstate $n$ of the target system is:

$$E = \frac{(-Z_\alpha \frac{1}{137})^2}{2} m_\mu m_r c^2 \frac{1}{n^2} \qquad (C37)$$

and therefore the energy difference

$$\Delta E = \frac{(-Z_\alpha \frac{1}{137})^2}{2} m_\mu m_r c^2 \left(\frac{1}{n^2} - \frac{1}{n'^2}\right). \qquad (C38)$$

The kinetic initial energy $E_i$ of the projectile are given by:

$$E_i = \frac{\hbar^2}{2} \cdot \frac{K_i^2}{M}. \qquad (C39)$$

The Born approximation disregards completely the Coulomb deflection of the projectile by the target system. A better approximation can be obtained if the hyperbolic trajectory of the projectile is taken into account [19].

The **T** matrix will than contain the Coulomb deflection factor $\exp(-\frac{1}{2}\pi\xi)$ :

$$T_{if}^{modified} = e^{-\frac{1}{2}\pi\xi} T_{if}^{Born}, \qquad (C40)$$

where $\xi = \eta_f - \eta_i$ with

$$\eta = \frac{Z_\alpha Z_t e^2}{\hbar v}. \qquad (C41)$$

The Coulomb deflection factor used in the present calculations is the dominant correction term as calculated by Bang and Hansteen [58] assuming a hyperbolic path for the projectile.

The total inelastic Coulomb excitation cross section in the modified Born approximation is then given by:

$$\sigma^{modified}/a_\mu^2 = \frac{8\pi}{(v_i \cdot 137/c)^2}\left(\frac{Z_t}{Z_a}\right)^2\left(\frac{n'n}{n'+n}\right)^2(2l'+1)$$

$$\sum_\lambda (2\lambda+1)\begin{pmatrix} l & l' & \lambda \\ 0 & 0 & 0 \end{pmatrix}^2 \int_{t_-}^{t_+} |F_{if}^\lambda|^2 \exp(-\pi\xi)\frac{dt}{t^3}. \qquad (C42)$$

## APPENDIX D

## NONLINEAR DENSITY DEPENDENCE OF STOPPING POWER

The stopping power of muonic helium ions $(\alpha\mu)^+$ in hydrogen can be derived from the proton stopping power since the stopping power of ions depends only on the charge $Z_p$ and velocity $v$ but not on the mass of the projectile as expressed in Bethe's stopping power formula [59]

$$\frac{-dE}{dx} = \frac{4\pi Z_p^2 e^4}{mv^2}\rho Z_t(ln\frac{2mv^2}{I} + ln\frac{1}{1-\beta^2} - \beta^2 - C), \qquad (D1)$$

where $m$ is the electron mass, $\rho Z_t$ is the average electron density, and $I$ is the mean ionization potential of the target electrons, $v$ is the ion velocity in atomic units, $\beta = v/c$ and $C$ describes shell corrections arising from the local inhomogeneity of the target electron distribution. This formula predicts the energy loss accurately at energies larger than 1 $MeV$ per atomic mass unit [amu]. There two physical parameters, the mean ionization potential $I$ and the shell corrections $C$, successfully express the influence of the electronic structure of the target material on the rate of energy loss. At very low projectile velocities non-electronic energy-loss mechanisms become important. In the intermediate energy region (between 30 $keV/amu$ and 1 $MeV/amu$) no simple theoretical description exists, as will be discuss below. However, precisely this energy range is sampled in the muonic reactivation process; the excitation cross sections peak around $v = 2$ [amu], corresponding to an energy of 100 $keV/amu$.

In the framework of linear response theory, the rate of energy loss of a charged particle penetrating through matter can be expressed in terms of the dynamical structure factor [60]

$$F(q,\omega) = \sum_f \frac{1}{Z_t}|\langle f|\rho(q)|i\rangle|^2\delta(\omega + E_i - E_f), \qquad (D2)$$

where $i$ and $f$ denote the initial and final state of the target, $\rho(q)$ is the Fourier transform of the electron density operator, and $Z_t$ is the number of electrons per target atom. (For thermally excited targets an ensemble average over initial states must be included in the definition of $S(q,\omega)$.) The rate of energy loss is then given by the rate of energy transfer to the medium

$$-\frac{dE}{dt} = \int d^3p' \int \omega d\omega \int d^3q (\frac{2Z_p e^2}{q^2})^2 F(q,\omega)\delta(E' + \omega - E)\delta^3(p' + q - p), \quad (D3)$$

where $E, p$ and $E', p'$ are the initial and final energy and momentum of the projectile, respectively. For projectiles much heavier than an electron the delta functions yield a connection between energy and momentum transfer:

$$\omega = vq, \qquad (D4)$$

where $v$ is the projectile velocity. On the other hand, the dynamical structure factor is related to the imaginary part of the longitudinal dielectric constant:

$$F(q,\omega) = \frac{q^2}{4\pi^2 e^2}(1+n(\omega))\Im\left(\frac{-1}{\epsilon_L(q,\omega)}\right), \qquad (D5)$$

where $n(\omega)$ is the occupation probability of excited electronic states. Assuming that the target is initially in its ground state, *eqs.*(3,4,5) become

$$-\frac{dE}{dt} = (\frac{Z_p e}{\pi})^2 \int_0^\infty \omega d\omega \int \frac{d^3q}{q^2}\delta(\omega - qv)\Im\left(\frac{-1}{\epsilon_L(q,\omega)}\right), \qquad (D6)$$

which forms the basis of the Lindhard-Winther theory of electronic stopping power [61]. It can also be derived within the framework of the classical theory of electromagnetism in continuous media [62].

The Bethe formula is obtained in the limit of vanishing q-dependence of the dielectric constant. The momentum integration can be carried out, (note $qv = qv\sin(\theta)$) paticularly easily if an upper cut-off $q_{max} = 2mv$ is introduced, yielding:

$$S = -\frac{1}{v\rho}\frac{dE}{dt} = \frac{2}{\pi\rho}(\frac{Z_p e^2}{v})^2 \int_0^\infty \omega d\omega \Im\left(\frac{-1}{\epsilon_L(\omega)}\right)\ln\left(\frac{2mv^2}{\omega}\right), \qquad (D7)$$

where $\rho$ is the atom target density. Without the logarithmic term the frequency integral is related to the plasma frequency $\omega_p$:

$$\int_0^\infty \omega d\omega \Im\left(\frac{-1}{\epsilon_L(\omega)}\right) = \frac{\pi}{2}\omega_p^2 = \frac{2\pi e^2}{m}n, \qquad (D8)$$

where $n$ is the electron density in the target: $n = rhoZ_t$. Defining the average ionization potential $I$ through the relation

$$\frac{2}{\pi}\frac{1}{\omega_p^2}\int_0^\infty \omega d\omega \Im\left(\frac{-1}{\epsilon_L(\omega)}\right)\ln(\omega) = \ln I, \qquad (D9)$$

the first term in the Bethe formula is derived. The remaining terms are relativistic corrections and shell corrections which result from the inhomogeneity of the electron density in the target [59].

For velocities in the range $(I/2m)^{1/2}$ these approximations no longer hold, and the stopping power must be calculated using a realistic description of $\epsilon_L(q,\omega)$. For gases, atomic or molecular, exact dipole strength calculations are available for that purpose. Such calculations yield, e.g. $I = 15\ eV$ for atomic hydrogen and $I = 19\ eV$ for molecular hydrogen [59], showing a definite dependence of the stopping power on the chemical composition of the target. For solid

targets the random phase approximation (RPA) to the homogeneous electron gas has found widespread use [63].

Differences in the stopping power $S$ between gaseous and condensed matter target of the same chemical composition have been noted by many experimenters (see e.g. the review by Thwaites [64]). Systematic investigations of this effect were carried out by Ziegler et al.[65] using alpha particles, who found $S$ not only to decrease below theoretical expectations for small velocities, but also a marked difference in the size of this effect between gases and solids. The difference was especially large for targets with low atomic number, rising to 40% at 600 *keV* alpha particle energy. Very similar behavior was found by Palmer et al. for liquid targets used in biological radiation research and even for water [66]. At an alpha particle energy of 500 *keV* the stopping power in the gaseous phase was 39% higher than in the liquid phase.

That an explicit density dependence of $S$ can exist even inside the liquid phase was recently shown by Both et al. [67] in an experiment making use of the Doppler-shift attenuation method. From the measurement of $\gamma$-rays emitted by moving $^7$Li nuclei in liquid ethane ($C_2H_6$) they found that the stopping power decreases slightly with increasing density of the liquid. This decrease could be explained by the change in the electron density distribution inside a molecule due to proximity effects from neighboring molecules. Therefore there is strong experimental evidence for a density dependent reduction of stopping power in the liquid phase at low ion velocities, at least for materials which exhibit a tendency to form hydrogen bonds leading to the possibility of molecular clustering in the liquid.

At this level of the formalism, nonlinear density effects are contained in the nonlinear dependence of the dielectric function $\epsilon_L$ upon density. In principle, i.e. if $\epsilon_L$ would be taken to be the true dielectric function of the target, all density dependence of this kind would be exactly described, even the discontinuous changes across a phase boundary. Unfortunately, realistic *ab initio* calculations of $\epsilon_L(q,\omega)$ do not exist for most materials, in particular, none is known to us for liquid hydrogen. Sufficient experimental information about $\epsilon_L(q,\omega)$ is also usually not available, because the polarizability can be readily measured only for values of q and $\omega$ that correspond to the photon dispersion relation and, moreover, because only the transverse and not the longitudinal component is obtained in this way. Therefore the stopping power of materials that do not either classify as dilute gases or exhibit a well-defined conduction band cannot be predicted accurately.

The stopping power as given in Ziegler's TRIM-85 program [48] for solid

hydrogen targets differs considerably from that for hydrogen gas [47], which was used in previous calculations [16,44]. This is shown in *section 5* figure 17 depicting the stopping power function $S(v)$ as function of ion velocity $v$ [amu]. At $v = 2$ the reduction agrees rather well with the empirical findings of Palmer et al. [66], indicating that it is likely to be valid also for liquid hydrogen targets.

# References


[1] Alvarez L.W. *et al.*, Phys. Rev. **105**, 1127, (1957).

[2] Frank F.C., Nature **160**,525 (1947).

[3] Sakharov A.D., *Report of the Physics Institute, Academy of Sciences*, (1948).

[4] Zel'dovich Ya.B., Dokl. Akad. Nauk S. S. R. **95**, 493, (1954).

[5] Zel'dovich Ya. B., S.S.Gershstein Soviet Phys. Usp. **3**, 593 (1961).

[6] Jackson J.D., Phys. Rev. **106**, 330 (1957).

[7] Dzhelepov V.P. *et al.*, Soviet Phys. JETP **23**, 820 (1966).

[8] Vesman E.A., Soviet Phys. JETP lett. **5**, 113 (1967).

[9] Gershtein S.S. and L.I.Ponomarev, Phys. Lett.**72B**, 80 (1977).

[10] Vinitsky S.I. *et al.*, Soviet Phys. JETP **47**, 444 (1978).

[11] Rafelski J., ed. Crowe *et al.*, *Exotic Atoms* '**79**, 177, (1980).

[12] Jones S.E. *et al.*, Phys. Rev. Lett. **51**, 1757 (1983).

[13] Jones S.E. *et al.*, Phys. Rev. Lett. **56**, 588 (1986).

[14] Jones S.E., Nature **321**, 127 (1986).

[15] Rafelski J. and S.E.Jones, Sci. Am. **255**, 84 (1987).

[16] Bracci L. and G. Fiorentini, Nucl. Phys. **A364**, 383 (1981).

[17] Rafelski H.E. *et al.*, *Muon Catalyzed Fusion* **1**, 315 (1987).

[18] Eichler J.K.M., Phys. Rev. **A23**, 498 (1981).

[19] Trautmann D. *et al.*, J. Phys. **B16**,3005 (1983).

[20] Ceperley D. and B.J.Alder, Phys. Rev. **A31**, 1999 (1985)

[21] Hu C.-Y., Phys. Rev. **A34**, 2536 (1986).

[22] Haywood S.E. *et al.* Phys. Rev. **A37**, 3393 (1988).
Szalewicz K. *et al.*, to be published in Proc. of the Florida MuCF workshop 1988; AIP, New York.

[23] Gershtein S.S. *et al.* Soviet Phys. JETP **53**, 872 (1981).

[24] Rafelski J. and B. Müller Phys. Lett. **164B**, 223 (1985).

[25] Danos M. *et al.* Phys. Rev. **A34**, 3642 (1986).

[26] Danos M. *et al.* Phys. Rev. **A35**, 2741 (1987). *Muon Catalyzed Fusion* **3**, 443 (1988).

[27] Biedenharn L. *et al.*, to be published in Proc. of the Florida MuCF workshop 1988; AIP, New York.

[28] Cohen J.S., *Muon Catalyzed Fusion* **1**, 179 (1987).

[29] Cohen J.S., *Muon Catalyzed Fusion* **3**, 499 (1988).

[30] Leon M. and H.A. Bethe, Phys. Rev. **127**, 636 (1962).

[31] Takahashi H., *Muon Catalyzed Fusion* **3**, 453 (1988).

[32] Markushin V.E., *Muon Catalyzed Fusion* **2**, (1987);
also in: Proc. of *Muons and Pions in Matter*, 246 (Dubna 1987).

[33] Basu D. *et al.*, Phys. Rep. **42C**, 147 (1978).

[34] Trautmann D. *et al.*, Nucl. Instr. Meth. **214**, 21 (1983).
D.Trautmann, Basel, *private communication.*

[35] Watts M.F. *et al.*, J. Phys. **B19**, L355 (1986).

[36] Takahashi H., Phys. Lett. **174B**, 133 (1986).

[37] Bossy H., to be published in Proc. of the Florida MuCF workshop 1988; AIP, New York.

[38] Cohen J.S., *Muon Catalyzed Fusion* **3**, 421 (1988).

[39] Menshikov L.I. and L.I.Ponomarev, JETP Lett. **41**, 623 (1985).

[40] Jones S.E. *et al.*, *private communication.*

[41] Breunlich W.H. *et al.*, *Muon Catalyzed Fusion* **1**, 67 (1987).

[42] Nagamine K., *Muon Catalyzed Fusion* **1**, 137 (1987).

[43] Bossy H. *et al.*, Phys. Rev. Lett. **59**, 2864 (1987).

[44] Cohen J.S., Phys. Rev. Lett. **58**, 1407 (1986).

[45] Balin D.V. *et al.*, Phys. Lett. **141B**, 173 (1984).
Soviet Phys. JETP Lett. **40**, 1112 (1984).

[46] Bossy H. *et al.*, Phys. Rev. Lett. **55**, 1870 (1985).

[47] Anderson H.H. and J.F.Ziegler, *Hydrogen Stopping Power and Ranges in All Elements*, Pergamon Press (1977), [see also references therein].

[48] Ziegler J.F. *et al.*, *The Stopping and Ranges of Ions in Solids*, Pergamon Press (1985), [see also references therein].

[49] Caffrey A.J., to be published in Proc. of the Florida MuCF workshop; AIP, New York.

[50] Struensee M.C. and J.S.Cohen, preprint LA-UR-87-4049, Los Alamos (1988).

[51] Ponomarev L.I. and G. Fiorentini, *Muon Catalyzed Fusion* **1**, 3 (1987).

[52] Alexander S.A. *et al.*, to be published in Proc. of the Florida MuCF workshop 1988; AIP, New York.

[53] Szalewicz K. *et al.*, Phys. Rev. **A35**, 965 (1987).

[54] Chan F.T. and J.K.M. Eichler Phys. Rev. Lett. **42**, 58 (1979).

[55] Eichler J.K.M. and F.T.Chan Phys. Rev. **A20**, 104 (1979).

[56] Chan F.T. and J.K.M. Eichler Phys. Rev. **A20**, 1841 (1979).

[57] Marbach G., *Diploma Thesis*, University of Basel (1986), [see also references therein].

[58] Bang J. and J.M. Hansteen, K. Dan. Vidensk. Selsk. Mat. Fys. Medd. **31**, 1 (1959).

[59] Fano U., Ann. Rev. Nucl. Sci. **13**, 1 (1963).

[60] Arista N.R. and W. Brandt, Phys. Rev. **A23**, 1898 (1981).

[61] Lindhard J. and A.Winther, K. Dan. Vidensk. Selsk. Mat. Fys. Medd. **34**, 4 (1964).

[62] Hubbard J., Proc. Roy. Soc. **A68**, 976 (1955).

[63] Lindhard J., K. Dan. Vidensk. Selsk. Mat. Fys. Medd. **28**, 8 (1954).

[64] Thwaites D.I., Rad. Res. **95**, 495 (1983).

[65] Ziegler J.F., *et al.*, Ap. Phys. Lett. **27**, 387 (1975).

[66] Palmer R.B.J. and A.Akhavan-Rezayat, J. Phys. **D11**, 605 (1978).

[67] Both G. *et al.*, Phys. Rev. **A28**, 3212 (1983).